Dissertation

Carlos Andres Rivera Villarreyes

Institute of Earth and Environmental Sciences
Water and Matter Transport in Complex Landscapes Group

Cosmic-ray Neutron Sensing for Soil Moisture Measurements in Cropped Fields

Cumulative Dissertation
for the academic degree of Doctor of Natural Science
"doctor rerum naturalium" (Dr. rer. nat.)
in the scientific discipline of Geoecology - Hydrology

submitted to the
Faculty of Mathematics and Natural Sciences
at the University of Potsdam, Germany

by
Carlos Andres Rivera Villarreyes

Potsdam, 31th October 2013

Contents

List of Figures

List of Tables

Abstract

This cumulative dissertation explored the use of the detection of natural background of fast neutrons, the so-called cosmic-ray neutron sensing (CRS) approach to measure field-scale soil moisture in cropped fields. Primary cosmic rays penetrate the top atmosphere and interact with atmospheric particles. Such interaction results on a cascade of high-energy neutrons, which continue traveling through the atmospheric column. Finally, neutrons penetrate the soil surface and a second cascade is produced with the so-called secondary cosmic-ray neutrons (fast neutrons). Partly, fast neutrons are absorbed by hydrogen (soil moisture). Remaining neutrons scatter back to the atmosphere, where its flux is inversely correlated to the soil moisture content, therefore allowing a non-invasive indirect measurement of soil moisture.

The CRS methodology is mainly evaluated based on a field study carried out on a farmland in Potsdam (Brandenburg, Germany) along three crop seasons with corn, sunflower and winter rye; a bare soil period; and two winter periods. Also, field monitoring was carried out in the Schaefertal catchment (Harz, Germany) for long-term testing of CRS against ancillary data.

In the first experimental site, the CRS method was calibrated and validated using different approaches of soil moisture measurements. In a period with corn, soil moisture measurement at the local scale was performed at near-surface only, and in subsequent periods (sunflower and winter rye) sensors were placed in three depths (5 cm, 20 cm and 40 cm). The direct transfer of CRS calibration parameters between two vegetation periods led to a large overestimation of soil moisture by the CRS. Part of this soil moisture overestimation was attributed to an underestimation of the CRS observation depth during the corn period (5-10 cm), which was later recalculated to values between 20-40 cm in other crop periods (sunflower and winter rye).

According to results from these monitoring periods with different crops, vegetation played an important role on the CRS measurements. Water contained also in crop biomass, above and below ground, produces important neutron moderation. This effect was accounted for by a simple model for

neutron corrections due to vegetation. It followed crop development and reduced overall CRS soil moisture error for periods of sunflower and winter rye.

In Potsdam farmland also inversely-estimated soil hydraulic parameters were determined at the field scale, using CRS soil moisture from the sunflower period. A modelling framework coupling HYDRUS-1D and PEST was applied. Subsequently, field-scale soil hydraulic properties were compared against local scale soil properties (modelling and measurements). Successful results were obtained here, despite large difference in support volume. Simple modelling framework emphasizes future research directions with CRS soil moisture to parameterize field scale models.

In Schaefertal catchment, CRS measurements were verified using precipitation and evapotranspiration data. At the monthly resolution, CRS soil water storage was well correlated to these two weather variables. Also clearly, water balance could not be closed due to missing information from other compartments such as groundwater, catchment discharge, etc. In the catchment, the snow influence to natural neutrons was also evaluated. As also observed in Potsdam farmland, CRS signal was strongly influenced by snow fall and snow accumulation. A simple strategy to measure snow was presented for Schaefertal case.

Concluding remarks of this dissertation showed that (a) the cosmic-ray neutron sensing (CRS) has a strong potential to provide feasible measurement of mean soil moisture at the field scale in cropped fields; (b) CRS soil moisture is strongly influenced by other environmental water pools such as vegetation and snow, therefore these should be considered in analysis; (c) CRS water storage can be used for soil hydrology modelling for determination of soil hydraulic parameters; and (d) CRS approach has strong potential for long-term monitoring of soil moisture and for addressing studies of water balance.

Zusammenfassung

In dieser kumulativen Dissertation wird die Detektion des natürlichen Hintergrunds von schnellen Neutronen, das sogenannte "Cosmic-Ray Neutron Sensing" (CRS), zur Messung von Bodenfeuchte auf der Feldskala in landwirtschaftlich genutzten Flächen untersucht. Die kosmische Primärstrahlung durchdringt die oberste Atmosphäre, und interagiert mit atmosphärischen Teilchen. Durch diese Wechselwirkungen entstehen Kaskaden hochenergetischer Teilchen die bis in die Erdoberfläche eindringen, wobei schnelle Neutronen entstehen. Teilweise werden diese durch Wasserstoff (Bodenfeuchte) absorbiert, teilweise zurück in die Atmosphäre gestreut. Dieser Neutronenfluss über dem Boden korreliert invers mit der Bodenfeuchte, was so eine non-invasive und indirekte Bodenfeuchteschätzung ermöglicht.

Die CRS-Methode wird vor allem in einer Feldstudie auf einem Ackerland in Potsdam (Brandenburg, Deutschland), einschließlich dreier Phasen mit Anbau von Mais, Sonnenblume und Winterroggen getestet und beurteilt. Darüber hinaus wurde ein Feldmonitoring im Schäfertaleinzugsgebiet (Harz, Deutschland) durchgeführt, um das Potential von Langzeit-CRS-Messungen gegenüber herkömmlich erhobenen bodenhydraulischen Daten abzuschätzen.

Im ersten Untersuchungsgebiet wurde die CRS-Methode kalibriert und mittels verschiedener Bodenfeuchtemessansätze validiert. In der Maisanbauphase wurden die Bodenfeuchte-Punktmessungen zunächst nur an der nahen Bodenoberfläche durchgeführt. In den folgendenen Anbauphasen (Sonnenblume und Winterroggen) wurden dann die Sensoren in drei unterschiedlichen Tiefen (5 cm, 20 cm und 40 cm) installiert. Die direkte Übertragung der CRS-Kalibrierparameter zwischen zwei Vegetationsperioden führte zu einer starken Überschätzung der CRS-Bodenfeuchte. Ein Teil der überschätzten Bodenfeuchte wurde der Unterschätzung der CRS-Beobachtungtiefe während der Maisperiode ($\sim$ 5-10 cm) zugeschrieben, welche später basierend auf Werten zwischen 20-40 cm in anderen Anbauperioden (Sonnenblume und Winterroggen) neuberechnet wurde.

Gemäß der Ergebnisse dieser Beobachtungsperioden mit verschiedenen Feldfrüchten, spielte die Vegetation eine wichtige Rolle für die CRS-Messungen,

da das Wasser, das in der über- und unterirdischen Biomasse vorhanden ist, die Neutronen bedeutend abdämpft. Dieser Effekt, sowie der Einfluss des Getreidewachstums und des reduzierten Gesamt-CRS-Bodenfeuchte-Fehlers, wurden in ein einfaches Model zur vegetationsbedingten Neutronenkorrektur berücksichtigt.

So wurde ein gekoppelter HYDRUS-1D- und PEST-Ansatz angewendet, um bodenhydraulische Parameter auf dem Feldmassstab während der Sonnenblumen-Phase invers abzuschätzen. Dann wurden die inversen Schätzungen der effektiven bodenhydraulischen Eigenschaften innerhalb des von CRS beobachteten Volumens durch die lokalen Bodeneigenschaften (Modellierung und Messungen) validiert. Abgesehen von Unterschieden auf Grund der Beobachtungtiefe und somit des Volumens, wurden hierbei erfolgreiche Ergebnisse erzielt. Dieser einfache Ansatz unterstreicht das zukünftige Forschungspotential, z.B. um mit Hilfe von Bodenfeuchten aus CRS-Messungen Modelle auf der Feldskala zu parametrisieren.

Im Schäfertaleinzugsgebiet wurden die Langzeit-CRS-Messungen mit Niederschlags- und Evapotranspirations-Raten abgeglichen. Bei einer monatlichen Auflösung korrelierte die Änderung des CRS-Bodenwasserspeichers mit diesen beiden Wettervariablen. Die Wasserbilanz konnte jedoch auf Grund fehlender Informationen bezüglich Grundwasser, Abfluss des Einzugesgebiets, etc. nicht geschlossen werden. Darüber hinaus wurde, wie auch am Potsdamer Standort, festgestellt, dass das CRS-Signal stark von Schneefall und Schnee-akkumulationen beeinflusst wird. Eine einfache Anwendung zur Schneemessung mittels CRS wurde für den Schäfertalfall vorgestellt.

Abschließend zeigte sich, dass (a) „Cosmic-Ray Neutron Sensing" (CRS) ein großes Potential hat, Messungen der mittleren Bodenfeuchte auf der Feldskala im Bereich landwirtschaftlich genutzter Flächen zu realisieren; (b) die CRS-Bodenfeuchte stark durch andere Wasserspeicher, wie Vegetation und Schnee beeinflusst wird, und dies im Rahmen von Analysen berücksichtigt werden sollte; (c) die CRS-Messungen über eine bodenhydraulische Modellierung zur Bestimmung von bodenhydraulischen Paramtern genutzt werden kann; und (d) der CRS-Ansatz ein großes Potential für Langzeit-Bodenfeuchte-Monitoring und für Wasserbilanzstudien hat.

Resumen

Esta tesis doctoral explora el uso de los neutrones producidos por radiación cósmica (CRS por sus siglas en inglés) para la medición del contenido de humedad del suelo en la escala de un campo agrícola.

Los rayos cósmicos primarios penetran la atmósfera superior e interactúan con partículas atmosféricas. Como resultado de estas interacciones una cascada de neutrones altamente energizados es producida. Estos neutrones continúan viajando a través de la atmósfera hasta que finalmente penetran la superficie del suelo, donde una segunda cascada de neutrones es creada nuevamente (neutrones rápidos). Parcialmente, los neutrones rápidos son consumidos por el Hidrógeno presente en el contenido de humedad del suelo. Los neutrones restantes logran escapar del subsuelo y regresan a la atmósfera, donde su tasa de flujo es inversamente proporcional al contenido de humedad del suelo.

El método CRS es principalmente investigado en base a trabajo de campo realizado en un terreno agrícola, en Potsdam (Brandeburgo, Alemania), a lo largo de tres periodos de cultivo con maíz, girasoles y centeno de invierno; un periodo con suelo sin vegetación; y dos periodos de invierno con nieve. En paralelo, el mismo trabajo de campo fue llevado a cabo en la cuenca Schaefertal (Harz, Alemania) para testear el método CRS por un largo periodo de tiempo consecutivo.

En el primer sitio de estudio, la metodología CRS fue calibrada y validada usando diferentes métodos de referencia. En el periodo con maíz, las mediciones de contenido de humedad del suelo a la escala local (valores puntuales) fueron conducidas a una profundidad cercana a la superficie. En los periodos siguientes, girasoles y centeno de invierno, los sensores fueron instalados en tres distintas profundidades (5 cm, 20 cm y 40 cm). La transferencia directa de los parámetros de calibración entre los dos periodos conllevó a una larga sobreestimación del contenido de humedad del suelo mediante el método CRS. Parte de esta sobreestimación fue atribuida a una subestimación de la profundidad de observación del nuevo método dentro del subsuelo. Inicialmente un valor entre 5-10 cm fue considerado para el periodo con maíz,

el cual fue recalculado entre 20 y 40 cm para los periodos con girasoles y centeno de invierno.

De acuerdo con los resultados de estos periodos de cultivo, el efecto de la vegetación es preponderante en el método CRS. El agua contenida en la biomasa produce una importante disminución de los neutrones. Este efecto fue corregido por un simple modelo basado en desarrollo vegetativo del cultivo. Correcciones produjeron una reducción significativa del desviación del contenido para los periodos con girasoles y centeno de invierno.

En el terreno agrícola en Potsdam, propiedades hidráulicas del suelo fueron estimadas a la escala de campo usando los valores de contenido de humedad por el método CRS en el periodo con girasoles. El flujo de agua en la zona no saturada fue modelado con HYDRUS-1D y PEST. Posteriormente, las propiedades hidráulicas del suelo obtenidas a la escala del terreno agrícola fueron validadas con valores a escala local (mediciones y simulaciones). Resultados satisfactorios fueron obtenidos en la comparación, a pesar del contraste de las escalas de medición. Esta metodología enfatiza futuras direcciones de investigación con el método CRS para la parametrización de modelos de flujo a la escala de un terreno agrícola.

En la cuenca Schaefertal, las mediciones con el método CRS fueron llevadas a cabo por un largo periodo y verificadas en base a mediciones de precipitación y evapotranspiración. A una escala temporal mensual, el contenido de humedad del suelo calculado por el método CRS fue adecuadamente correlacionado con estas dos variables climatológicas. El balance hídrico no pudo ser cerrado debido a la falta de información relacionada al agua subterránea, escorrentía en la cuenca, etc. También se investigó la influencia de la nieve en los neutrones medidos en Schaefertal. Al igual que en Postdam, la señal del método CRS fue fuertemente influenciada por la caída y acumulación de nieve. Adicionalmente, una simple metodología para medir el equivalente en agua de nieve es presentada para la cuenca Schaefertal.

El trabajo expuesto en esta tesis doctoral concluye que (a) la medición de neutrones producto de los rayos cósmicos tiene un gran potencial para la cuantificación del contenido medio de humedad del suelo a la escala de un terreno agrícola; (b) el contenido de humedad por este método es considerablemente afectado por el agua en la vegetación, nieve u otros, por lo que el análisis de estos factores es recomendado; (c) valores de contenido de humedad del suelo medido con el método de rayos cósmicos pueden ser utilizados para la modelación de flujo variablemente saturado y para la determinación de parámetros hidráulicos del suelo; y (d) el método de rayos cósmicos puede ser usado para el monitoreo a largo plazo y en estudios de balances hídricos.

Chapter 1

Introduction

1.1. Motivation

1.1.1. Importance of soil moisture measurements

Soil moisture is a key state variable for understanding major hydrological processes involved in a variety of natural processes such as geomorphic, climatic, ecological, etc. that act at different spatio-temporal scales (Entin et al., 2000; Pan and Wang, 2009). Soil moisture is arguably the most important state variable that controls near-surface hydrologic and energy balance variability (Western et al., 2002; Western et al., 2004). Agricultural and irrigation management practices, especially in semi-arid and arid zones, depend on accurate quantifications in time and space of soil moisture at the root zone (Vereecken et al., 2008). Therefore, there is a direct impact of soil moisture on the production and health status of crops and soil salinization.

From the regional to global scales, soil moisture plays an important role on controlling the exchange and partitioning of water and energy fluxes at the land surface. The coupling that takes place between soil moisture and the atmosphere can have profound impacts on the planet's climate systems (Seneviratne et al., 2010).

In hydrological studies, soil moisture is a critical component to control the partitioning between infiltration and run-off (Graeff et al., 2009). Infiltration amount determines the amount of water available for vegetation growth and possible deep percolation to the aquifer. Runoff has a strong impact on the rate of surface erosion and river processes. In combination with hydrological and climatological processes, soil moisture can impact many environmental phenomena from extreme events like droughts and flooding to state patterns such as the ecological distribution of homogeneous vegetation zones (Kornelsen and Coulibaly, 2013). Despite the many advantages that can

be derived from the knowledge of soil moisture distribution, measurement of soil moisture at the field or small catchment scale remains difficult and unclear. This is largely due to the difficulty and cost associated with obtaining spatially representative in situ soil moisture measurements by point scale sampling. In the following sections, literature is presented to review the controlling factors of soil moisture and measurement techniques along the scales.

1.1.2. Controlling factors of soil moisture at different scales

The large spatial and temporal variability of soil moisture is determined by different factors such as atmospheric forcing, topography, soil properties, and vegetation. All of these interact in a complex and non-linear manner (Western et al., 2004). Studying scales of soil moisture variation is very important for understanding many aspects of weather and mesoscale phenomena and for climate change. For instance, climate modelling requires prior information of the autocorrelation lengths in order to define the size of spatial grids and time steps. Moreover, the analysis of scales shows how much soil moisture varies due to small-scale processes (short-term influences) and large-scale processes (long-term influences) (Entin et al., 2000). The variation of soil moisture in time or space can be expressed by two different components, (i) a small scale influenced by land-surface components and (ii) a large scale influenced by atmospheric components. The land-surface components affect soil infiltration and water holding capacity in a specific location (e.g. field-scale variability of soil hydraulic properties). The atmospheric components modify soil moisture through the precipitation and through the evaporative demand. Such regime of fluxes depends on temperature, radiation, humidity and wind speed in a specific region (Entin et al., 2000). The small scale shows differences in soil moisture by different local soils, topography, root structure and vegetation. This scale is of the order of a few days, temporally, and tens of meters, spatially. In the case of large scale, this is of the order of months and hundreds of kilometres (Entin et al., 2000). The measurement and modelling scales of soil moisture consist of a scale triplet expressed as function of spacing, extent and support (Blöschl and Sivapalan, 1995). The "spacing" refers to the distance between samples or model elements; "extent" refers to the overall coverage; and "support' refers to the integration volume or area (Western and Blöschl, 1999). For example, for a transect of FDR (Frequency Domain Reflectometry) sensors located at 5 cm depth, the scale triplet may be defined as 10 m spacing (distance between measurement points), 150 m

extent (i.e. total length of transect) and 6 cm support (i.e. length of FDR sensor rods). Beside the measurement scale, the scale of the natural variability is termed as "process scale" (Blöschl and Sivapalan, 1995) and relates to whether the natural variability is small-scale variability or large-scale variability (Western and Blöschl, 1999). This last point deals with the spatial organization of soil moisture in the environment (Famiglietti et al., 2008; Vivoni et al., 2010; Gaur and Mohanty, 2013; Graham Milledge et al., 2013). Soil moisture is often topographically organized with connected bands of high soil moisture in the depression zones of a catchment and near the streams. Especially at the catchment scale, these patterns are often quantified with topography index (Western and Blöschl, 1999; Pellenq et al., 2003; Lane et al., 2009; Graham Milledge et al., 2013). In others cases, soil moisture patterns are fractal (Rodriguez-Iturbe et al., 1995; Giménez et al., 1997), soil- and rock-dependent (Blöschl and Sivapalan, 1995; Onda et al., 2006), landscape dominated (Venkatesh et al., 2011), or vegetation dependent (Geoff Wang, 2000; Graham Milledge et al., 2013). Especially, the relation between vegetation patters and soil moisture variability has been rarely explored by hydrologist. However, Graham Milledge et al. (2013) pointed out the large potential of using remote sensing images to identify vegetation patterns and resolve spatial soil moisture patters at a resolution sufficient to characterize its fine scale spatial variability. Moreover, it is clear that the influence of a specific pattern to soil moisture variability is likely to depend on the relevant hydrological processes in a specific location and its climatic, and topographical properties (Tetzlaff et al., 2008).

1.2. Different measurement techniques for quantifying soil moisture

Soil moisture is a key state variable and varies substantially in support scale (or volume). From our current capabilities (Robinson et al., 2008), soil moisture is measured from the point scale to global scale by using different physical properties such as thermogravimetric measurement, neutron thermalization, electrical conductivity, dielectric properties and soil thermal properties. In last years a number of experimental techniques and equipment have been developed that allow measurements of soil moisture in different spatio-temporal scales, some techniques for field estimation of soil moisture are briefly reviewed:

1.2. DIFFERENT MEASUREMENT TECHNIQUES FOR QUANTIFYING SOIL MOISTURE

a. Point measurements

Surely within all measurement techniques at the point scale, Time Domain Reflectometry (TDR) and Frequency Domain Reflectometry (FDR) have become very popular and well recognized in the scientific community. The high spatial resolution of field soil moisture can be achieved increasing number of sensors; however, this is limited to cost of devices. The TDR approach is based on the travel time analysis of a defined pulse along a wave guide (Ponizovsky et al., 1999; Greco, 2006; Moret et al., 2006; Greco and Guida, 2008; Calamita et al., 2012). This travel time measured by the TDR sensor is related to soil bulk dielectric constant, which is a function of soil moisture, porosity, soil salinity, clay content, and among others. There are well established equations to relate soil moisture and soil bulk dielectric constant (Topp et al., 1980). Further applications have considered retrieval of soil moisture profiles along the TDR wave guide by special inversion algorithms (Graeff et al., 2010). The FDR approach determines the soil permittivity by measuring the frequency changes induced by a changing value of the soil permeated by the fringing fields of the capacitor sensor (Baumhardt et al., 2000).

The accuracy for soil moisture measurement with TDR and FDR approaches depends on the probe calibration. Calibration can be carried out for specific soil conditions (Ponizovsky et al., 1999; Lesmes and Friedman, 2005), by (i) extracting soil samples from the field and reproducing different moisture contents in the laboratory, or by (ii) measuring sensor output at a specific time in the field and compare it with ground-truth values (e.g. soil cores). Additionally, a sensor calibration can be carried out by relating sensor output with different permittivity constants (e.g. water, ice, acetone, etc.).

b. Geophysical methods

Geophysical methods provide an opportunity to estimate field soil moisture in a non-invasive or minimal-invasive form (Robinson et al., 2008). Some of these techniques for observing spatial variability of soil moisture at the field scale are described below:

Ground Penetrating Radar (GPR)

The GPR is an electromagnetic method that uses the transmission and reflection of high-frequency (1 MHz - 1 GHz) electromagnetic waves within the subsurface (Huisman et al., 2003). The measurements provide information about the permittivity of subsurface materials; because of the link between permittivity and soil moisture (Davis and Annan, 1989). Huisman et al. (2001) and Grote et al. (2010) showed how GPR ground wave data could

be used effectively to map near surface changes of soil moisture. The GPR performance is optimal in a soil with a coarse texture, but the performance decreases in electrically conductive media such clayey soils (Michot et al., 2003). The depth of investigation can be sub-meter to tens of meters or even greater in resistive materials. The determination of soil moisture based on GPR method has been evaluated by different approaches such as off-set profiling (Lunt et al., 2005), estimation of ground-wave velocity (Hubbard et al., 2002), common midpoint measurements (Greaves et al., 1996), and surface reflectivity (Serbin and Or, 2004).

Electromagnetic Induction (EMI)
The EMI method is one of the more promising technologies for determination of soil properties and soil moisture (Robinson et al., 2008). The instrument measures the ground conductivity. The penetration depth of the EMI method depends on the conductivity of the soil, penetration depth reducing slightly as the soil becomes more conductive (Callegary et al., 2007). Brevik et al. (2006) observed a maximum depth of 0.9 m. Some examples of using EMI for soil moisture measurements are Scanlon et al. (1999); Reedy and Scanlon, (2003); Martínez et al. (2010), and among others. The major difficulty of this approach is interpreting the signal and its causes. One approach has been to try to calibrate the signal response using directed soil sampling based on the signal response surface and using a multiple linear regression (Lesch et al., 1995a; b). An alternative approach might be to use the instrument to assess changes in ground conductivity before and after rainfall events (Robinson et al., 2008).

Electric Resistivity Tomography (ERT)
The ERT method is very sensitive to subsurface changes in soil moisture and pore water salinity (Daily et al., 2004). The method is potentially able to provide realistic spatial characterization in several hydrological context such as unsaturated water flow (Daily et al., 1992), snow melting (French and Binley, 2004), saline tracer monitoring (Slater et al., 2000), groundwater studies (Barker and Moore, 1998), solute transport monitoring (Binley et al., 1996), carbon sequestration (Breen et al., 2012), permafrost identification (You et al., 2013), etc. ERT could provide a continuous image of the main hydrological processes occurring within the soil by integrating information on large volume, and subsequently defining a conceptual hydrological model (Travelletti et al., 2012). The resistivity values are not directly measured from surface-based ERT surveys. Electrode spacing, electrical current intensity and electrical potential are the measured parameters used to calculate the apparent resistivity values which are subsequently inverted to estimate the

true resistivity values (Samouélian et al., 2005; Rings and Hauck, 2009). For
the temporal monitoring of water infiltration, differences between resistivity
measurements are more accurate than absolute values (Samouélian et al.,
2005). Resistivity anomalies are often calculated in relation to the resistivity
at the initial state (Travelletti et al., 2012).

d. Distributed Temperature Sensing (DTS)

Distributed temperature sensing using fiber optic cables has the potential
to monitor soil moisture at high temporal resolutions (0.10 Hz) and at high
spatial resolution ($\leq$ 1 m). For a given soil, thermal conductivity varies
as a function of the ambient temperature and soil moisture. Under normal
environmental conditions, these variations of thermal conductivity can be
mainly related to changes of soil moisture (Olmanson and Ochsner, 2006).
The method could monitor soil moisture along cables exceeding 10 km in
extent (Sayde et al., 2010; Steele-Dunne et al., 2010) with spatial resolutions
as fine as 1 m (Selker et al., 2006). For instance, buried DTS fiber optic ca-
bles at multiple shallow depths were used to passively monitor soil moisture
through near-surface soil temperature fluctuations due to diurnal radiative
heating (Krzeminska et al., 2012). Some difficulties of DTS method arise in
(i) placing the cables at consistent depths and spacing to accurately calcu-
late soil moisture and (ii) monitoring diurnal soil temperature fluctuations
at depth because dense canopy and cloud cover limit induced temperature
variation. Another major disadvantage of DTS method is the strongly inva-
sive installation.

e. Global Positioning System (GPS)

For typical applications of GPS, reflected signals are considered a source of
error (Braun et al., 2001; Larson et al., 2007), rather than useful information.
This phenomenon is referred to the multi-path of the reflected signal, which
travels more than one way before reception. Larson et al. (2008) related the
GPS "error" signal to fluctuations of near-surface soil moisture. This is due
to GPS receivers gather energy from ground reflections in addition to the
direct signal that travels between the GPS satellite and receiving antenna.
The characteristics of the reflected signal change as soil moisture, and there-
fore the dielectric constant of the ground varies. GPS-derived soil moisture
represents an area approximately of 300 m^2 (Larson et al., 2008). The GPS
signals are L-band, thus GPS receivers are an optimal in-situ data source to
combine with future satellite measurements. The major advantage of this
approach is to make use of existing GPS instrumentation ($>$ 5000) installed
on the Earth's surface for other purposes. Therefore, GPS products become
a promising technique for near-real time estimates of soil moisture for hy-

drology, climate and ecology studies. Nevertheless, GPS method presents two major disadvantages (i) signal reflections may be affected by vegetation covers and (ii) soil moisture can be overestimated in periods following precipitation events (Larson et al., 2008; Larson et al., 2010).

g. Wireless sensor networks

The wireless sensor network technology allows real-time soil moisture monitoring at unprecedented spatial and temporal resolution for observing hydrological processes in small watersheds (0.1-80 km^2). Such a network can be linked to an automated rain gauge and the sampling frequency could be increased during precipitation events to allow high temporal resolution during the event (Bogena et al., 2007; Bogena et al., 2010). The high spatial resolution of field soil moisture can be achieved by increasing number of sensors; however, this is limited to high cost of devices. The major disadvantage of this approach is its disturbance of natural soil conditions during sensor installation. Moreover, extensive sensor network is impractical for monitoring inside agricultural fields, where farmer activities (e.g. ploughing) are continuously carried out.

h. Remote sensing of soil moisture

Remote sensing of soil moisture is a completely non-invasive technique. Spatio-temporal variability of soil moisture is inferred through the soil's influence on electric, magnetic and gravitational fields. Three major groups cover the remote sensing techniques for soil moisture. The first two are related either to the electromagnetic radiation naturally emitted by the target (passive remote sensing) or the radiation scattered by the target after this has been irradiated (active remote sensing). The third group is related to the gravity potential field above the soil (Robinson et al., 2008).

The support scale of remote sensing products depends on the measurement sensor. For instance, the active remote sensing ASAR/ENVISAT has a very high resolution of about 12.5 x 12.5 m for soil moisture mapping (Baup et al., 2007a; Baup et al., 2007b; Zribi et al., 2007). Passive devices such as AMSR-E and SMOS have a coarse resolution between 5 km and 70 km (Merlin et al., 2008; Albergel et al., 2010; Albergel et al., 2012; Collow et al., 2012).

The temporal resolution, especially in airborne sensors, is quite limited. For instance, SMOS overpasses twice per day. ENVISAT with the ASAR radar offers repetitiveness of measurements less than 5 days compared to 35 days for ERS/SAR (Zribi et al., 2009). Therefore, this temporal limitation hinders the comparison remotely-sensed soil moisture with other techniques.

The drawback of these techniques is its limitation of penetration depth,

i.e. up to 5 cm in optimal conditions (Albergel et al., 2010; Albergel et al., 2012), and signal attenuation due to surface roughness, distribution of soil moisture in depth, soil temperature and vegetation cover (Fernández-Gálvez, 2008; Hajnsek et al., 2009; Koyama et al., 2010).

At the global scale, GRACE (Gravity Recovery and Climate Experiment) mission provides monthly measurements of the Earth's gravity field (Tapley et al., 2004). The dominant GRACE signal reflects changes in vertically integrated stored water, including variations from snow pack, glaciated areas, surface water, soil moisture, and groundwater at all depths (Lettenmaier and Famiglietti, 2006; Ramillien et al., 2006; Güntner, 2008; Grippa et al., 2011). In this manner, GRACE data clearly differs to other remote-sensed products observed at the near-surface depth. The disaggregation of any water compartment observed by GRACE requires modelling approaches and/or observation of other water compartments (Werth et al., 2009; Wziontek et al., 2009). Among others, some examples of soil moisture and groundwater retrieval with GRACE are Leblanc et al. (2009); Rodell et al. (2009); Tiwari et al. (2009); among others.

1.3. Filling gap at the intermediate scale: Gravimeter vs. Cosmic-ray neutron probe

From brief literature review above as well in Robinson et al., (2008) and Vereecken et al. (2008), current measurement capabilities of field soil moisture reveal a gap at the intermediate scale between point-observation scale and remote sensing scale. To overcome these limitations, two techniques are being currently investigated high-precision gravimeter (Superconductive Gravimeters, SG) and cosmic-ray neutron probes. These two measuring approaches provides an integral observation within its support volume of water storage.

Gravimeter measurements are influenced by water storage due to the Newtonian attraction of masses. The major sources of temporal gravity variations are the tides of the solid Earth, ocean tide loading, changes in the atmosphere and polar motion. The variations of water mass from the hydrology part are considered as noise. Measurements of gravity are frequently expressed in Gal units (1 cm s^2). High-precision gravimeters measure with a resolution of 0.01 μGal (Van Camp et al., 2005). Gravity measurements can be used to determine temporal changes in the mass of a conceptual col-

umn of water in the near surface and subsurface (Creutzfeldt et al., 2010a; Creutzfeldt et al., 2010b). The SG measurements are influenced by large and local water storage changes (WSC). The large-scale effect is generated in a zone with a radius of 200 km to 10,000 km around the SG and may amount to a few μGal. The local-scale hydrology effect may amount to 14 μGal (e.g. Wettzell's case in Germany, Creutzfeldt et al., 2010a; Creutzfeldt et al., 2010b), where 52 μGal corresponds to 1 m of water mass change. The gravity response of different WSC was calculated at the German Wettzell site for a square with a side length of 4 km (Creutzfeldt et al., 2008). The disadvantage as well as the advantage of gravity measurements is their integrative nature. It makes gravity observations difficult to interpret, and therefore, extreme caution should be applied when interpreting a gravity signal for hydrological studies, if a single water storage is studied. For instance, a groundwater table rise of 4 m from 10 m to 6 m below surface in a aquifer with specific yield of 11 %, results in a gravity change of $\sim$ 22 μGal. A soil moisture change of only 7 % causes a gravity response of 17 $\pm$ 10 μGal. Vegetation water may cause a change up to 0.07 μGal. Snow contribution to gravity measurements could be positive or negative in respect to location of SG building (Creutzfeldt et al., 2008).

The major limitation of the high-precision gravimeters are (i) its elevated costs (Robinson et al., 2008), (ii) low mobility (i.e. need of a building), (iii) high influence from surrounding local conditions, (iv) high fluctuable radius of influence (i.e. gravity is not only a function of distance of mass changes, but also depends on topography and distribution of water mass over depth), and (v) large contribution from groundwater storage, therefore it hinders to derive measurements of soil moisture only.

Cosmic-ray neutron sensing (Zreda et al., 2008; Desilets et al., 2010; Rivera Villarreyes et al., 2011; Franz et al., 2012b; Zreda et al., 2012; Franz et al., 2013; Rivera Villarreyes et al., 2013a) provide a great opportunity to cover the measuring gap between point-scale observations and remote-sensing observations. The physical basis of the method is the crucial role of hydrogen for the moderation of natural neutrons (fast neutrons), product of cosmic radiation. The measurement footprint is a diameter approximately of 600 m with a penetration depth (few decimetres) depending on the soil moisture level (Franz et al., 2012). Value of footprint is well accepted so far, although it is needed a verification for hill-slope sites. Fast neutrons are moderated for any kind of hydrogen allocated on the air-ground interface, therefore in principle, the cosmic-ray neutron sensing is able to observe any kind of hydrogen pool. Since penetration depth fluctuates between 12 and 70 cm only, method is not influenced by groundwater in major cases. Contrarily

to the gravimeter which vegetation water storage is negligible to other compartments, the cosmic-ray method highly observes crop water content. The signal disaggregation of the cosmic-ray neutron sensing on different water compartments is feasible (Franz et al., 2003).

Major advantage of the cosmic-ray neutron sensing is that methodology is straightforward and practical. The probe can be used stationary or in a mobile manner (i.e. rover set-up). Single field calibrations are needed to convert fast neutrons to soil moisture amounts for long-term monitoring (Zreda et al., 2012).

For feasible measurement of soil moisture at the intermediate scale, in order to fill measuring gap between point scale and remote sensing, the cosmic-ray neutron method provides best capabilities compared to gravimeter approach. This dissertation is focused on the development and test this methodology for field applications. A deep literature review is provided in following section of introduction as well as in the chapters.

1.4.   Major research objectives and research direction

From short literature review presented in previous section, as well as in (Robinson et al., 2008), there is a measurement gap of field soil moisture between local scale (point observations) and remote sensing scale. This gap mainly covers the horizontal extent of an agricultural field or small catchment, and the vertical extension of the root zone. The main objective of this dissertation is to investigate a recently-introduced approach, cosmic-ray neutron sensing (Zreda et al., 2008; Desilets et al., 2010; Rivera Villarreyes et al., 2011; 2013a), which is able to cover this measurement gap at the intermediate scale. The applicability of the cosmic-ray neutron sensing for hydrological applications is mainly verified with long-term field monitoring at two experimental sites (cf. 1.3.3). The main research objectives are:

a. To evaluate the use of the cosmic-ray neutron sensing for soil moisture measurements in cropped fields
This objective tries to cover the need of research on testing the cosmic-ray neutron sensing in cropped fields. Previous studies (Zreda et al., 2008; Desilets et al., 2010) have mainly focused on the evaluation of the cosmic-ray neutron sensing in semi-arid landscapes in absence of agricultural crops. Therefore, here crop influence is irrelevant or can be considered as a con-

stant effect (Franz et al., 2013). However, high fluctuation of biomass water content and other crop characteristics may impose an additional uncertainty to the cosmic-ray neutron sensing approach. In this dissertation, it is also intended to identify major disadvantages of using the cosmic-ray neutron sensing on cropped fields (e.g. how large is the soil moisture deviation from the ground-truth soil moisture during the growing season).

b. To test new calibration approaches and vegetation corrections for using the cosmic-ray neutron sensing in cropped fields
Complementing the previous objective, it is clear that a stable and accurate calibration approach is needed for optimal measurements of soil moisture via the cosmic-ray neutron sensing. Since the methodology is influenced by any kind of water storage inside its support volume, the question of calibration clearly arrives. Which parameters are the most suitable for calibration? In which temporal scale, calibration period, should this process carried out? When is the best time to calibrate this approach, initial season with low water contribution from crop or middle season when crop reaches its maximum development? The answer of all these questions is not straightforward because it may depend on crop type and its characteristics, field conditions, etc. Moreover, here I also intend to answer the question if it is possible to provide a simple, but robust time-variable vegetation correction to account for crop influence on the cosmic-ray signal.

c. To test applicability of the cosmic-ray neutron sensing for soil hydrological modelling
The cosmic-ray neutron sensing provides an integral observation of soil water storage in its entire support volume (few hectares in horizontal direction and decimetres in vertical direction). Therefore, it is an adequate compartment size for large model parametrization. However, first it is needed to validate effective model parameters at the cosmic-ray support volume with parameters inside such volume. The research question in this section is oriented in the following objectives:

- Implementation of the cosmic-ray neutron sensing for modelling of soil water fluxes.

- Verification of effective soil hydraulic properties derived with integral observations of soil water storage from cosmic-ray neutron sensing in respect to inside-volume local soil properties.

d. To investigate the benefits of using cosmic-ray neutron sensing at the small catchment scale

The fact that the natural neutrons may be influenced by several water storing environmental compartments such as soil moisture, biomass water, snow, intercepted water, etc. (cf. section 1.3) at the intermediate measuring scale, methodology provides a great opportunity to investigate two major hydrological state variables at the catchment scale: soil moisture and snow water equivalent. Here, I present the benefits of using a single device for measurements of soil moisture and snow water equivalent depending on the season at the Schaefertal catchment in Germany. Moreover, the methodology approach is oriented to test the cosmic-ray neutron sensing in a remote-sensing manner. The device is calibrated once and operates continuously for a long-term period, using ancillary data to test sporadically the cosmic-ray signal. The specific objectives of this section are:

- Use of cosmic-ray neutron sensing as a monitoring network for integral measurements of soil and snow water storage

- Investigate benefits on using the cosmic-ray neutron signal for monitoring of snow water equivalent and identify which energy level (thermal neutrons, fast neutrons or a combination) is best suitable for this purpose

1.5. COsmic-ray Soil Moisture Observing System (COSMOS)

The COsmic-ray Soil Moisture Observing System (COSMOS, http://cosmos.hwr.arizona.edu/), funded by the US National Science Foundation in 2009 (Zreda et al., 2012), comprises 48 cosmic-ray neutron probes installed at sites through the USA and five abroad. The network is planned to grow up to 500 probes. Each COSMOS probe has two neutron detectors to measure both fast neutrons and thermal neutrons. Probes are independent and can be installed anywhere with sufficient sky view for solar panels and Iridium reception.

The COSMOS is designed to improve the availability of continental-scale soil moisture measurements by ultimately deploying a network across the USA. Each probe will measure average soil water content within a diameter of a few hectometres and to a depth of a few decimetres without consideration of soil heterogeneity.

The cosmic-ray neutron probes at the COSMOS network were preferentially installed at sites where other meteorological and hydrological measurements are being made. The main idea of this data combination is to understand primarily the probe response to varying moisture amounts under different land-surface and ecohydrological processes, developing data assimilation techniques, calibrating and/ or validating satellite microwave sensors, and evaluating the soil moisture from weather and seasonal prediction.

Beside this dissertation, COSMOS network provides other peer-reviewed publications on the use of cosmic-ray neutrons for soil moisture measurements. A brief description of the state of the art is presented below chronologically, further discussion is included in next chapters.

- **Zreda et al., (2012)** Presentation and description of COSMOS network. Neutron corrections due to atmospheric pressure, incoming high-energy cosmic rays and water vapour pressure are defined.

- **Franz et al., (2012a)** Development of the effective sensor depth for the cosmic-ray neutron probe. The penetration depth or effective depth was evaluated based on neutron transport simulations. The effective depth was defined as the region of the soil profile where 86 % of the neutron counts aboveground are originated.

- **Franz et al., (2012b)** A field verification of the cosmic-ray soil moisture with a distributed sensor network. A field calibration of the cosmic-ray neutron probe was carried out at a site covered by a 24 % with slowly-changing vegetation, primarily composed of creosotebush, grasses, forbes, cacti and mesquite. The cosmic-ray soil moisture indicated underestimation of ground-truth from distributed sensor network, especially during infiltration process.

- **Franz et al., (2013)** The universal calibration function for the cosmic-ray neutron probe. Based on neutron transport simulations and measuring full chemistry at 40 COSMOS sites, a universal calibration function was developed in order to relate fast neutrons and hydrogen molecular fraction. This equation requires information from hydrogen pools existing at the atmosphere, soil moisture, lattice water, soil organic carbon, and above- and below-ground vegetation. This study has only covered cases in forests assuming a constant value of aboveground biomass and constant ratio fresh mass to dry mass.

- **Chrisman and Zreda (2013)** Quantifying mesoscale soil moisture with the cosmic-ray rover. Soil moisture mapping within a footprint

of 25 km x 40 km, equivalent to footprint of SMOS footprint, was surveyed in Arizona basin by using the cosmic-ray rover. A cosmic-ray neutron probe was mounted on car and mesoscale soil moisture was sampled approximately at the monthly resolution. Moreover, soil moisture profiles were derived by combining rover data with surface soil moisture from satellite microwave sensors. Finally, evapotranspiration was computed from basin-wide water balance using interpolated soil moisture and soil moisture profile estimates.

1.6. Experimental approach

1.6.1. Origin of natural cosmic-ray neutrons

Natural fast neutrons, named as well albedo neutrons (Kodama, 1984) or ground albedo neutrons (Rivera Villarreyes et al., 2011), originated from cosmic radiation are inversely correlated to the hydrogen content at the ground-air interface. This natural cosmic radiation is mainly divided in primary cosmic rays, originated from the space, and secondary cosmic rays, generated by the interactions of primary cosmic rays with atmospheric particles. Therefore, fast neutrons depend on the temporal and spatial variability of both primary and secondary cosmic radiation.

Primary cosmic rays, mainly formed by protons, originate from the space (galactic cosmic rays) and the sun (solar cosmic rays). Galactic cosmic rays occur in a permanent form compared to solar cosmic rays that are sporadic and individual events. In general, primary cosmic rays correspond to particles with energy up to 1020 eV and are temporally variable due to the solar modulation.

The outer atmosphere of the sun, the solar corona, is in continuous hydrodynamical expansion, producing a flow of plasma known as the solar wind (Parker, 1965). A magnetic field is frozen into this plasma and is dragged radially outward from the sun. The charged extrasolar cosmic rays particles are strongly influenced by this magnetic field as they penetrate from the outside into the heliosphere (Schlichkeiser, 2002). Cosmic ray intensity in the inner solar system is lowest when the solar activity, as measured by the sunspot number, is highest (Forbush, 1954).

Additionally, primary cosmic rays have a spatial variability at the global scale, because partly these particles are deflected at the top atmosphere by Earth's magnetic field. At certain locations on the Earth, the magnetic field provides an effective shield against cosmic ray particles (Heinrich et al., 1999).

In the atmosphere, the primary cosmic ray particles collide with the atoms

of the air. They lose energy in ionization interactions with air atoms and thus are slowed down continuously. This energy is spent on the production of new particles like protons, neutrons, and mesons named as secondary cosmic rays (Lal and Peters, 1967). The target nuclei may produce protons, neutrons and alpha particles by evaporation, which have typical energies below 10 MeV. High-energy neutrons continue travelling through the atmosphere and they can be absorbed or moderated in their way, thus creating neutrons with lower energies. This collision process depends strongly on the atmospheric column and its composition (Phillips et al., 2001). Therefore, secondary neutrons are generally classified according to their energy level (Krane, 1988) such as thermal neutrons (~ 0.025 eV), epithermal neutrons (~ 1 eV), slow neutrons (~ 1 keV) and fast neutrons (~ 100 keV $- 10$ MeV). These neutrons continue travelling until they penetrate the soil porous media and collide with soil nuclei and hydrogen nuclei (soil moisture), or in the snow pack mainly with hydrogen. At the end, some neutrons are able to leave their containing medium (e.g. soil or snow) with a decrease of energy and others are completely absorbed.

In the soil, hydrogen is far the best neutron moderator compared to other atoms. This moderation is due to its large neutron scattering cross section (Sears, 1992) and higher stopping power (Krane, 1988). Therefore, this allows a passive and indirect estimation of soil moisture from natural neutrons. From the different types of natural neutrons, those at the fast energy level present the better estimation of soil moisture (Zreda et al., 2008). From neutron transport simulations, Zreda et al. (2008) found out that neutrons at the thermal level are not very sensitive to changes of soil moisture (i.e. only 2-3 % neutron variability by high changes of soil moisture) and sensitive to different soil minerals. By using commercial devices placed aboveground, named cosmic-ray neutron probes, Zreda et al. (2008) and Desilets et al. (2010) showed the first intent to measure field soil moisture by quantifying fast neutron backscattered to the atmosphere. However, their approach was a modification of the original version from Kodama (1984), who quantified the relation between soil moisture and natural neutrons with a detector located below-ground. The cosmic-ray sensor has a footprint of approximately 600 m diameter (Zreda et al., 2008) and penetration depth depending on soil moisture (Franz et al., 2012), which fluctuates from 12 cm down to 70 cm (silica sandy soil without lattice water). The mathematical equation for relating fast neutrons and soil moisture (or snow water equivalent or total water content) is described in detail in next chapters.

1.6.2.   Neutron corrections

Prior to any computation of CRS water content, neutron counts have to be corrected by local changes of atmospheric pressure, water vapour and incoming high-energy cosmic radiation. Corrections of atmospheric pressure are the most important of the three mentioned above. Local changes of pressure produces an important neutron attenuation. The moderation of a neutron which travels through the atmospheric column is controlled mainly by the mass attenuation for high-energy neutrons. This parameter is typically expressed in nuclear physics with units of $g\,cm^{-2}$ and varies between ~ 128 $g\,cm^{-2}$ at high altitudes and 142 $g\,cm^{-2}$ at the equator (Zreda et al., 2012). The effect of mass attenuation on cosmic ray neutrons has been deeply studied by Bachelet et al. (1965), who addressed effects of latitude, altitude and geomagnetic latitude (i.e. expressed as cut-off rigidity) on mass attenuation.

Neutron corrections due to incoming high-energy cosmic rays are based on observations from worldwide neutron monitoring stations http://www.nmdb.eu/nest/search.php. For example, the four most proximal stations to field sites in Germany (described in next chapters) are KIEL (Kiel, Germany), LMKS (Lomnickystit, Slovakia), JUNG (Jungfraujoch, Switzerland) and ROME (Rome, Italy). Time resolution in stations varies from minutes, days, months and years. Neutron counts in monitoring stations are corrected by pressure and efficiency of detector. Correction factor due to incoming radiation assumed that neutron measured in experimental sites are proportionally affected by changes of neutrons in a neutron monitor station.

The corrections by changes of atmospheric water vapour are computed from temperature and relative humidity records only (Rosolem et al., 2013). . A reference air density is defined (e.g. dry air or value at day of calibration).

Finally, all neutron corrections are taken into account as follows:

$$N_{cor} = N_{unc} \cdot \frac{f_p \cdot f_{wv}}{f_{in}} \tag{1.1}$$

where N_{unc} is the uncorrected neutron counts [cph], N_{cor} is the corrected neutron counts by atmospheric pressure (f_p), incoming radiation (f_{in}) and water vapour (f_{wv}) in cph.

1.7.   Structure of the dissertation

This dissertation is focused mainly on the use of cosmic-ray neutron sensing for soil moisture measurements at the intermediate scale and root zone.

In the last chapter, as complementary benefit of this approach, it is also presented an evaluation for monitoring of snow water equivalent. The research aims are mainly achieved with field monitoring in two experimental sites. The structure of this dissertation follows a cumulative form with original research articles developed during the doctorate study period. The dissertation is divided into six chapters, brief description of next chapters is:

Chapter 2 Integral quantification of seasonal soil moisture changes in farmland by cosmic-ray neutrons (Rivera Villarreyes et al., 2011)
The study presents the first monitoring period of cosmic-ray fast neutrons at an agricultural field (Bornim). New methodology was evaluated and compared against a network of FDR soil moisture sensors located at near-surface for a summer period with corn crop and a later autumn-winter period without crop and a longer period of snow cover in 2010 and 2011. Here it will be presented a calibration approach using ground-truth soil moisture at 5 cm depth only. Moreover, influence of snow cover on soil moisture via cosmic-ray neutron sensing is also discussed.

Chapter 3 Calibration approaches of cosmic-ray neutron sensing for soil moisture measurement in cropped fields (Rivera Villarreyes et al., 2013a)
This study continues the evaluation of the cosmic-ray neutron sensing for soil moisture in cropped fields. Measurements of cosmic-ray neutrons (fast neutrons) were performed at farmland Bornim cropped with sunflower and winter rye in 2011 and 2012. Three field calibration approaches and four different ways of integration the soil moisture profile to an integral value for cosmic-ray neutron sensing were tested. Calibration variability is identified by choosing different calibration periods along the growing season. Using crop height as simple proxy, deviation of cosmic-ray soil moisture is related to crop development. Finally, an approach for correcting neutrons due to vegetation is presented.

Chapter 4 Inverse modelling of cosmic-ray soil moisture for field-scale soil hydraulic parameters (Rivera Villarreyes et al., 2013b)
Here it is presented the first application of cosmic-ray neutron sensing in hydrological modelling. The objective is to investigate the inverse modelling of soil moisture measurements via the cosmic-ray neutron sensing in order to estimate soil hydraulic properties at the field scale and root zone. Field measurement used for inverse simulations corresponded to sunflower period in Bornim (cf. Chapter 3). HYDRUS-1D model was used to simulate soil water dynamics and its automatic calibration was carried out with PEST

(Parameter Estimation Software). Effective parameters at the field scale were compared against local measurements and other inversely estimated soil parameters from independent FDR soil moisture profiles.

Chapter 5 The benefits of the cosmic-ray neutron sensing for measuring integral soil and snow water storages at the small catchment scale
Four cosmic-ray sensors were implemented to monitor fast and thermal neutrons in Schaefertal catchment. The cosmic-ray neutron sensor was used in a strictly remote-sensing manner with a single day calibration and use of ancillary data (e.g. weather station) for signal verification. Analysis of temporal variability of soil moisture at the CRS scale is performed. The response of the CRS signal (thermal neutrons and fast neutrons) and CRS penetration depth is evaluated for snow periods. Finally, CRS snow water equivalent is derived using the so-called universal calibration function. This study proves the applicability and benefits of the cosmic-ray neutron sensing in a small catchment.

Chapter 6 General discussion and final conclusions
This section covers the overall discussion from the previous chapters and final conclusions of this dissertation.

Chapter 2

Integral quantification of seasonal soil moisture changes in farmland by cosmic-ray neutrons

Abstract

Soil moisture at the plot or hill-slope scale is an important link between local vadose zone hydrology and catchment hydrology. However, so far only a few methods are on the way to close this gap between point measurements and remote sensing. One new measurement methodology that could determine integral soil moisture at this scale is the aboveground sensing of cosmic-ray neutrons, more precisely of ground albedo neutrons. The present study performed ground albedo neutron sensing (GANS) at an agricultural field in northern Germany. To test the method it was accompanied by other soil moisture measurements for a summer period with corn crops growing on the field and a later autumn-winter period without crops and a longer period of snow cover. Additionally, meteorological data and aboveground crop biomass were included in the evaluation. Hourly values of ground albedo neutron sensing showed a high statistical variability. Six-hourly values corresponded well with classical soil moisture measurements, after calibration based on one reference dry period and three wet periods of a few days each. Crop biomass seemed to influence the measurements only to minor degree, opposed to snow cover which has a more substantial impact on the measurements. The latter could be quantitatively related to a newly introduced field neutron ratio estimated from neutron counting rates of two energy ranges. Overall,

our study outlines a procedure to apply the ground albedo neutron sensing method based on devices now commercially available, without the need for accompanying numerical simulations and suited for longer monitoring periods after initial calibration.

2.1. Introduction

Soil moisture plays an important role in the hydrological cycle. It influences climate and weather (Wu and Dickinson, 2004), and also determines surface runoff after precipitation events and controls groundwater recharge. In addition, soil moisture is a key factor for chemistry, biology, infiltration and matter transport processes in soil, e.g. it provides the main storage of water available for vegetation (Robinson et al., 2008). Despite the importance of soil moisture, its representative measurement is still a big challenge in hydrological research. Observation techniques of soil moisture have improved at various scales. Measurements of soil moisture at the point-scale ($\sim$1 dm^3) have advanced significantly in the last decades for a wide range of sensors. These are usually the basis for calculation of water storage and its changes at the field scale (up to 1 km^2). Point measurements are scaled up to large areas applying geostatistical techniques (Western et al., 2002; Bogena et al., 2010). However, inherent small-scale soil heterogeneities and non-linearity of processes dominate spatial and temporal variability of soil moisture and introduce sources of error that can produce significant misinterpretation of hydrological scenarios and unrealistic predictions. At the basin scale (2500–25 000 km^2), remote sensing technology, both active and passive, has demonstrated the potential to map and monitor surface soil moisture changes over large areas at regular intervals in time (Barrett et al., 2009). Satellites with L-band radiometers, e.g. SMOS (Kerr et al., 2001), and the planned SMAP mission (Entekhabi et al., 2010), or gravity change detection, GRACE (Tapley et al., 2004), provide a spaceborne Earth observation with opportunities to estimate soil water content at continental scale.

Although these techniques are promising, current measurement capabilities still do not cover the crucial need of hydrological observations corresponding to soil moisture in the root zone at the scale of a field, a small watershed scale or a hydrologic response unit. New measurement methodologies of soil moisture are investigated to obtain more information on this intermediate scale, e.g. spatial TDR soil moisture measurements (Graeff et al., 2010), ground penetrating radar (GPR) measurements (Huisman et al., 2003), electrical resistivity tomography (ERT) measurements (Garre et al., 2011), or ground-based microwave radiometry (Schwank et al., 2009). In

practice, these techniques are limited to the estimation of soil moisture at
the very surface, influenced by soil chemistry, hindered by vegetation cover,
and limited in temporal or spatial coverage. In general, there are either
invasive methods that can detect also deeper soil moisture, but in a point-
like manner, or non-invasive or remote sensing methods with high spatial
coverage but representing shallow soil only. Ground penetrating radar can
do a deeper assessment non-invasively, but it is costly and only an indirect
measurement.

Recently two novel methods were introduced that potentially can fill the
gap of soil moisture measurements at the field scale: (i) the cosmic-ray neu-
tron sensing method (Zreda et al., 2008), preferably called ground albedo
neutron sensing (GANS), and (ii) measuring water storage changes by a
high-precision gravimeter (Creutzfeldt et al., 2010a). While both are non-
invasive and detect water storage changes in a similar integration area, called
footprint or support scale, the gravimeter is less mobile and its measurement
includes also water stored in shallow groundwater (Christiansen et al., 2011;
Leirião et al., 2009); and thus an estimation of soil moisture itself is more com-
plicated. We will focus here on the ground albedo neutron sensing method,
which counts background neutrons generated in land surface materials by
secondary cosmic rays, following a terminology according to Kodama (1980)
and Kodama et al. (1985) instead of the name "cosmic-ray (neutron) sensing"
used by Zreda et al. (2008).

In earlier studies, Kodama (1984) described the possible applications of
measuring cosmic radiation for estimations of snow water equivalent and also
soil moisture by below-ground measurements (Kodama et al., 1985). At the
laboratory scale, Oswald et al. (2008) and Tumlinson et al. (2008) presented
an imaging technique (2-D and 3-D) based on a beam of low energy neutrons
to investigate water redistribution and plant water uptake of a single plant
in detail. Recently, using neutron transport simulations and field measure-
ments, Zreda et al. (2008) and Desilets et al. (2010) introduced a new method-
ology of soil moisture measurements via counting natural aboveground fast
neutrons, generated primarily by interactions of secondary cosmic-ray neu-
trons with terrestrial and atmospheric nuclei. These neutron intensities are
inversely correlated with soil moisture over an integration area, called foot-
print, with diameter of ca. 600 m (at sea level). The penetration depth of
the measurement of ground albedo neutrons, taken as the depth up to which
86 % (i.e. all but two e-folds) of the counted neutrons originate, ranges up to
few decimetres. The method is based on the crucial role of hydrogen as neu-
tron moderator due to its scattering cross-section of ca. 20 barns (Horsley,
1966) compared to others elements present in parents rocks (e.g. 2.167 barns
for Si, see Table 2.1) (Sears, 1992).

Neutrons at the air/ground interface are moderated by any chemical and physical form of hydrogen ^{1}H in or above soil surface, e.g. soil moisture, snow, intercepted water, biomass, and carbohydrates. Therefore, there is still an open question if the non-invasive ground albedo neutron sensing method is suitable to quantify water stored in different reservoirs at the field scale.

In this manuscript, we present a study of aboveground albedo neutrons for the estimation of soil moisture at an agricultural site in northern Germany. We quantified the relative influence of crop biomass during summer and investigated the impact of snow during winter. This study has been designed to

- extend the first applications of the GANS methodology, there called cosmic-ray (neutron) sensing, to a different geographical context,

- monitor ground albedo neutrons under two different vegetative situations (cropped field and bare soil) and different seasonal conditions (summer and winter),

- measure temporal variability of soil moisture at the ground/air interface and to evaluate the effective response of the ground albedo neutron method to hydrological events.

2.2. Materials and methods

2.2.1. Basis of the GANS method to detect soil moisture

Primary cosmic rays that hit the Earth consist mostly of charged protons. Partly these primary cosmic rays are deflected before the top atmosphere by Earth's magnetic field. Because of the spatial variability of Earth's magnetic field, e.g. with latitude, the intensity of high-energy cosmic rays varies in space. The incoming cosmic-ray intensity also varies with the solar activity (Parker, 1965). However, this variability will be neglected here because it is mainly a longer term modulation and is usually of the order of 1 % or less in amplitude (Kodama et al., 1985).

In the atmosphere, incoming protons generate a cascade of secondary cosmic rays as product of their collision with atmospheric nuclei (Lal and Peters, 1967). The intensity of this secondary cascade is related to how much air mass was encountered during the transit through the overlying atmosphere. Therefore, variations of air pressure affect the intensity of secondary cosmic ray fluxes at the near-surface atmosphere.

Table 2.1: Nuclear properties of major rock constituents: atomic number
(Z), atomic weight (A) in grams, total scattering cross section (σ_S), absorption cross section (σ_a) for $2200\,\mathrm{m\,s^{-1}}$ neutrons ($20\,^\circ\mathrm{C}$), average number of collisions (NC) required to reduce a neutron's energy from $2\,\mathrm{MeV}$ to $0.025\,\mathrm{eV}$ by elastic scattering, average logarithmic energy decrement per collision (ξ), and neutron stopping power (SP). Cross sections units in barn
(1 barn $= 10^{-24}\,\mathrm{cm^2}$) and values were extracted from Sears (1992). Calculations are based on equations presented in Rinard et al. (2009) and
Krane (1988)*.

Element	Z	A	σ_S	σ_a	NC	ξ	SP
H	1	1.00794	22.02**	0.3326	26	1.000	22.020
B	5	10.811	5.24	767	108	0.174	0.913
C	6	12.0107	5.551	0.0035	119	0.158	0.876
N	7	14.0067	11.51	1.9	137	0.136	1.569
O	8	15.9994	4.232	0.00019	155	0.120	0.508
Na	11	22.98987	3.28	0.53	219	0.085	0.277
Mg	12	24.305	3.71	0.063	230	0.080	0.297
Al	13	26.98154	1.503	0.231	255	0.072	0.109
Si	14	28.0855	2.167	0.171	265	0.070	0.151
Cl	17	35.453	16.8	33.5	332	0.055	0.930
K	19	39.0983	1.96	2.1	365	0.050	0.099
Ca	20	40.078	2.83	0.43	374	0.049	0.139
Mn	25	54.938	2.15	13.3	509	0.036	0.077
Fe	26	55.845	11.62	2.56	517	0.035	0.411
Ag	47	107.8682	4.99	63.3	991	0.018	0.092

* Information for other materials is presented in the auxiliary material mentioned in Zreda et al. (2008)
and available at: ftp://ftp.agu.org/apend/gl/2008gl035655/.
** See Horsley (1966) for values in different energies.

Once the secondary cascades of cosmic rays arrive at the ground level,
these collide with the land surface, where lower energy neutrons are created
as product of these new interactions between secondary cosmic rays and land
surface materials (soil, snow, plant canopies, etc.). Cosmic-ray neutrons in
the intermediate energy level (1–2 MeV), fast neutrons (Hess et al., 1961),
penetrate the soil. They are scattered and randomly distributed below- and
above-ground losing kinetic energy in the course of several successive collisions with nuclei in the soil, land surface cover and near-surface atmosphere,
while some are absorbed at some stage.

Hydrogen plays an important role on the moderation of neutrons. For
example, a fast neutron requires only 26 collisions with hydrogen nuclei to
decrease its energy from 2 MeV (fast level) to 0.025 eV (thermal level), com-

pared to other common elements such as C (119 collisions), O (155 collisions), N (137 collisions), Al (255 collisions), Si (265 collisions), etc. (Table 2.1). In conclusion, hydrogen in water molecules is the key factor to moderate these neutrons and thus the intensity of neutrons above the ground surface strongly depends on the water mass present in soil. This allows a non-invasive indirect measurement of soil moisture.

2.2.2. Quantitative soil moisture estimation by ground albedo neutron measurements

Ground albedo neutrons can be detected by special counters. They count events resulting from neutrons passing the detector during a preset integration period. Based on neutron transport modeling studies an equation was derived by Desilets et al. (2010, Appendix A, A1) that could be used to relate albedo neutron flux and soil moisture, as follows below. However, we specify here also the approach to normalize and correct the neutron counting rates, with the aim to ease the practical application of the method.

$$\theta = \left[\frac{a_o}{(N_R - a_1)} - a_2 \right] \cdot \rho_{\mathrm{b}}/\rho_{\mathrm{wat}} \tag{2.1}$$

where θ is the volumetric areal mean soil moisture $[\mathrm{m^3\,m^{-3}}]$, N_R is the normalized and pressure-corrected neutron counting rate $[-]$ (specified in Eq. 2.3), ρ_{b} is the mean bulk density $[\mathrm{kg\,m^{-3}}]$, ρ_{wat} is water density $[\mathrm{kg\,m^{-3}}]$, and a_i are fitting parameters $[-]$.

The intensity of secondary cosmic rays reaching the land surface fluctuates with changes in the mass density of the atmosphere, i.e. actually atmospheric pressure. Thus, neutron counting rates can be corrected by accounting for fluctuations of atmospheric pressure as follows (e.g. Bachelet et al., 1965):

$$N = N_{\mathrm{raw}} \cdot \exp\left[\beta\left(P - P_{\mathrm{mean}}\right)\right] \tag{2.2}$$

where N_{raw} is the value of ground albedo neutrons observed in a moderated counter and measured in a fixed time period, β is the atmospheric attenuation coefficient for ground albedo neutrons $[\mathrm{mbar^{-1}}]$, P is the local pressure corresponding to the period when N_{raw} was observed and P_{mean} is the long-term mean local pressure [mbar].

The integration period of ground albedo neutrons depends on the desired accuracy of soil moisture measurements. Events of neutron counting rates follow a Poisson distribution, which suggests that the standard deviation of neutrons counted in a fixed interval is equal to the square root of the total counts. The accuracy also depends on both detection efficiency and effective

volume of the detector (Kodama et al., 1985). The range of neutron counting
rates depends on several variables (e.g. site altitude, fluctuation of incoming
protons due to solar activity changes, and other types of moderation such
as biomass or open water bodies nearby), where site altitude usually is the
predominant one. Neutron counting rates are substantially lower in altitudes
at sea level than at mountain altitudes; therefore, GANS measurements of
soil moisture at lower altitudes require longer integration periods of neutron
counts.

Based on Eq. (2.2), the normalized and pressure-corrected neutron count-
ing rate (N_R) is defined as

$$N_R = \frac{N_{\mathrm{raw}} \cdot \exp\left[\beta\left(P - P_{\mathrm{mean}}\right)\right]}{N_{\mathrm{dry\_raw}} \cdot \exp\left[\beta\left(P_{\mathrm{dry}} - P_{\mathrm{mean}}\right)\right]} = \frac{N_{\mathrm{raw}}}{N_{\mathrm{dry\_raw}}} \cdot \exp\left[\beta\left(P - P_{\mathrm{dry}}\right)\right] \quad (2.3)$$

where $N_{\mathrm{dry\_raw}}$ is the number of ground albedo neutrons observed in a
moderated counter and measured under dry soil conditions and P_{dry} is the lo-
cal pressure corresponding to the dry condition when $N_{\mathrm{dry\_raw}}$ was observed.
The attenuation coefficient (β) for neutron fluctuations induced by local air
pressure was calculated from historical data of ground albedo neutrons and
air pressure from the most proximal station of the worldwide network of stan-
dardized neutron monitors in Kiel, Germany, located at $54.34°\,\mathrm{N}$, $10.12°\,\mathrm{E}$
and $54\,\mathrm{m\,a.s.l.}$ (see more below).

The dry condition state chosen to normalize the neutron counting rates
have an influence on the parameter values in Eq. (2.1). It can be shown, that
using a different dry condition state and accordingly a different neutron count
rate ($N'_{\mathrm{dry\_raw}} = \alpha\,N_{\mathrm{dry\_raw}}$; $P'_{\mathrm{dry}} = \gamma\,P_{\mathrm{dry}}$) leads to a conversion of parameters
a_0 and a_1 , i.e. they have only to be divided by a constant factor $\alpha \cdot e^{\beta \cdot P_{\mathrm{dry}} \cdot (\gamma - 1)}$,
leaving the calibration curve Eq. (2.1) otherwise unchanged (see Appendix).
This implies that using a different dry condition state for normalization, e.g.
a drier state observed later, will not change the derived values of soil moisture
θ, if converted values of a_0 and a_1 are used in the equation.

The second type of corrections of neutron counting rates in the air/ground
interface is due to variations of high energy primary cosmic rays. Existing
databases of neutron monitoring worldwide stations observe spatial variations
and temporal fluctuations of incoming cosmic rays. The four most proximal
stations KIEL (Kiel, Germany), LMKS (Lomnicky stit, Slovakia), JUNG
(Jungfraujoch, Switzerland) and ROME (Rome, Italy) were selected to ob-
tain hourly changes of neutron counting rates exclusively due to fluctuations
of incoming high energy cosmic rays. Time series of hourly ground albedo
neutron counts were normalized to the maximum value observed in each sta-
tion during the selected period. Normalized neutron fluxes in all these sta-

tions were quite similar despite different detection sensitivities, e.g. different neutron detectors (18-NM64 in KIEL, 8-SNM15 in LMKS, 18-IGY in JUNG and 20-NM64 in ROME). Our analysis showed that incoming cosmic rays did not substantially vary during our observation period. For example, mean value and standard deviation were 174.3 and 1.5 counts per second at KIEL station, respectively. This standard deviation is far less than the variability, between maximum and minimum periods of solar activity, of 40 counts per second, reported from this station during the last decades. Therefore, we assumed that a correction of neutron counting rates for the variations of incoming primary cosmic rays is not necessary, at least for our observations.

2.2.3. Horizontal and vertical coverage of the GANS method

Horizontal spatial coverage of the cosmic-ray neutron sensing method or GANS method can be defined as the region within which 86 % of the counted albedo neutrons are originated (Zreda et al., 2008). Since ground albedo neutrons depend on atmospheric pressure, also the footprint is inversely proportional to atmospheric pressure. Probability of neutron collisions with nuclei in air is significantly less than in soil because of its lower water content (specifically H) compared to soil. This probability is expressed on the basis of length (macroscopic cross-section, $\Sigma = N\sigma \ [\mathrm{m}^{-1}]$) and is a function of the atom density (N) and energy-dependent element cross-section (σ). Therefore, the neutron counting rate above the ground surface is a measure of intensity in soil (Shuttleworth et al., 2010). By means of simulations, Zreda et al. (2008) suggested to adopt a 600 m diameter footprint at sea level, rather independent of soil moisture level.

The depth of measurement of the GANS method depends mostly on soil moisture, because the probability of neutron scattering and absorption events depends on the number of hydrogen molecules. Hydrogen has a higher scattering cross-section compared to common elements in rocks. Numerical simulations by the Monte Carlo Neutron Particle (MCNP) transport code (Briesmeister, 1997) suggest in silica matrix a vertical coverage by albedo neutrons counted aboveground ranging from about 0.8 m in dry soils to 0.1 m in wet soils (Zreda et al., 2008). A very descriptive feature of the transmission of ground albedo neutrons produced by secondary cosmic rays through the soil porous media is the mean-free path length, $\overline{\lambda_m}$ [m], given as follows:

$$\overline{\lambda_m} = \frac{1}{\Sigma_{\mathrm{t}}} = \frac{1}{\theta\,(\Sigma)_{\mathrm{water}} + (1-n)\,(\Sigma)_{\mathrm{soil}} + (n-\theta)\,(\Sigma)_{\mathrm{air}}} \qquad (2.4)$$

where Σ_t is the total material cross-section $[\mathrm{m}^{-1}]$, θ is volumetric soil moisture $[\mathrm{m}^3\,\mathrm{m}^{-3}]$, n is soil porosity $[-]$, and Σ_i is the macroscopic cross-section of material i (water, soil or air) as described above $[\mathrm{m}^{-1}]$. Equation (5) is derived from Eq. (12.8) in Rinard et al. (2009) assuming a volumetric mixture of water, soil and air in the porous media. The mean-free path length is an indicator of the soil depth from which ground albedo neutrons can be detected assuming homogeneous soil chemical characteristics under variable-saturation conditions (neutron moderation by air in void volume). It depends not only on the type of material but also on the energy of the neutron penetrating the medium, because their total macroscopic cross-section changes with neutron energy (Horsley, 1966).

However, if only ground albedo neutrons (from epithermal to fast level) are counted aboveground, the mean-free path length depends only weakly on the chemical composition of the soil, as shown by Zreda et al. (2008). Therefore, a count of ground albedo neutrons in this energy range will predominantly depend on soil moisture. And worth mentioning, the neutrons detected in the sensor come from a broad range of angles, including almost horizontal ones. However, this deflected angle after collision does not strongly affect the counting probability, because mean-free path length in air is typically in the order of tens of meters. This is also the reason why the height of a neutron counter above ground surface is not sensitively influencing counting rates as long as it is not shielded by surface structures and is lower than the mean-free path length in air.

2.2.4.   Experimental site

The non-invasive GANS method for estimation of soil moisture was tested in a 30 ha agricultural field in Bornim (Brandenburg, Germany). The test site is located close to Potsdam, and 30 km west of Berlin (Figure 2.1). The landscape at the site was formed during the last ice age. Soil consists in the upper one meter of 75 % sand, 17.2 % silt and 7.8 % clay (Gebbers et al., 2009). Texture analysis was done for a number of near-surface samples, and a loamy sand type is predominant in all 19 selected sampling locations (Fig. 2.1). Percentages of sand (between 77.8 and 86.2 %), silt (between 8 and 14.8 %) and clay (between 4.8 and 9.4 %) always indicated this soil classification, in agreement with the previous work in the area nearby (Gebbers et al., 2009).

The period of highest precipitation in Potsdam usually is between May and August, but varying between the years. Total annual precipitation ranged between 374.6 mm (1976) and 825.9 mm (2007), based on the long term meteorological record of the period 1893–2010 (Meteorological Station

Potsdam Telegrafenberg – Germany). Averaged in this period, the mean monthly relative humidity seasonally varies between 67.6 % (May) and 89.3 % (December). Analogously, the monthly averaged daily mean air temperature were recorded as $-1\,^\circ$C (January) to $18\,^\circ$C (July) in this period.

The monitoring period started on 27 August 2010 when the field was cropped with corn (*Zea Mays*). The monitoring continued until corn was harvested on 14 September 2010. A second monitoring period started on 26 November 2010 in a condition of bare soil and continued until the end of March 2011. Thus, the first period covered a part of late summer and the second period covered the transition from late autumn to the beginning of spring. Weather data was provided from the nearby station of Leibniz Institute for Agricultural Engineering Potsdam-Bornim (ATB) located about 1 km from the field site. Snow fall data were taken from the Meteorological Station Potsdam Telegrafenberg located about 6 km to the east.

2.2.5. Biomass and the GANS method

The role of biomass on estimations of soil moisture by means of the GANS method is still under debate. The presence aboveground biomass could affect the ground albedo neutrons in two ways: (1) the biomass produces moderating effects on incoming cosmic rays and on ground albedo neutrons before they reach the detector, mainly by its water content, and (2) scattering and absorption properties of other biomass constituents (e.g. carbohydrates) also reduce neutron fluxes at the ground/air interface. It can be expected that vegetation with lower biomass will have a less important influence on incoming cosmic rays and albedo neutrons emanating from soil.

In order to understand the influence of biomass on the GANS method, spatial and temporal variability of corn was monitored. Two field campaigns (19 August 2010 and 6 September 2010) were performed to measure the crop height for a total of 96 points according to the sampling grid shown in Fig. 2.1. Moreover four areas of $1\,\mathrm{m^2}$ with four different mean crop heights, covering the full range of heights observed previously were selected for biomass measurements. Biomass samples were subsequently dried in the oven. Crop height, wet biomass and dry biomass measurements were used to establish an empirical relationship between biomass water in corn and crop height.

2.2.6. Ground Albedo Neutron Sensing (GANS)

At the experimental field site, two "types" of cosmic-ray neutron sensors (CRS-1000, Hydroinnova, Albuquerque, USA) were installed. These devices only recently became available commercially. One probe contained two pro-
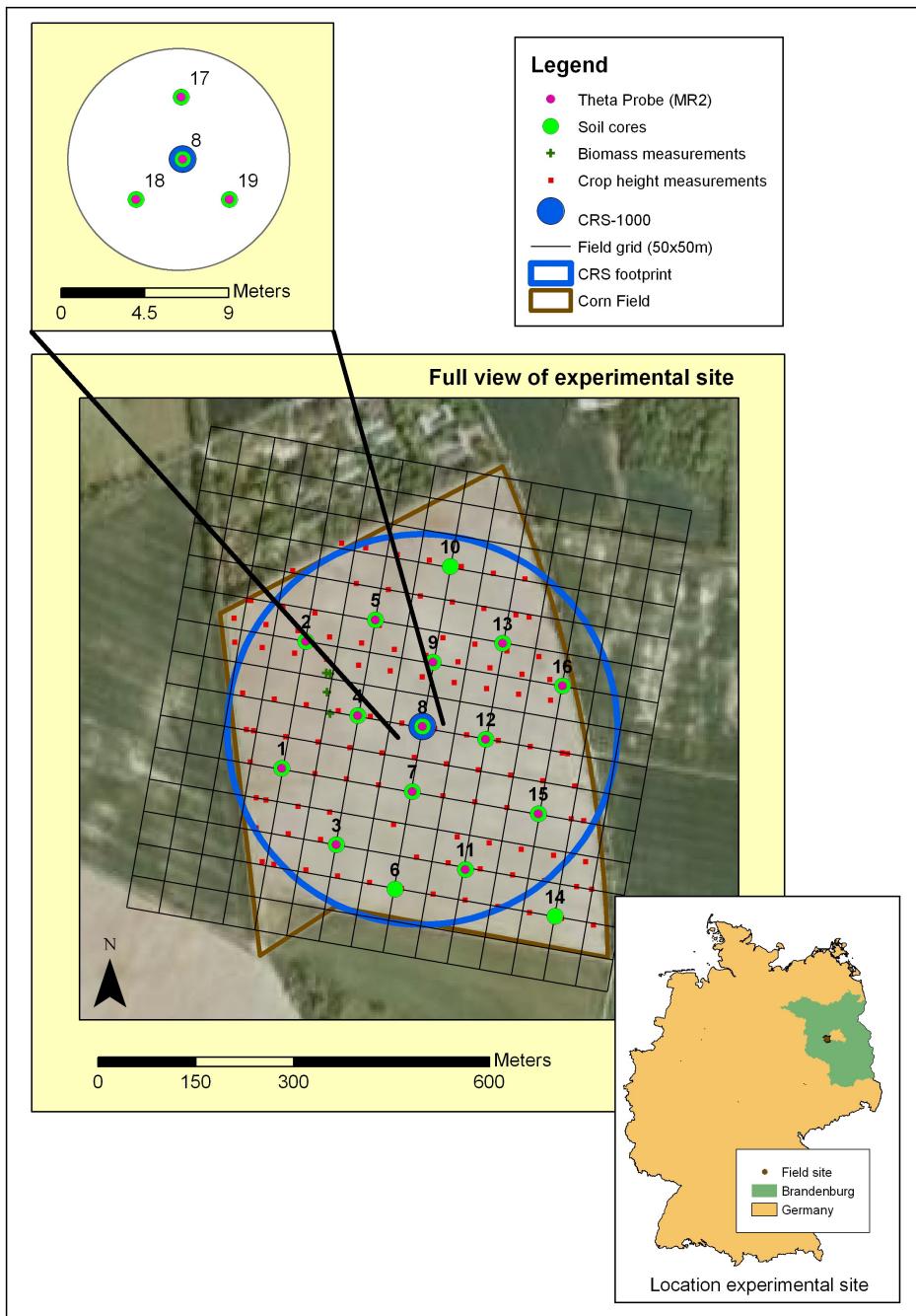
Figure 2.1: Location of experimental site and its hydrological instrumentation.

portional counters, one counter surrounded by a low-density polyethylene and a second, bare counter (Fig. 2.2a). The second CRS-1000 had a moder-

ated proportional counter only. Moderated counters monitor epithermal to fast neutrons, whereas the bare counter measures neutrons predominantly in the thermal energy range. All these neutron detectors applied at the field site are proportional counters filled with He-3 gas (2 atm pressure). Neutron detector tubes interface directly to a Neutron Pulse Module, NPM, (Q-NPM-2000-HV, Quaestra Instruments LLC, Tucson, AZ) with integrated 2000 V high voltage supply and Multi-Channel Analyzer (MCA).

The sensors were mounted on a pole in the middle of the field (52.431° N, 13.021° E, WGS84, 84 m a.s.l.) at a height of 1.5 m aboveground surface in order to collect ground albedo neutrons from a footprint (Fig. 2.1), ca. 600 m diameter, as specified by Desilets et al. (2010). The two CRS-1000 were placed 6 m apart, thus purposely with a large overlap in their footprint (Fig. 2.2b). Neutron pulse counting modules of the CRS-1000 were set-up to record counts every 20 min; in data processing, neutron counts were integrated in one-hour time intervals.

2.2.7. Soil moisture network and field campaigns

In parallel to measurements of ground albedo neutrons, soil moisture data at point-scale was monitored by using classical techniques. A soil moisture network consisting of 16 Theta probes MR2 (Delta-T Devices Ltd., Cambridge, UK) with data loggers was installed at the experimental site. The probes measure the soil moisture based on the Frequency Domain Reflectometry (FDR) approach. Sampling design in the first monitoring period used 16 MR2s on the surface level spaced as shown in Fig. 2.1. Some of the MR2s were damaged during this period by animals or intruding water. The second monitoring period used only five locations in the experimental field: point 8 (center), point 9 (north), point 7 (south), point 4 (west) and point 12 (east) as shown in Fig. 2.1. Each location in the second period had three different depths for MR2 probes (surface representing 5 cm, 20 cm and 40 cm).

Calibration of classical soil moisture devices was carried out collecting undisturbed soil samples during the different seasons (Table 2.2). Soil samples, 100 cm^3 soil cores (UGT, Muencheberg, Germany), were used for gravimetrical estimation of soil moisture and bulk density. Also, soil texture was measured by means of the hydrometer method (Beverwijk, 1967), and classified by the United Stated Department of Agriculture (USDA) classification.

2.2.8. Calibration of CRS-1000

In literature, the calibration technique for CRS-1000 is only done by modeling neutron transport. Zreda et al. (2008) and Desilets et al. (2010) evalu-
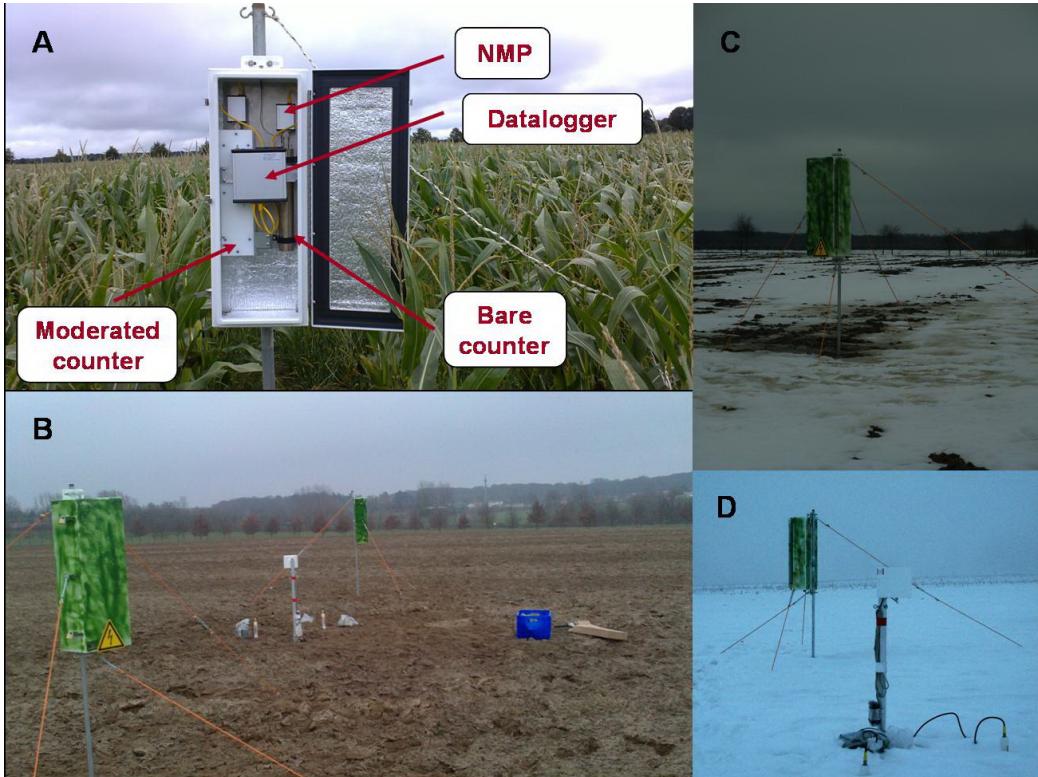
Figure 2.2: Ground albedo neutron sensors (CRS-1000) under different field conditions in Bornim: **(a)** two-counters CRS-1000 and its parts in cropped corn field, **(b)** picture of two CRS-1000s in bare field condition, **(c)** picture of CRS-1000 at the beginning of snow cover condition, and **(d)** picture of CRS-1000, rain gauge and Theta Probes (MR2) during a day with maximum snow cover.

ated the fitting parameters of Eq. (2.1) by means of simulating the relative neutron flux for a given volumetric soil moisture under simplified conditions in via the code Monte Carlo N-Particle Extended (MCNPX). Subsequently, an equation such as Eq. (2.1) was adjusted to match field soil moisture values (two points in time) by translating the curve until a least-squares fit was achieved. This calibration approach requires neutron modeling. Furthermore, these simulations currently are restricted to simple geometries.

To overcome these limitations we suggest a modified procedure to ease the practical application of the methodology without the need of modeling neutron scattering, and requesting intensive, but viable monitoring activities. In the particular approach implemented in this study we performed a calibration of CRS-1000 devices based on continuous data from a classical soil

Table 2.2: Description of soil sampling campaigns at experimental site.

Campaign	Date [dd/mm/yy]	Season	No. of samples	Mean soil moisture [m^3 m^{-3}]	Standard deviation [m^3 m^{-3}]
1	03/08/10	Summer	18	0.169	0.028
2	11/08/10	Summer	18	0.066	0.015
3	16/08/10	Summer	19	0.198	0.029
4	06/09/10	Summer	19	0.132	0.052
5	11/02/11	Winter	5	0.238	0.014

moisture network (see Sect. 2.7). Firstly, ground albedo neutron counting rates measured in the moderated counter (N_{raw}) were normalized to a counting rate observed during dry conditions ($N_{\text{dry\_raw}}$). This neutron counting rate under dry conditions was taken from a period when lowest soil moisture values were measured in the MR2s. Classical soil moisture data here was only used to identify the drier period, but these data were not applied in the calibration procedure itself.

An important point of this calibration is that the penetration depth of the GANS method is variable depending on mean soil moisture values in the footprint. On the other hand, this penetration is relatively well known for wet conditions, and then the penetration depth, or vertical footprint, is about 10 cm. Because of this, our calibration approach used spatially averaged surface soil moisture values from MR2s at 16 locations inside the footprint (Fig. 2.1), taken during periods when vertical penetration depth of CRS-1000 is comparable to the vertical coverage of surface MR2 devices. With this dataset a good calibration was achieved, as described in the following sections. However, an assessment of the actual vertical coverage of a CRS-1000 is an important topic that needs to be investigated further.

Since Eq. (2.1) presents three unknown fitting parameters, three short periods of soil moisture data were selected from the first monitoring period in order to calibrate the CRS-1000 devices. These periods are chosen to cover a range of medium moist and the close-to-saturation conditions. A single set of calibration parameters using these periods was estimated by minimizing the root mean square error (RMSE) between MR2 and CRS-1000 data defined

as follows:

$$\text{RMSE} = \sqrt{\frac{\sum\limits_{i=1}^{i=n_\text{p}} \left(\theta_{\text{GANS},i} - \theta_{\text{MR2},i}\right)^2}{n_\text{p}}} \qquad (2.5)$$

where $\theta_{\text{GANS},i}$ is the areal mean soil moisture inferred via the GANS method $[\text{m}^3\,\text{m}^{-3}]$, $\theta_{\text{MR2},i}$ is the hourly value of soil moisture (mean value from 16 locations) $[\text{m}^3\,\text{m}^{-3}]$, each at data point i of a time series, and n_p is the number of data points considered in the calibration data. Subsequently, the soil moisture determined using the set of calibrated parameters was applied for the whole summer observation period and another period after harvest in winter.

The datasets used to estimate RMSE included hourly soil moisture data. Soil moistures values derived by GANS in Eq. (2.5) were estimated by using six-hours moving average of neutron counting rates. Either a moving average or longer integration periods of neutron data is required to achieve the desired accuracy of soil moisture measurements, because at a low altitude site such as Bornim, counting rates are notably smaller than at higher altitudes, e.g. previous studies of Zreda et al. (2008) and Desilets et al. (2010).

2.3. Results and discussion

2.3.1. Ground albedo neutrons under different field conditions

Different scenarios observed at the field site showed a first opportunity to distinguish the influence of different sources of water (biomass water, soil moisture and snow pack) on the ground albedo neutron flux. In Table 2.3, we summarize ranges of neutron counting rates observed for three types of field conditions. Although, periods when the field was cropped or bare did not show significant difference in neutron counting rates, we found it useful to plot counting rates of ground albedo neutrons in different energy levels. Here, we introduce the Field Neutron Ratio (N_f) that could be an useful information to identify different field conditions from ground albedo neutron data alone, and probably also water in different environmental reservoirs, as follows:

$$N_\text{f} = \frac{C_\text{B}}{C_\text{M} - C_\text{B}} \qquad (2.6)$$
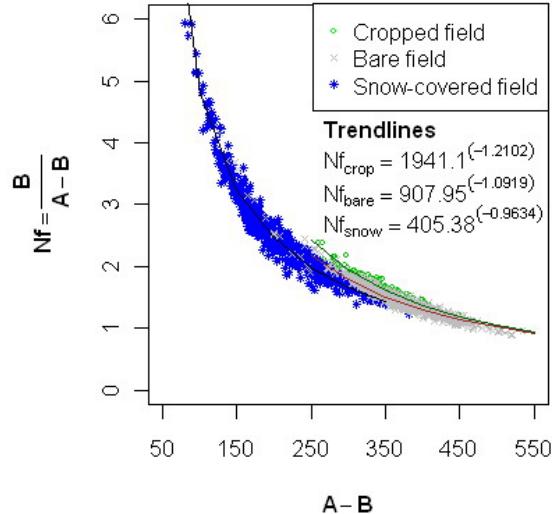
Figure 2.3: Neutron counts in different field conditions. In the vertical axis, N_f is a field neutron ratio, here defined as ratio of bare counts per hour (B) over difference of moderated counts per hour (A) and bare counts per hour (B). In the horizontal axis, difference of moderated counts minus bare counts per hour.

where C_B and C_M are the ground albedo neutron counts per hour observed in the bare and in the moderated counter, respectively. Evaluation of N_f values for cropped field, for bare soil and for snow cover is shown in Fig. 2.3. This plot presents slightly different properties than usual in neutron physics, since CRS-1000 devices do not give exact energy information about neutrons recorded in the detector. This is the reason why we defined N_f using rates recorded in "bare" and "moderated" counters, which is more practicable. A similar approach was presented in the so-called "Cd-difference" by Kodama et al. (1985).

The ratio N_f ranged between 1.21 and 2.38 for cropped-field and between 1.24 and 2.34 for bare-field conditions. In both scenarios, N_f follows well a similar power law relation. Though N_f is slightly higher for cropped than bare field, the result overall corroborated that there was no significant difference between bare and cropped conditions.

One important issue in the ongoing-development of the GANS method is to quantify the influence of biomass. Therefore, direct measurements of plant biomass were carried out in this study. We determined an empirical relationship between wet and dry corn biomass per m^2 and mean corn height ($r^2 = 0.98$, data not shown). Biomass water and dry biomass in the CRS-1000

34

Table 2.3: Range of neutron counting rates observed in different field conditions.

Condition	Period* [dd/mm/yy]	Moderated counter [neutrons per hour]			Bare counter [neutrons per hour]		
		Range	Mean	St. Dev.	Range	Mean	St. Dev.
Cropped soil	27/08/10 until 14/09/10	790–1067	918	52	500–659	573	32
Bare soil (without snow)	26/11/10 until 01/12/10	802–1045	900	43	489–650	557	30
	10/01/11 until 25/03/11	687–1060	838	79	398–649	500	45
Bare soil (with snow cover)	02/12/10 until 09/01/11	521–930	730	85	387–621	519	48

* Short gaps due to battery failure.

footprint were evaluated by measuring crop height at a number of locations. Two field campaigns (cf. Sect. 2.5) showed that height of corn (*Zea Mays*) strongly varied, showing values between 50 and 190 cm with a mean of 143 cm. These campaigns took place only a few weeks before harvest. Thus, the biomass and especially biomass water may have not increased further, or even declined, because maize tends to dry at the end of summer. Very sandy locations showed reduced crop height. In the center and east, for example, soil had a higher silt and clay content and supported better crop growth. Assuming the maximum crop height for everywhere in the footprint, biomass water was at most $100\,\mathrm{Mg\,ha^{-1}}$. In comparison to soil moisture, this estimation constitutes only $14.95\,\%$ of the water mass for a $0.45\,\mathrm{m}$ soil column (mean CRS-1000 penetration) with mean soil moisture of $0.15\,\mathrm{m^3\,m^{-3}}$. This can be taken as a maximum estimate. We infer that a corn crop, in terms of biomass and biomass water, as a moderator of ground albedo neutrons, is of substantially less influence on neutron counting rates than soil moisture. This impact on neutron counting rates may be higher only for even drier conditions, e.g. $\theta < 0.05\,\mathrm{m^3\,m^{-3}}$, or higher biomass cover than our maximum estimate for corn. However, these are quite unlikely conditions, more in combination, and therefore, we hypothesize that this assumption is true for cropped fields in general. This behavior can be expected to be different for other types of vegetation, especially forest.

During winter there was an early and relatively long period with a snow cover, starting on 2 December 2010 with $8\,\mathrm{cm}$. Snow water equivalent was measured as $19 \pm 3\,\mathrm{mm}$, $23 \pm 4\,\mathrm{mm}$ and $36 \pm 8\,\mathrm{mm}$ on 23 December 2010, 3 January 2011 and 7 January 2011, respectively based on four samples each day taken in the proximity of CRS-1000. Evaluating a five weeks period with continuous presence of snow cover (until 9 January 2011), neutron counting rates were slightly less than observed under bare field and cropped-field conditions (Table 2.3). Moreover, periods with and without snow cover could be distinguished by N_f (Fig. 2.3). Values of N_f were clearly shifted to larger values if a snow cover was present. Values of N_f between 1.24 and 5.93 corresponded to the snow-covered period.

Neutrons are slowed down and absorbed efficiently in water. Therefore, numbers of ground albedo neutrons detected aboveground are substantially different when a snow layer is present. This explains why neutron counting rates observed during winter differ between periods with or without a snow layer. Kodama et al. (1979) reported that the attenuation character of neutrons in snow cover is influenced by the so-called boundary effect of air-snow-soil layers. During the initial phase of snow accumulation ($\sim 30\,\mathrm{cm}$ water depth) there is a steep decrease of neutron counting rates due to air-water boundary low energy neutrons (as observed in a bare counter). But

Kodama et al. (1979) observed also that this behavior disappeared when
neutrons of higher energy (e.g. those observed in a moderated counter) were
measured. Based on observations at our field site, we also can conclude that
snow cover plays a substantial role on moderation of neutrons, and shifts
counting rates to higher N_{f} values more strongly than both biomass and soil
moisture (Fig. 2.3).

2.3.2. Calibration for soil moisture estimations

Classical monitoring network

Due to the relative homogeneous classification of the soil type in the
field (cf. Sect. 2.4), the same calibration function for all MR2 probes could
be used. A standard calibration function for mineral soil type provided by
MR2 was tested against soil samples (Fig. 2.4). Gravimetric soil moisture
was converted to volumetric soil moisture by multiplying bulk density es-
timated from undisturbed soil cores. The mean value of bulk density was
$1.40\,\mathrm{g\,cm^{-3}}$ with a standard deviation of $0.12\,\mathrm{g\,cm^{-3}}$. Soil moisture estimated
from undisturbed soil cores varied between 0.049 and $0.233\,\mathrm{m^3\,m^{-3}}$ with a
mean value of $0.14\,\mathrm{m^3\,m^{-3}}$. The MR2 measurements gave values between
0.106 and $0.283\,\mathrm{m^3\,m^{-3}}$ with a mean value of $0.16\,\mathrm{m^3\,m^{-3}}$. The coefficient
of correlation and RMSE between MR2 data and field measurements of soil
moisture (soil cores) were 0.84 and $0.034\,\mathrm{m^3\,m^{-3}}$, respectively. A specific
calibration for each MR2 could be evaluated for further research focused on
the assessment of the spatial variability inside the footprint. However, con-
sidering the aim of this study and the relatively few number of samples at
each location, the standard calibration function for mineral soil type was
considered to give a sufficient representation and thus was used for all MR2.

Ground albedo neutron sensor CRS-1000

Ground albedo neutrons observed in the two different probes had a similar
response during the entire two monitoring periods. Neutrons monitored in
the two moderated counters of the CRS-1000s showed a correlation coefficient
of 0.81 for one-hour integration periods (Fig. 2.5a). For an integration period
of six hours, and thus a lower statistical variability of counts, the correlation
between the two moderated counters increased to 0.97 (data not shown). This
demonstrates that the counters functioned in the same way and also that the
distance of 6 m between probes did not lead to significant differences.

Neutron rates were indeed inversely correlated to local atmospheric pres-
sure as expected (Fig. 2.5b). After local correction of neutron counting rates
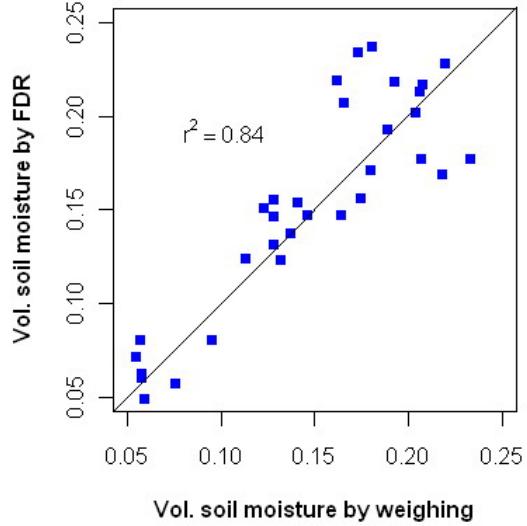
Figure 2.4: Calibration of Theta Probes (MR2): observed soil moisture from soil cores and soil moisture measured by MR2s.

due to fluctuations of atmospheric pressure (between 1000.10 and 1026.96 mbar), ground albedo neutrons ranged between 781 and 1103 counts per hour. The maximum value of ground albedo neutrons per hour (1067), which coincided with a period of no precipitation events and minimum soil moisture value, was used as $N_{\mathrm{dry\_raw}}$ for normalizing neutron counts of Eq. (2.3).

In order to relate neutron counting rates with soil moisture according to Eq. (2.1), three datasets representing soil moisture values shortly after rain events with maximum cumulative values (16.7, 8.2 and 4.9 mm) were selected as calibration data. These soil moisture measurements come from three separate time periods of about a day only each, and are jointly used for a single fit of calibration parameters. They were chosen to cover a range of medium soil moisture values, but avoiding situations where the top part of the soil had dried out while the lower part may still be much moister. The latter is to ensure that the local soil moisture measurements represent a similar soil moisture state than the CRS-1000 signal. No weighting of the local soil moisture measurements was applied (cf. Eq. 2.5), though shallower and horizontally closer locations contribute more to the neutron counts in the CRS-1000 than deeper and more distant locations in the footprint. The spatial coverage in the vertical and horizontal will have to be investigated further to be able to define a suitable weighting scheme, with the aim to improve the calibration of a GANS probe and to better understand how neutron counts represent soil moisture in the footprint. It can be expected that such
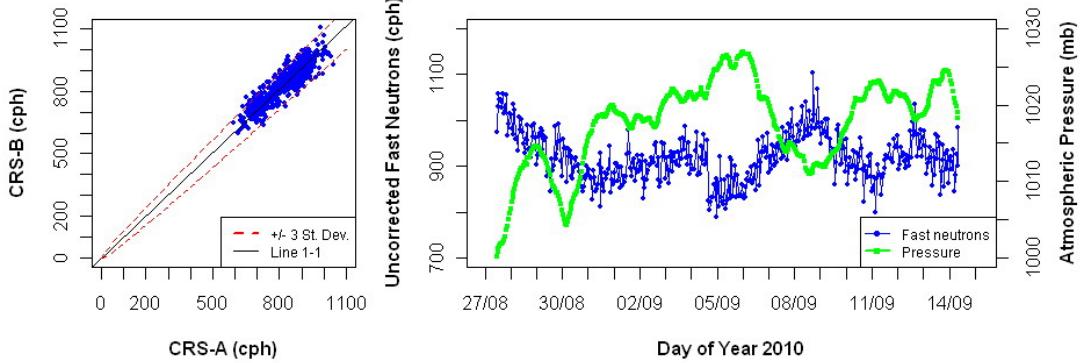
Figure 2.5: Ground albedo neutrons in moderated counter under cropped field conditions: (left) correlation of ground albedo neutron counting rates per hour between two CRS-1000 sensors, and (right) temporal variability of uncorrected ground albedo neutron counting rates per hour and local atmospheric pressure.

a weighting is required the less homogeneous the footprint is in respect to soil texture, vegetation type and aboveground biomass. At our cropped field the conditions were relatively homogeneous and thus a procedure without spatial weighting of local soil moisture data seems appropriate, opposed to, e.g. a forest site.

These datasets of 26 h (between 29 August 2010 13:00 LT and 30 August 2010 14:00 LT), 20 h (between 4 September 2010 17:00 LT and 5 September 2010 12:00 LT) and 14 h (between 13 September 2010 17:00 LT and 14 September 2010 06:00 LT) had soil moisture mean values of 0.261, 0.191 and 0.141 $m^3 m^{-3}$, respectively (Figs. 2.6a and 2.7). By calibration, a good fit between the soil moisture MR2 data and soil moisture measurements by the GANS method was obtained with values of 0.465, 0.1125 and 0.49 for the fitting parameters a_0, a_1 and a_2, respectively. These fitting parameters showed a small minimum RMSE of 0.019 $m^3 m^{-3}$. This value of RMSE is similar to the accuracy of CRS-1000 for a six-hour integration period (0.013), which can be inferred from the standard deviation of the mean neutron counting rate (5504 counts in six hours). The coefficient of correlation between CRS-1000 soil moisture measurements and the mean value of MR2 soil moisture observations was 0.98 (Fig. 2.6b).

The fitting parameters presented in this study were derived via the data from the three selected periods of the measured soil moisture time series. In these periods values of N_R ranged between 0.784 and 0.906. This normalization was based on the reference N_{dry_raw} used to calculate N_R. This reference
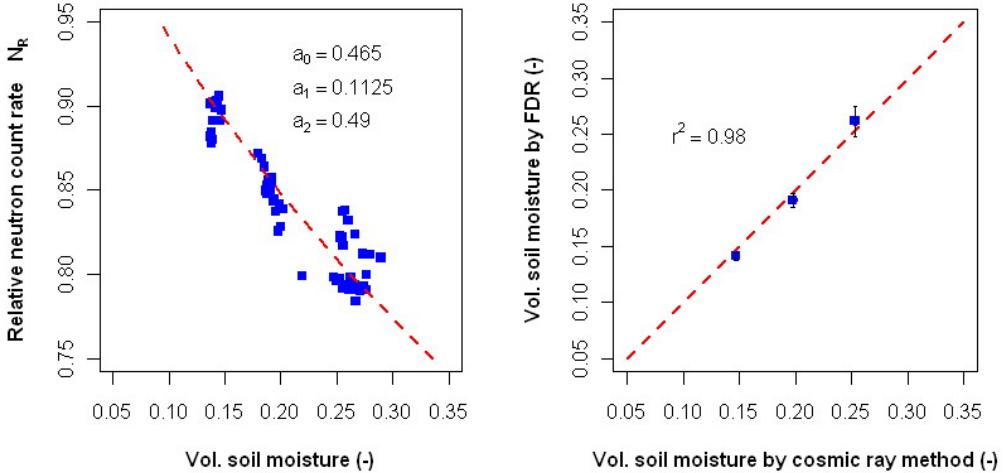
Figure 2.6: Calibration of the CRS-1000: (left) calibrated function of soil moisture estimation by ground albedo neutrons (Eq. 2.1) and (right) correlation between soil moisture measured by CRS-1000 and measured by MR2 probes, where each data point represents the mean value of each calibration period.

value to represent dry conditions was taken from another period, identified by soil moisture measurements in the field.

The applicability of the calibration function is not limited to the values occurring in the three selected periods used for the calibration, as an empirical calibration would be, because the form of our calibration function is based on the results from a statistical simulation of neutron transport, fully based on physical principles (Desilets et al., 2010; A1). Therefore, this equation should allow also evaluating soil moisture for a broad range of sensible soil moisture values. However, there is a mathematical limitation for N_R when it approaches a_1, but this is not to be expected to occur, at least for our field site (cf. Fig. 2.6). However, the calibration function type, derived by Desilets et al. (2010), might depend on some sensor characteristics such as its geometry, He-3 gas pressure, moderator material surrounding the neutron counter, etc., since all this information was included in the neutron transport simulations performed by these authors. Therefore, Eq. (2.1) might be restricted to similar counter specifics.

The values of fitting parameters derived for our field site did not coincide with values reported by Desilets et al. (2010). They reported values of 0.0808, 0.372 and 0.115 for the fitting parameters a_0, a_1 and a_2, respectively. These values were derived by neutron flux simulations for a generic pure silica soil matrix (SiO_2) and successfully applied for measurements at

a location in Lewis Springs, Arizona, USA ($31.562°$ N $110.140°$ W, WGS84,
1233 m a.s.l.). For the fitting parameters a_0 and a_1 identical values cannot be
expected, just because of the dependence on the reference dry condition used
for normalization (see above). For the third fitting parameter, a_2, offsetting
the minimum soil moisture, a dependence on site soil conditions or detector
characteristics would not be surprising.

Thus, the mathematical relation between counting rates of ground albedo
neutrons and soil moisture seems applicable, as supported by the good fit of
data measured at our field site. Moreover, it seems possible to calibrate at
a specific site using independent soil moisture measurements from at least
three short time periods. The calibrated parameters can be applied also for
soil moisture observations at other times and possibly at similar locations
(e.g. at the same hillslope or small catchment with similar soil and land use
characteristics), if the same counter type is used. However, transferability
of calibration parameters to other locations is still an open question to be
evaluated in further investigations.

In the following we report how we tested the CRS-1000 soil moisture
measurements during the complete observation period in summer, and also
during a winter period with snow cover. In both periods, parameters cali-
brated were not changed anymore.

2.3.3. Test period during summer

Applying these fitting parameters, soil moisture values derived from hourly
ground albedo neutron counts are shown in Fig. 2.7 A good agreement was
observed between time series of soil moisture data by CRS-1000 and mean soil
moisture from the MR2s located in the CRS-1000 footprint. Furthermore,
the temporal patterns of soil moisture inferred from MR2s and CRS-1000 are
similar, despite their different measurement volumes. Mainly, the GANS-
derived soil moisture pattern was inside a range of one standard deviation
of MR2s, except in two periods: (i) between 2 September 2011 00:00 LT and
2 September 2011 14:00 LT, and (ii) between 9 September 2011 11:30 LT and
11 September 2011 11:30 LT. Values in this first period fall into a range of
two standard deviations of MR2 average mean values. However, during the
second period there was a clear overestimation of soil moisture by CRS-1000
compared to MR2 values, longer and more than to be expected by statisti-
cal deviations. The reason for this probably is not a measurement error of
the MR2, but from the CRS-1000. However, an easy explanation could not
be found and requires further research. After this period, the soil moisture
measurements of CRS-1000 decreased again to the level of the MR2 values
and responded properly to precipitation events.

Overall, the RMSE between hourly soil moisture values by CRS-1000 and spatial mean hourly values of soil moisture from MR2s was $0.039 \, \mathrm{m^3 \, m^{-3}}$ for the complete cropped field period. This RMSE is similar to the accuracy (cf. Sect. 2.2) of CRS-1000 (0.033) expected from a mean counting rate of 918 ground albedo neutrons per hour.

Furthermore, the GANS method responded well and quickly to precipitation events, as neutron counting rates decreased during precipitation events and stayed lower afterwards; thus GANS-derived soil moisture values increased for those periods as they should (e.g. after events 29 September 2010 and 4 September 2010). However, when CRS-1000 data were smoothed with a six-hour moving average, to compensate for the statistical variability of neutron counting rates, fast changes of soil moisture may not be reflected perfectly. For example, the CRS-1000 estimations resulted in an increase of soil moisture a few hours ($\sim$6–7 h) before precipitation actually occurred (e.g. events 8 September 2010 06:00 LT with 0.9 mm and 12 September 2010 23:00 LT with 0.3 mm).

2.3.4. Test period during winter with periods of snow cover

After harvest of corn, the CRS-1000s were operated at the field site again by end of November 2010. The CRS-1000 data retrieved were used for assessing the difference to the cropped field of the summer period and to test for the impact of snow cover. Values in different depths during the winter period were similar and for a consistent interpretation between summer and winter campaign we used only values of 5 cm depth (Fig. 2.8). This winter had an early cold period with snow fall. Classical soil moisture sensors, MR2 probes, could not provide a true measurement of the total soil moisture during parts of the winter period with freezing conditions. Since the classical devices used in this study actually measure the bulk dielectric constant of the soil surrounding the probe, a decrease of MR2 signal under freezing conditions could be expected. The soil's bulk dielectric constant is dominated by the dielectric constant of the liquid water (81 at 20 °C), as the dielectric constants of other soil constituents are much smaller; e.g. soil minerals range between 3 and 5, frozen water is about 4, and air is about 1 (Jones et al., 2002). Therefore, a change of states from unfrozen soil moisture to frozen soil moisture causes significant changes of soil's bulk dielectric constant. Moreover, we observed that when air temperature (measured in CRS-1000) falls below 0 °C, electrical output of MR2s sharply decreased, and then for negative air temperatures stayed below the usual range of 200 to 850 mV, observed
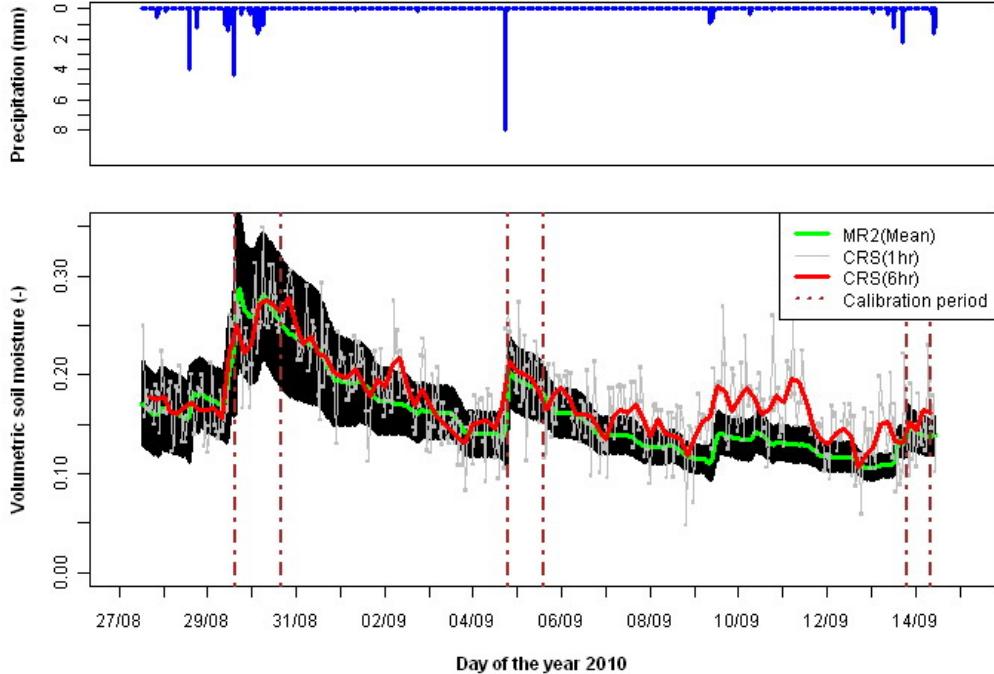
Figure 2.7: Soil moisture inferred by the GANS method plotted for a period
of cropped field condition. Upper graph: hourly precipitation time series data
measured in ATB weather station. Lower graph: soil moisture time series
data measured by MR2 probes (spatial mean hourly value in green and one
standard deviation in black band) and CRS-1000 (1-h estimations and 6-h
moving average in gray and red colors, respectively). The three periods used
for calibration of CRS-1000 are shown between vertical dashed lines.

under cropped and bare conditions. Overall, we found quite good correlation
between air temperature and functionality of MR2 probes (not shown) in
order to identify periods where MR2s data could be used. Thus, these peri-
ods when MR2 probes were not giving real soil moisture values are marked
with an arrow between vertical dashed lines in Fig. 2.8. In the intermediate
periods of varying length the MR2 data seem to reflect realistic soil moisture
conditions, except a period of one week in the beginning of March showing
strong fluctuations.

In this winter period the CRS-1000 calibration via Eq. (2.1) with soil
moisture data from cropped-field conditions was applied without modifica-
tions. Therefore, the CRS-1000 derived data could be tested for these bare
field conditions, including periods with and without snow cover. During pe-
riods of bare soil without snow cover, soil moisture by CRS-1000 reproduced
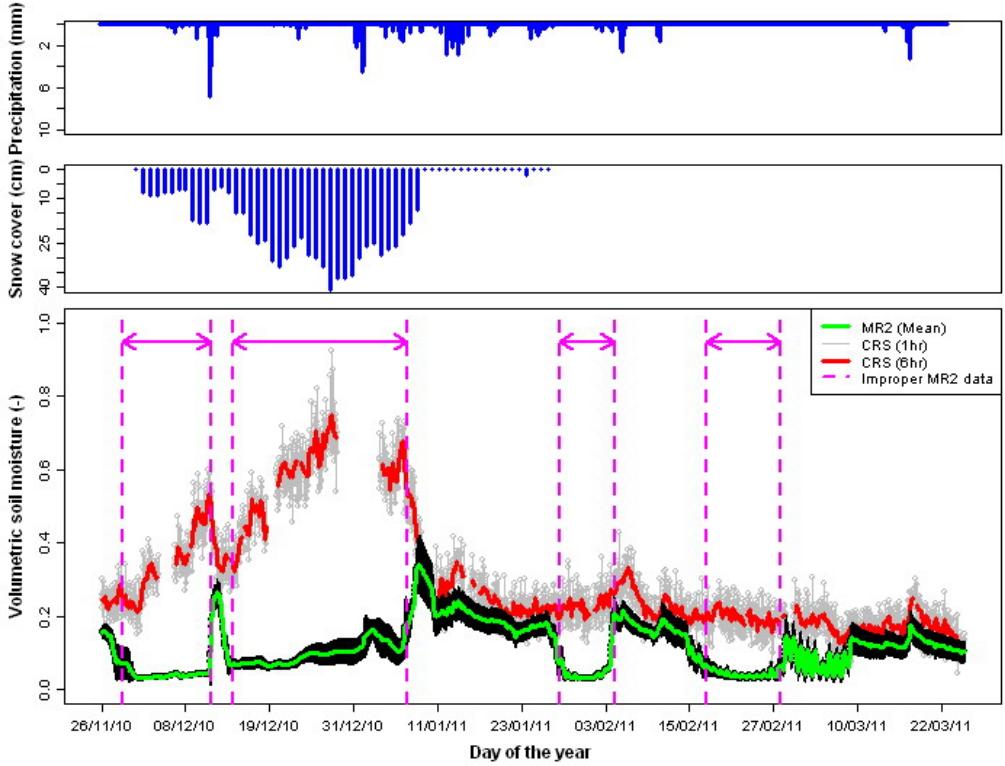
Figure 2.8: Total volumetric water content (soil moisture and snow water) measurement by GANS method during the winter period. Two upper graphs: hourly precipitation (mm) in ATB weather station and daily snow cover in PIK weather station. Lower graph: soil moisture time series data measured by MR2 probes (spatial mean hourly value in green and its standard deviation in black band) and CRS-1000 estimations (1-h estimations and 6-h moving average in gray and red colors, respectively). Periods where MR2 did not work properly due to low soil temperature conditions, are shown between vertical dashed lines.

well the values observed in the field (Fig. 2.8), as long as the MR2s were able to provide correct data, e.g. mid and end of March. In cold periods without snow cover the GANS method gave plausible values, opposed to the MR2, e.g. for the period end of January to the first days of February. It also showed an increased response to precipitation (not resulting in snow cover). Moreover, CRS-1000 measurements of soil moisture were unaffected by sharp drops of air temperature.

Because the MR2s did not properly estimate soil moisture under low temperatures, estimations of CRS-1000 were also validated with results from a fifth soil sampling campaign (Table 2.2). In this campaign, mean soil

44
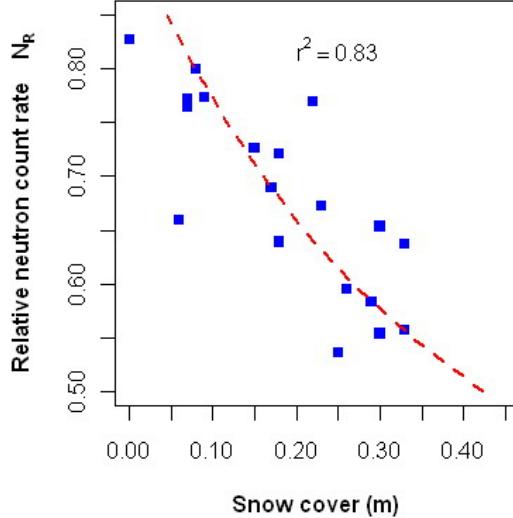
Figure 2.9: Normalized daily neutron counting rate (N_R) versus daily snow cover in PIK weather station (Telegrafenberg-Potsdam, Germany).

moisture was $0.238\,\mathrm{m^3\,m^{-3}}$ with a standard deviation of $0.014\,\mathrm{m^3\,m^{-3}}$. This is comparable to the areal mean soil moisture of $0.22\,\mathrm{m^3\,m^{-3}}$ estimated by means of the GANS method (averaged over the time interval required for the sampling campaign).

In the period when bare soil was covered with snow, neutron counting rates were significantly lower, thus Eq. (2.1) predicted higher values of θ. Such soil moisture values inferred by GANS method have to be seen as a measurement of the water mass stored in and on the soil in the footprint of the CRS-1000. Nominal soil moisture values derived for these periods exceed porosity values of loamy sand (0.38) in the field. This over-estimation of soil moisture reflects the additional moderation of hydrogen mass in snow, as has to be expected (Kodama et al., 1979), and requests a different interpretation of these nominal soil moisture values.

Normalized neutron counting rates and snow cover data, both as a daily average, suggest that these two could well be related with the calibration curve based on Eq. (2.1) as shown in Fig. 2.9. This is in agreement with previous studies of Kodama et al. (1979) and Kodama (1984). In Bornim, lower values of N_R were measured for higher snow cover. Maximum and minimum daily snow covers of $41\,\mathrm{cm}$ and $8\,\mathrm{cm}$ corresponded to N_R values of 0.47 and 0.80 (daily integration), respectively.

The presence of snow modifies the energies of the neutrons detected, as can be seen clearly in Fig. (2.3). However, we have not applied a procedure

to distinguish between snow moderated and non-snow moderated neutrons, though this could be aimed for in principle. Instead, we take this shift as indication of the impact of snow and otherwise limit our interpretation to nominal soil moisture, which represents the combination of real soil moisture (possibly frozen) and snow water mass equivalent on the soil surface, as discussed above.

When snow started to melt neutron counting rates increased resulting in a steep drop of (nominal) soil moisture until 10 January 2011, when there was no more snow cover on the field. N_R values were higher again (0.72) and therefore measurements by CRS-1000 corresponded again to soil moisture measurements by MR2.

2.4.   Summary and conclusions

The work presented has tested the novel cosmic-ray neutron sensing methodology, especially in a new geographical context that may allow for the application of the method in investigations of local soil water balance and catchment hydrology. Furthermore, an application procedure was explored that now could be adopted by others relatively easily for measuring integral soil moisture at intermediate spatial scales.

An operational procedure suggested for application of integral soil moisture measurements on farmland via sensing of ground albedo neutrons, similar to the one used, in summary is:

1. selection of field site location with a 100–300 m radius with relatively homogeneous soil, vegetation, and relief;

2. installation of a (commercially available) neutron counter, such as a CRS-1000, on a pole with a height of around 1.5 m, best with a moderated and a bare counter, data logger, solar panel, air humidity and temperature measurement and possibly remote data transfer;

3. monitoring site specific soil moisture data in periods of a few days covering at least one dry period and three periods varying between medium wet to wet conditions; use these data for calibration of ground albedo neutron values on the basis of Eq. (2.1) by adapting the three fitting parameters after correcting neutron counting rates for air pressure variations;

4. derivation of integral soil moisture values on hourly basis, with possible subsequent accumulation or smoothing;

5. observation of snow cover or at least checking the relative difference of
counts in moderated and bare counters for N_f values shifted to values
outside the bare-field values; possibly use a relation as shown in Fig. 2.9
to identify count rates influenced by snow cover, if distinguishing be-
tween snow and soil water is desired.

Results show that the cosmic-ray neutron method, more precisely ground
albedo neutron sensing (GANS), can be successfully applied also for agricul-
tural fields, even at low altitudes where neutron counting rates are lower than
in highlands. This inherent disadvantage of lowland applications limits the
temporal resolution and implies that an integration period of several hours,
or an equivalent smoothing window, are needed to obtain results without too
much statistical variability.

Times series of precipitation in comparison with GANS soil moisture val-
ues show overall an excellent response of the GANS method to these hydro-
logical events, also smaller precipitation amounts. These observations are
in agreement with Kodama's measurements (1985). The GANS-derived soil
moisture values are consistent with other measurements in the first 10 cm
of topsoil, but shall also reflect water somewhat deeper than that. There
may be short periods of a few days, when soil moisture derived via GANS
exhibit a systematic deviation, e.g. observed once in this study between 9
and 11 September 2010, with a shift towards higher values of soil moisture
by about $0.05 \, \mathrm{m^3 \, m^{-3}}$. Such shifts might be caused by small changes in in-
coming primary cosmic ray intensity, local air pressure differences or heavy
cloud cover. However, this will have to be investigated further. Furthermore,
investigations will be needed to specify the real extension of the horizontal
footprint for different conditions, e.g. vegetation or topography, as well as
how actual soil moisture distribution with depth affects the GANS count
rates and vertical albedo neutrons' penetration depth.

Another aspect is the influence of hydrogen stored in other forms besides
soil moisture such as water in soil materials or plant roots, carbohydrates,
aboveground biomass water or snow. There may be an influence of bound
water and carbohydrates in soil which may impact the values of fitting param-
eters; however, these will not cause a systematic deviation of calibrated soil
moisture values. Also, aboveground crop biomass seems not to lead to signif-
icant changes in GANS-derived soil moisture values and therefore, biomass
of agricultural crops does not necessarily need to be accounted for explic-
itly in applications of the ground albedo neutron sensing method. However,
other vegetation cover, for example trees, probably may have more substan-
tial impact on neutron counting rates and therefore, derived soil moisture
values.

47

Snow cover of the soil has a major influence on neutron counting rates, shifting the nominal soil moisture values easily to more than double or even triple of the real soil moisture values. Since there is good inverse relation with snow height and additionally a shift towards relatively more counts in the bare than the moderated CRS-1000 counter, it could be possible to subtract the snow water mass contribution or even use it to estimate snow height (or snow water equivalent). Moreover, the CRS-1000 was giving reliable values of soil moisture also for periods of freezing conditions without snow cover, opposed to the measurements with MR2 failing in these periods. The use of this methodology to detect snow condition is promising, however further investigation is needed to evaluate a possible quantification procedure.

Overall, this study suggests that the GANS methodology, based on above-ground neutron counting, can successfully be applied at agricultural fields, also in lowlands, provided that similar or higher counting rate levels can be recorded. Nevertheless, methodological improvements will be required. In general, the GANS method has the potential to become a worthwhile and not too expensive extension of soil hydrological measurement methods. It lends itself to extended monitoring as well as shorter-period observations due to the relatively simple installation and mobility. This data could be a valuable input for the observation of hydrological water balances and especially the hydrological modeling of small to medium catchments.

Edited by: H.-J. Hendricks Franssen

Chapter 3

Cosmic-ray neutron sensing of soil moisture in a cropped field: testing calibration approaches during a vegetation period

This is a revised version of the one published by Rivera Villarreyes, C. A., Baroni, G., and Oswald, S. E.: Calibration approaches of cosmic-ray neutron sensing for soil moisture measurement in cropped fields, Hydrology and Earth System Sciences Discussions, 10, 4237-4274, 2013; a proceedings-type publication.

Abstract

This study evaluates the applicability of the Cosmic-Ray Neutron Sensing (CRS) for soil moisture measurements in cropped fields. Measurements were performed at a lowland farmland (Bornim, Brandenburg, Germany) cropped with sunflower and winter rye. The CRS probe was calibrated against local soil moisture profiles. Three field calibration fitting approaches and four different ways of integration the soil moisture profile were compared in this study. Calibration periods were defined according to each crop growing stage (initial, development, middle and late seasons). Furthermore a simple approach to account for neutron attenuation by vegetation is presented also.

The results of the different fitting calibration approaches were in general very similar (RMSE ~ 0.02 m^3 m^{-3}). On the one hand, the applicability and limitations arise mainly from practical aspects as availability of relatively long time series of soil moisture for calibration and strong variability of neutron fluxes. On the other hand, it could be shown that the vegetation growth had a strong influence on the neutron counting rate, independently

from the fitting approaches. The selection of the calibration period, as representative of the average condition in the monitoring season, became the most crucial issue in respect to represent real soil moisture. To overcome this limitation, a time-variable correction of neutron counts for vegetation influence was applied. After this vegetation correction, the CRS soil moisture was significantly improved (RMSE ~ 0.015 m^3 m^{-3}) for both studies crops and vegetation periods, independently from the calibration period considered. Therefore, neutron corrections due to vegetation cover are indeed an important research direction in this methodology, especially for further applications in cropped fields and agricultural water management.

3.1. Introduction

The understanding of soil moisture variability across spatio-temporal scales is of great interest for several fields such as flood prediction and forecasting (Brocca et al. 2010; Koster et al. 2010; Steenbergen and Willems, 2012), weather prediction (Albergel et al. 2010), climate modelling (Team et al. 2004), agriculture management (Champagne et al. 2011; Vico and Porporato, 2011), and groundwater recharge (Patterson and Bekele, 2011).

Despite the important role of soil moisture in the hydrological cycle (e.g. Porporato and Rodriguez-Iturbe 2002, Robinson et al. 2008 and Vereecken et al. 2008), there is still a gap of current soil moisture measurement capabilities covered between point-scale and large-scale remote sensing (Tapley et al. 2004; Entekhabi et al. 2010). Especially at the intermediate scale (e.g. small catchment scale, agricultural-field scale, etc.), measurement techniques for soil moisture are still under development. Indeed, many methodologies of soil moisture measurements at this intermediate scale are investigated such as wireless soil moisture monitoring networks (Bogena et al. 2010), spatial TDR network (Graeff et al. 2010), ground penetrating radar (GPR) measurements (Huisman et al. 2003), electrical resistivity tomography (ERT) measurements (Garre et al. 2011), time-lapse gravity data (Christiansen et al. 2011) or ground-based microwave radiometry (Schwank et al. 2009). Recently, integral quantifications of seasonal soil moisture in the root zone at the scale of a field, a small watershed scale or a hydrologic response unit have become possible with a novel methodology introduced by Zreda et al. (2008) and Desilets et al. (2010), named cosmic-ray sensing.

The very first steps of this methodology were presented in a case study of Kodama (1984) in which estimations, both snow water equivalent and below-ground soil moisture, were indirectly derived by measuring "albedo neutrons", secondary products of cosmic radiation. More recently, based on

using neutron transport simulations and field measurements in grassland, first reliable measurements of soil moisture by counting above-ground natural fast neutrons were presented (Desilets et al. 2010). This methodology has been implemented in the Cosmic-ray Soil Moisture Observing System (COSMOS, Zreda et al. 2012). This type of measurement has been cited in literature in different ways, referring to the method itself (Kodama et al. 1980, Kodama et al. 1985, Zreda et al. 2008, Desilets et al. 2010, Rivera Villarreyes et al. 2011) or to the probe (Franz et al. 2012a, Franz et al. 2012b and Franz et al. 2013). According to the physical basics of the methodology that will be described in the sections below, in the following text, we refer to the methodology with the name Cosmic-Ray Neutron Sensing (CRS), which reflects that natural neutrons as product of the cosmic-ray are detected.

Indeed, the cosmic-ray neutron sensing shows a lot of potential for covering data requirements for large-scale studies, e.g. calibration and validation of land surface models and satellite-based soil moisture retrievals. Additionally, this data can improve existing world wide initiatives of soil moisture monitoring such as the International Soil Moisture Network (ISMN, Dorigo et al. 2011). However, there are still some open questions on this methodology that have to be evaluated such as (i) field verification of measurement volume (vertical penetration depth and horizontal footprint) in complex topographies (i.e. hill slopes); (ii) field verification of influence from other water environmental compartments (e.g. interception water, biomass water, ponded water, etc.), (iii) calibration approaches without using complex neutron transport models; (iv) transferability of calibration parameters to other locations; etc. Especially in agricultural fields, it was noted (Hornbuckle et al. 2012) that fast temporal variability of the vegetation by its growth contributes to an important modification of the neutron counting rate. Therefore, limitations can arise for the application of this methodology at agricultural sites and in general on agricultural water management. Therefore, in this study, our motivation is directed to investigate the following main points:

- to verify the reliability of using a single calibration curve for cosmic-ray neutron sensing in agricultural fields with continuous crop rotation. Field calibration approaches of different complexity will be considered in the analysis;

- to quantify the vegetation influence on the CRS and to investigate a neutron correction to account for the temporal variability of the vegetation.

3.2. Materials and methods

3.2.1. Basis of the cosmic-ray neutron sensing

Primary cosmic radiation (galactic and solar) penetrates the top atmosphere and creates a cascade of secondary cosmic rays after its interaction with atmospheric particles. Major composition of these secondary cosmic rays consists on neutrons. High-energy neutrons continue traveling through the atmospheric column until penetrate the ground surface. Some neutrons are absorbed completely, and others can randomly escape back to the atmosphere with a reduce energy (fast level). Intermediate-energy neutrons called fast neutrons (1–2 MeV; Hess et al., 1961) are so created as the product of interactions (collisions) between secondary cosmic ray particles and land surface materials such as soil, snow, plant canopies, etc. In these collisions, the hydrogen molecules play an important role due to its large neutron-moderation capabilities (elastic scattering cross section and stopping power) compared to other common elements found in soil minerals. Based on this interaction, first measurements were initially presented in a case study by Kodama (1984) in which estimations, both snow water equivalent and below-ground soil moisture, were derived. More recently, based on using neutron transport simulations and field measurements in a grassland, first reliable measurements of soil moisture by counting natural above-ground fast neutrons were presented (Zreda et al. 2008, Desilets et al. 2010). Neutron transport simulations were computed for specific soil moisture conditions (from 0 $\mathrm{m^3\,m^{-3}}$ to 0.40 $\mathrm{m^3\,m^{-3}}$) in silica-based soil with porosity of 0.40. Based on this modelling study, authors proposed a function to convert fast neutrons into soil moisture based on a probe installed above ground as:

$$\theta_{\mathrm{CRS}} = \frac{a_0}{\frac{N}{N_0} - a_1} - a_2 \tag{3.1}$$

where θ_{CRS} is the volumetric soil moisture [$\mathrm{m^3\,m^{-3}}$], N is the corrected neutron counting rate [-], a_i are dimensionless calibration parameters [-], and N_0 is defined as the corrected neutron counting rate over dry soil under the same reference conditions used for N. Calibration parameters were defined as $a_0 = 0.0808$, $a_1 = 0.372$ and $a_2 = 0.115$ from the modelling study. Equation and parameters are valid for soil moisture higher than 0.02 kg $\mathrm{kg^{-1}}$ (Desilets et al. 2010).

Further understanding of interactions between neutron and environmental H pools was achieved by Franz et al. (2013). The authors applied a universal calibration function to account for all different H pools in the CRS support volume. In the case of vegetation, constant aboveground biomass

was assumed for USA forest sites and provided improvements in relation
neutrons vs. hydrogen (expressed as hydrogen molecular fraction).

Horizontal spatial coverage of the CRS, called horizontal footprint, can
be defined as the land surface region from which 86 % of the counted fast
neutrons originate. Zreda et al. (2008) suggested adopting a value of approx-
imately 600 m as diameter, which was also verified by Desilets and Zreda
(2013). The measuring depth of the CRS, called effective depth, depends
on the mean free path length for elastic collisions in soil. This is on the
scale of tens of centimeters. Soil moisture controls CRS measuring depth
because the probability of neutron scattering and absorption events depends
mainly on the number of hydrogen molecules. Very recently, Franz et al.
(2012a) presented an equation based on the hydrogen contribution from the
soil moisture profile and mineral water content (or lattice water), as follows:

$$z^* = \frac{5.8}{\rho_b \cdot (\tau + SOC) + \theta + 0.0829} \qquad (3.2)$$

where z^* is the effective depth of the CRS probe [cm], ρ_b is the soil dry
bulk density [$\mathrm{g\,cm^{-3}}$], τ is the weight fraction of lattice water in the mineral
grains defined as the amount of water released at 1000 ^{o}C preceded by drying
at 105 ^{o}C [g of water per g of dry minerals], SOC is the soil organic matter
[$\mathrm{g\,g^{-1}}$] and θ is the average volumetric pore water content [$\mathrm{m^3\,m^{-3}}$] in the
profile, considering an average depth down to 40 cm as proposed in Zreda et
al. (2008).

3.2.2. Experimental site

Field measurements and monitoring activities were carried out at a low-
land farmland in Bornim (Brandenburg, Germany). The experimental site
consisted of a 30 ha agricultural cropped field and is located close to Potsdam
(30 km west of Berlin, Figure 3.1). At the same field in 2010, when cropped
with corn (Zea mays), Rivera Villarreyes et al. (2011) measured field-scale
soil moisture via the cosmic-ray neutron sensing. The climate in the study
area is classified as temperate oceanic climate (Cfb) according to Köppen-
Geiger classification (Köppen, 1936). The period of highest precipitation in
the area usually is between May and August, but varying between the years.
Based on historical data recorded at the meteorological station located 6 km
from the experimental site (Weather station Telegrafenberg, Potsdam), total
annual precipitation ranged between 374.6 mm (1976) and 825.9 mm (2007).
The mean monthly relative humidity seasonally varies between 67.6 % (May)
and 89.3 % (December). Analogously, the monthly averaged daily mean air

temperature were recorded as ranging from 1 ^{o}C (January) to 18 C (July) in this period.

According to geological and soil information (German national maps), the field site presents a homogenous geology (quartz sand) and homogenous sandy soil profiles. This information was extended with intensive measurements conducted in the field (Table 3.1). Texture analysis was conducted at the surface level (3 campaigns with 19 locations, asterisks in Fig. 3.1), top soil (0-40 cm at A-E, Fig. 3.1) and two deeper profiles (down to 150 cm with 10 cm intervals at B and D, Fig. 3.1). Measured texture revealed very high sand percentages from 80 % to 83 % and low clay percentages from 4.8 % to 8.5 $\sim$%. From soil profiles, predominant sandy texture decreases slightly with depth down to approximately 50-60 cm. Saturated hydraulic conductivity (K_{sat}), determined by constant head permeameter (Klute 1986), was also measured in undisturbed soil cores taken at 5 cm, 10 cm, 20 cm, 30 cm and 40 cm depth in five locations (A-E). The K_{sat} values are within order of magnitude of sandy soils (10^{-5} m s^{-1}, Hillel 1998). Shortly after sowing in two crop seasons (May 5th and Nov. 11th 2011), lattice water and organic matter was measured in five positions (locations A-E in Figure 3.1) at 5 cm, 20 cm and 40 cm depths. Lattice water in experimental site varied from 0.009 to 0.012 g g^{-1} and organic matter varied from 0.018 and 0.023 g g^{-1}. These low ranges are expected for sandy soils and geological conditions in experimental site. Values of lattice water tend in fact to be more relevant in soil types dominated by clay. In general, it is notable that the variability of soil properties is significantly lower (1 order of magnitude less) than at all COSMOS sites in USA (Zreda et al. 2012). This may also be related to farming activity (e.g. mechanical tillage, i.e. soil overturning, carried out before beginning of crop season). This process tends to homogenize soil structure and conditions every season in specific at first 30-50 cm of the soil that, as shown later, corresponds to the zone of investigation of the CRS.

3.2.3. Monitoring activities

The first monitoring period in this study consisted of the entire growing season of sunflower (Helianthus annuus) from 5th May 2011 (initial stage, shortly after sowing) until 5th September 2011 (harvest). Later field activities and monitoring were restarted from 11th November 2011 (initial stage, shortly after sowing) until 25th May 2012 (shortly before harvest), now cropped with winter rye (Secale cereale). We call these the sunflower period and the winter rye period. Because this study is focused on soil moisture estimations for the vegetative period, we do not present data during winter period 2011-2012 when soil was frozen and sometimes there was snow.
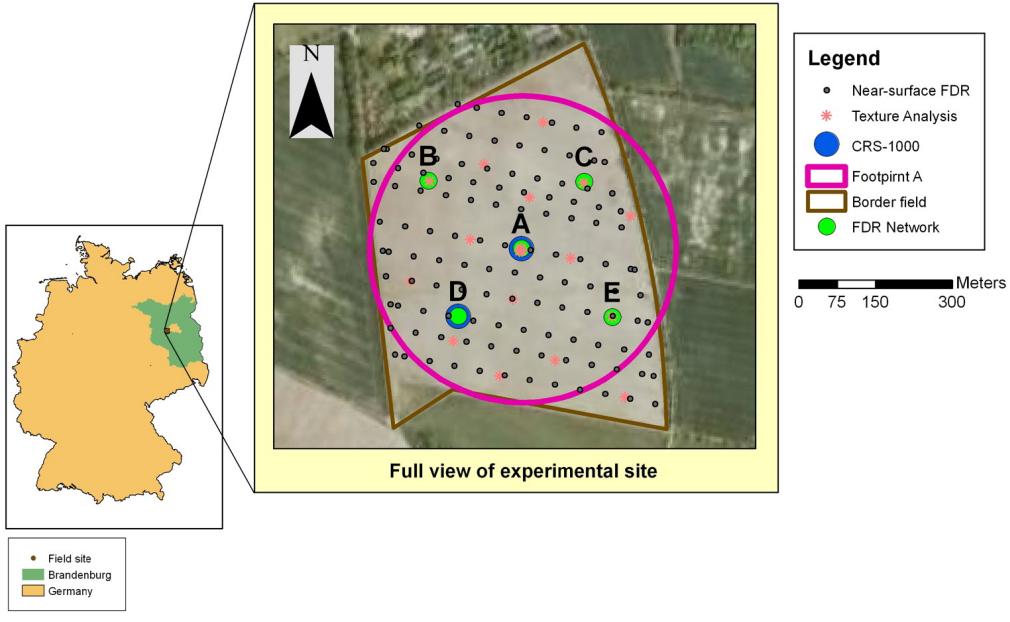
Figure 3.1: Monitoring network in Bornim during sunflower and winter rye
periods: FDR soil moisture positions (A, B, C, D and E) and CRS probe at
location A. Theoretical CRS probe footprint is represented by 600 m diameter
circle.

For purposes of understanding the cosmic-ray neutron sensing in cropped
fields and vegetation influence, crop survey and measurements of crop heights
were carried out throughout sunflower and winter rye season to identify the
different development stages. Crop height was monitored always in four
plants at five locations (A–E; see Fig. 3.1). Moreover, length of growing was
verified using data base from the Food and Agriculture Organization (FAO).

During the sunflower and winter rye periods, a cosmic-ray soil mois-
ture neutron sensor (CRS-1000, Hydroinnova, Albuquerque, USA), named
here with the abbreviation CRS probe, was installed. The probe contained
two proportional counters, a moderated counter surrounded by a low-density
polyethylene (for fast neutrons) and a second, bare counter (for thermal neu-
trons) installed in the center of the field (52.431^o N, 13.021^o E, WGS84, 84
m a.s.l.) named "A" in Figure 3.1. Only measurements from the moderated
counter are considered in the present study. The sensor was mounted on a
pole at a height of 1.5 m above-ground. The neutron pulse counting mod-
ules of the CRS probe was set-up to record counts during 20 min periods;
neutron counts were subsequently integrated into one-hour time intervals in

Table 3.1: Soil properties (texture, bulk density ρ_b, lattice water τ, organic matter OM and hydraulic conductivity K_{SAT}) in the CRS support volume measured at near-surface level and depths of FDR locations (5 cm, 20 cm and 40 cm). Standard deviation of each measure is presented in parenthesis. [*] Correspond to mean values from three campaigns. [**] Correspond to samples at 5 cm, 10 cm, 20 cm, 30 cm and 40 cm.

	Field	Sand [%]	Clay [%]	Silt [%]	ρ_b [$\mathrm{g\,cm^3}$]	τ [$\mathrm{g\,g^{-1}}$]	OM [$\mathrm{g\,g^{-1}}$]	K_{SAT} [$\mathrm{m\,d^{-1}}$]
19 locations (surface)*	Corn	81.2 (2.4)	7.3 (0.9)	11.6 (2.0)	1.40 (0.12)	-	-	-
FDR locations	Sunflower	74.7 (4.5)	10.2 (1.5)	15.1 (3.3)	1.32 (0.09)	0.012 (0.002)	0.023 (0.007)	2.62** (1.63)
FDR locations	Winter rye	74.9 (5.8)	13.7 (5.6)	11.4 (1.7)	1.43 (0.10)	0.009 (0.002)	0.018 (0.004)	-

data processing. It is well known that CRS signal variability increases in low altitudes, which is the case for our field site located 84 m a.s.l. In those conditions, a longer integration time of neutrons (e.g. 6 hrs–1 day) will give smoother soil moisture time series.

3.2.4. Ground-truthing soil moisture

In the present study, ground-truthing soil moisture for the CRS calibration and validation consisted in FDR (Frequency Domain Reflectometry, Theta Probes MR2, Delta-T Devices Ltd., Cambridge, UK) sensors installed inside CRS footprint. Zreda et al. (2012) recommended a CRS calibration with a soil moisture campaign collected in 18 locations wich a depth of 30 cm. The implementation of a continuous monitoring network of soil moisture facilitates a calibration-validation at any time of the season, as well understanding better a time-variable vegetation influence. However, major limitation in agricultural fields is that a monitoring network can not be placed permanently due to farmer's activities (tillage, fertilization and harvesting). Therefore, a small number of optimal FDR locations were identified for the estimation of the mean soil moisture. Locations were selected based on the specific characteristics of the experimental site (i.e. low spatial variability of soil properties within CRS support volume as discussed in previous section)

and the previous monitoring activities (Rivera Villarreyes et al. 2011).

In particular, five FDR locations (A-E, Figure 3.1) were chosen out of 18, based on their soil texture and the sensitivity radius for CRS calibration (25 m, 75 m and 175 m). Since the locations have to be representative of the mean soil moisture in the field, a further analysis of the locations was also conducted from time series of FDR soil moisture collected in 2010 in the same experimental site (Rivera Villarreyes et al. 2011). Time series of mean soil moisture from 19 FDR locations within the CRS footprint and the selected five FDR locations compared very well in terms of absolute value and temporal dynamics. The RMSE and correlation coefficient were $0.018 \, \mathrm{m^3 \, m^{-3}}$ and 0.952, respectively. The remained small deviation is partially explained by expected sensor and calibration error. Variability of soil moisture within CRS footprint was also intensively measured in two field campaigns during the previous season with corn in 2010. Using a mobile FDR sensor connected to a HH2 Moisture Meter (Delta-T Devices Ltd., Cambridge, UK), 121 near-surface locations (three replicates at each location) had been considered. These two campaigns had covered dry and medium wet conditions with mean values of $0.053 \, \mathrm{m^3 \, m^{-3}}$ and $0.14 \, \mathrm{m^3 \, m^{-3}}$, respectively and standard deviations of $0.014 \, \mathrm{m^3 \, m^{-3}}$ and $0.021 \, \mathrm{m^3 \, m^{-3}}$. Mean soil moisture from FDR mobile from first campaign were in good agreement with both mean soil moisture of 19 locations and mean of 5 locations selected. Mean values with 19 and 5 sensors slightly deviated from mean values of second campaign in 0.03 $\mathrm{m^3 \, m^{-3}}$, partly attributed to intrinsic sensor error ($\sim 0.01 \, \mathrm{m^3 \, m^{-3}}$). However, this is acceptable for our purpose, since CRS deviation due to vegetation changes, addressed in this study, is at least one order of magnitude higher than these deviations.

FDR were then installed at three depths (5 cm, 20 cm and 40 cm). The location of the deepest sensor was chosen according to predictions of CRS penetration depth (Eq. 3.2) and soil moisture values measured in 2010. This depth corresponds to maximum CRS effective depth estimated under driest conditions and considering lattice water and organic matter measured in the field.

As for the CRS probe, FDR sensors were set-up to record soil moisture every 20 min. Subsequently, FDR soil moisture was averaged to an hourly-time step and used for the CRS calibration/validation, as it is explained in the following sections. A standard calibration function for mineral soil type provided by FDR devices had been tested against soil samples in our previous study (Rivera Villarreyes et al. 2011) and was used now again. Verification of field-calibration was carried out with soil cores ($100 \, \mathrm{cm^3}$) taken shortly after harvest and before FDR installation (sunflower and winter rye). This former calibration function provides a RMSE of about $0.04 \, \mathrm{m^3 \, m^{-3}}$, where

most of this deviation appears at high soil moisture (≥ 0.20 m^3 m^{-3}).

3.2.5. Calibration of the CRS

Standard neutron corrections

Before the calibration of the CRS probe, fast neutrons were corrected by changes of local atmospheric pressure (Bachelet et al. 1965), incoming cosmic radiation (Zreda et al. 2012) and atmospheric water vapor (Rosolem et al. 2013). For the incoming cosmic-rays, neutron monitoring station Jungfraujoch in Switzerland (www.nmdb.eu) was used as reference station. Neutrons in Bornim were corrected by a factor defined as ratio of the measured neutrons in Jungfraujoch to its historical mean (179.71 counts s^{-1}). Correction of atmospheric water vapor is computed to take into account the daily variability of actual air density.

Fitting approaches for CRS equation

Soil moisture measurements (θ_{CRS}) via cosmic-ray neutron sensing were carried out using different fitting calibration approaches of Eq. 3.1 proposed in Desilets et al (2010). The universal calibration approach proposed very recently in Franz et al. (2013) is not considered in the present study, because for that approach all hydrogen pools needs to be quantified to disaggregate the hydrogen signal from soil moisture. In seasonal crops with fast-changing characteristics (i.e. aboveground biomass, biomass water content, root water content and others), these H pools may not easily be quantified due to limited frequency of measurements and invasiveness of existing measurement techniques (e.g. for roots and biomass). On the contrary, local calibration of Eq. 3.1 accounts already for the aggregation of the hydrogen contribution and the deviation from the ground-truthing soil moisture can be considered in the assessment of possible effects of different hydrogen pools (e.g., vegetation). We test three different fitting approaches to calibrate the CRS probe: (i) a three-parameter fitting approach altering a_0, a_1 and a_2 freely as proposed by Rivera Villarreyes et al. (2011), (ii) a one-parameter fitting approach with a factor, where θ_{CRS} is calibrated by downscaling and upscaling soil moisture (Hydroinnova, 2010), analyzing Desilets' parameters (2010), and (iii) a N_0-fitting approach according to Franz et al. (2012b) and Zreda et al. (2012). Mathematical relations and parameters fitted are presented in Table 3.2. Pros and cons of the different fitting calibration approaches are discussed in the result session (cf. section 3.2).

Table 3.2: Definition of three fitting approaches for Eq. 3.1. The N_0 value for the three parameter and factor-parameter fitting approaches was considered as the maximum counting rate measured in the field (1294 counts per hour).

Fitting approach	Equation	Fitting parameters
Three-parameters	$\theta_{\text{CRS}} = \frac{a_0}{N/N_0 - a_1} - a_2$	a_0, a_1 and a_2
Factor	$\theta_{\text{CRS}} = \left(\frac{0.0808}{N/N_0 - 0.372} - 0.115 \right) \cdot f_{cal}$	f_{cal}
Factor	$\theta_{\text{CRS}} = \frac{0.0808}{N/N_0 - 0.372} - 0.115$	N_0

CRS support volume

The CRS has a variable penetration depth depending on soil moisture (Eq. 3.2). In our former study (Rivera Villarreyes et al. 2011), CRS parameters were calibrating in a corn season assuming a significant decrease of the CRS depth ($\sim$ 5-10 cm) under wet conditions. However, these corn parameters results into a large overestimation of soil moisture (RMSE = $0.143\,\text{m}^3\,\text{m}^{-3}$) for sunflower and winter rye periods. The reason of this large difference may be attributed to the CRS penetration depth, which was recalculated using Eq. 3.2 and revealed a minimum observation depth of 20 cm. For this reason, in this study, we evaluated the CRS penetration depth for the three fitting approaches with four different ways of integrating reference FDR soil moisture:

- C1: constant penetration depth and equal neutron weights in depth,

- C2: variable penetration depth and equal neutron weights in depth,

- C3: constant penetration depth and variable neutron weights in depth, and

- C4: variable penetration depth and variable neutron weights in depth.

In all the cases the CRS values are taken to represent the soil water mass down to the effective penetration depth, with the given weighting with depth z^*. In the case of constant penetration depth (C1 and C3), the value of z^* was defined as 40 cm. This is the maximum value computed for driest conditions with Eq. (3.2), the mean penetration from ranges suggested by Desilets

(2010), and also coincides with deeper FDR sensor. In the case of variable penetration depth (C2 and C4), this was computed with the mean FDR soil moisture in Eq. (3.2). Cases C3 and C4 consider that neutrons from different depths are contributing differently to the total counts observed above-ground (Eq. 3.3-3.4). The neutrons measured aboveground are not produced uniformly in depth, also because of vertical distribution of soil moisture in the field. In terms of neutron moderation, neutron intensity tends to decrease exponentially when they penetrate a certain material (Hassanein et al. 2005 and Oswald et al. 2008). This exponential decrease is a function of the thickness and neutron scattering properties of the penetrating material; i.e. soil porous medium. Therefore, we adopt an exponential neutron weighting model to account for the neutron contribution from several depths as follows:

$$\alpha_z = e^{k \cdot z / z^*} \tag{3.3}$$

where α_z is the weighting neutron factor [-], z is the vertical depth [m], z^* is the penetration depth or effective depth for the CRS probe [m], and k is a negative constant which reflects how neutrons are originated from different depths. The value of k may reflect additionally some properties involved in the neutron transport such as macroscopic cross-section and stopping power. This parameter was simultaneously calibrated with the soil moisture equation, adding it in the optimization process; therefore, a direct parameter comparison between different cases, periods and calibration approaches is not possible. Discussion of using or not using a weighting function is based on values RMSE and performance of CRS soil moisture respect to ground-truth soil moisture. The weighted-value of soil moisture due to different neutron contributions in depth was defined as follows:

$$\theta_{FDR}^{av} = \frac{\int_0^{z^*} \alpha_z \cdot \theta_{FDR,z} \cdot dz}{\int_0^{z^*} \alpha_z \cdot dz} \tag{3.4}$$

where is the averaged FDR soil moisture used for CRS calibration with the cases C3 and C4 [$m^3\,m^{-3}$], is the FDR soil moisture observed at depth z [$m^3\,m^{-3}$], α_z is the weighting factor at depth z. The effective depth, z^* is constant for C3, but variable for C4. The definite integral in Eq. (3.4) was approximated by linear interpolation between the measurement depths.

In all the calibration approaches, no weighting function in the horizontal direction was applied to compute mean field soil moisture. It is expected that the contributing CRS signal decreases with radial distance. This CRS sensitivity distribution was partially accounted for by placing FDR profiles

(locations B, C, D and E in Figure 3.1) within the same sensitivity area defined by 175 m radius and one FDR profile in the area of maximum sensitivity (center, location A in Figure 3.1).

3.2.6. Calibration-validation of the CRS

The entire monitoring period with sunflower and winter rye was split into eight consecutive short periods (D1 to D8, Table 3.3), describing major vegetation stages. The periods D1-D4 for sunflower have approximately equal length (~ 30 days). In the case of winter rye, the initial stage (D5) is longer (~ 150 days), but the development stage (D6) is shorter (~ 20 days). Midseason and late stages (D7-D8) are comparable to stage length of sunflower period. Based on these periods, a split sampling calibration-validation was applied. All fitting approaches were separately calibrated for each crop growing stage (initial, development, middle and late/senescence) for sunflower and winter rye. The calibration was carried out minimizing the root mean square error (RMSE) between mean FDR soil moisture (5 profiles) and CRS soil moisture with the non-linear least square (NLS) library in R language and environment. Validation of the fitting parameters (a_0, a_1, a_2, f_{cal} and N_0) was carried out using periods outside of the calibration window.

The statistical significance of the calibration results (fitting approaches, cases and periods) was tested with an Analysis of Variance (ANOVA; Driscoll, 1996) test based on F-value (F-Statistics; Silvapulle, 1996) and a Student's t-test (Hedderich and Sachs, 2012). Here mean RMSE between fitting approaches (n = 32) and between calibration cases of depth integration (n = 24) was compared. For instance, the null hypothesis in ANOVA was defined as H_0: $\mu_3 = \mu_{f_{cal}} = \mu_{N_0}$, where μ_3, $\mu_{f_{cal}}$, and μ_{N_0} represent the mean RMSE for fitting approaches with three parameters, factor and N_0, respectively; and the alternative hypothesis (H_1) was set as "at least one of the RMSE is different". The Student's t-test was used to make one-by-one comparisons.

3.2.7. Neutron attenuation due to vegetation

The contribution of the vegetation to the CRS is investigated estimating the amount of neutrons attenuated by vegetation (N_{att}) as follows. The amount of neutrons expected (N_{exp}) by the soil moisture dynamics is computed from existing time series of soil moisture. In our case, Desilets' equation (2010) in Table 3.2 is inverted for known FDR soil moisture and compute values of N_{exp} for each fitting calibration approach proposed. The real number of counts observed during a specific vegetation period is directly measured in the CRS probe, which is called here N_{CRS}. Subsequently, the number of

Table 3.3: Field characteristics of the calibration periods during sunflower and winter rye periods. Notice that FDR soil moisture presented in table corresponds to the mean value at 5 cm, 20 cm and 40 cm depth.

Period	Crop	Growing stage	Duration [days]	Crop height [cm]	FDR soil moisture [$\mathrm{m^3\,m^{-3}}$]
D1	Sunflower	Initial	30	5 - 30	0.069 - 0.119
D2	Sunflower	Development	30	30 - 110	0.046 - 0.141
D3	Sunflower	Mid-season	30	110 - 150	0.090 - 0.224
D4	Sunflower	Late	34	110 - 125	0.122 - 0.165
D5	Winter rye	Initial	150	< 10	0.133 - 0.261
D6	Winter rye	Development	20	30 - 130	0.108 − 0.161
D7	Winter rye	Mid-season	40	130 - 140	0.045 - 0.105
D8	Winter rye	Late	33	140 - 150	0.057 - 0.179

neutrons attenuated by changes of vegetation outside of the calibration period (N_{att}) is defined as follows:

$$N_{att} = N_{exp} - N_{CRS} \tag{3.5}$$

Values of N_{att} are expected to have a temporal variability according to the vegetation stages. For instance, when calibration is conducted in a period of bare soil or shortly after sowing, N_{att} is expected to be positive for development, middle and late crop stages. Contrarily, when CRS is calibrated at maximum stage of vegetation, N_{att} in other periods (initial, development and late stages) becomes negative, since a reduction of vegetation biomass and vegetation water content happens. By definition, N_{att} is approximately zero within the crop stage when CRS probe was calibrated.

Since N_{att} should follow the crop stages, its temporal variability can be simplified according to the temporal dynamics of other vegetation parameters as defined in literature (e.g. FAO databases). This shape is mainly dominated by the length of crop stages, for example, considering constant values at the initial and middle crop stages, linear increase during development stage and linear decrease during late stage. Further information is described in detail in Allen et al. (1998). Accordingly, N_{att} is described by a piecewise linear function as follows:

$$N_{att}(t) = N_{att}^{Initial} \qquad\qquad 0 < t \leq t_1 \qquad (3.6)$$

$$N_{att}(t) = K_1 \cdot t + N_{att}^{Middle} \qquad\qquad t_1 < t \leq t_2 \qquad (3.7)$$

$$N_{att}(t) = N_{att}^{Middle} \qquad\qquad t_2 < t \leq t_3 \qquad (3.8)$$

$$N_{att}(t) = K_2 \cdot t + N_{att}^{Final} \qquad\qquad t_3 < t \leq t_4 \qquad (3.9)$$

where t_1, t_2, t_3 and t_4 are defined by the length of crop stages initial (L_i), development (L_d), middle (L_m) and final (L_f), respectively, which can be identified by measurements of crop heights or literature. The slopes in Eq. (3.7) and Eq. (3.9) are defined by:

$$K_1 = \frac{N_{att}^{Middle} - N_{att}^{Initial}}{L_d} \qquad (3.10)$$

$$K_2 = \frac{N_{att}^{Final} - N_{att}^{Middle}}{L_f} \qquad (3.11)$$

where $N_{att}^{Initial}$ and N_{att}^{Middle} are the averaged neutron attenuation at the initial and middle crop stages. The N_{att}^{Final} is the neutron attenuation observed at the end of the crop season (shortly before harvest), for instance it can be an average of the last measuring day.

Hence, the overall shape of attenuated neutrons (N_{att}) is defined with Eq. (3.6) through Eq. (3.11). These values are including to measured neutrons (N_{CRS}) according to Eq. (3.5) in order to compensate differences in vegetation along the entire growing season. Subsequently, a single set of calibration parameters can be applied for entire season using vegetation-corrected neutrons.

3.3. Results and discussion

3.3.1. Standard neutron corrections and integration time

The final range of corrected fast neutrons used for CRS probe calibration varied from 766 to 1294 counts per hour. The standard neutron correction due to changes of atmospheric pressure from the cosmic-ray neutron detector varied from 0.687 to 1.245. Neutrons at Jungfraujoch station showed a decreasing tendency (ranging from 0 to 10.7 %) of the incoming high-energy cosmic rays (data not shown) during the monitoring period, therefore the correction factor varied from 0.888 to 1.022. In the case of Jungfraujoch neutrons, best available data used was at the daily time resolution for our

monitoring period. Correction factor derived from Jungfraujoch was well comparable to Kiel neutron monitor station (Germany). However, neither of the two stations did not report a known cosmic-ray event (Ground Level Enhancements, GLE) on May 17th 2012 (www.nmdb.eu), but which coincides approximately, with a deviation of CRS soil moisture in comparison to the FDR (discussed later). Correction due to atmospheric water vapor (factor from 0.962 to 1.048) in our field conditions was more relevant during winter period 2011-2012, here air density drops significantly down in a longer cold period.

Neutron counts per hour (cph) detected at the experimental site at low altitude are relatively low in comparison to other studies, e.g. COSMOS site Mt. Lemmon (Arizona, 2745 m a.s.l.) with range from 1800 cph to 3600 cph (Desilets et al. 2010). Therefore, analysis in further sections is based on mean daily values of neutron counts in order to smooth natural variability of fast neutrons observable at shorter time resolution.

3.3.2. Comparison of fitting approaches

The summary of three approaches and cases for depth integration (C1-C4) is presented in Table 3.4 and Figure 3.2. Results of all calibration parameters from three fitting approaches are presented in appendix B.

In general, calibration approaches fitting one single parameter (f_{cal} or N_0) provide smaller mean values (n = 32) of RMSE between mean FDR soil moisture and CRS soil moisture, compare to approach fitting three parameters (a_0, a_1, and a_2). The mean values of RMSE were 0.033 $m^3\,m^{-3}$, 0.030 $m^3\,m^{-3}$ and 0.029 $m^3\,m^{-3}$ for the three-parameter, factor and N_0-calibration fitting approaches, respectively. Statistical difference was observed between three-parameter approach and single-parameter approaches (f_{cal} and N_0), but not between two single-parameter approaches.

Comparing simple case of depth integration (C1) and periods (D1-D8), different fitting calibration approaches were in general very similar, except some remarkable results. For instance, a period of calibration with wet soil moisture conditions (e.g. D5), three-parameter and N_0-parameter approaches provide similar calibration error (0.012 $m^3\,m^{-3}$ and 0.013 $m^3\,m^{-3}$, respectively). However, RMSE in validation period is larger for three-parameters (0.034 $m^3\,m^{-3}$) compared to single parameter with 0.030 $m^3\,m^{-3}$. Opposite situation occurred within another wet period (D3) with comparable RMSE ($\sim$ 0.013 $m^3\,m^{-3}$), but now the three-parameter approach provides lower validation RMSE (0.039 $m^3\,m^{-3}$) than N_0-parameter with 0.043 $m^3\,m^{-3}$. In the case of dry periods of calibration (e.g. D2 and D7), single-parameter approaches consistently provided higher calibration RMSE (0.018 $m^3\,m^{-3}$)

Table 3.4: Summary of averaged root mean square error (RMSE) in $\mathrm{m^3\,m^{-3}}$ from three fitting approaches (Table 3.2) of CRS calibration and four cases of integrating FDR soil moisture in depth (C1-C4). Same letters in superscript represent samples that are considered statistically the same, based on ANOVA test and Student's test at 95 % significance level.

Fitting approach	C1	C2	C3	C4	Avg. RMSE*
Three parameters	0.039^d	0.032^d	0.031^d	0.031^d	0.033^a
Factor	0.032^e	0.029^e	0.029^e	0.029^e	0.030^b
N_0-approach	0.029^f	0.028^f	0.029^f	0.029^f	0.029^b
Avg. RMSE**	0.033^c	0.030^c	0.030^c	0.030^c	-

* Computed for each approach.
** Computed for each case of depth integration.
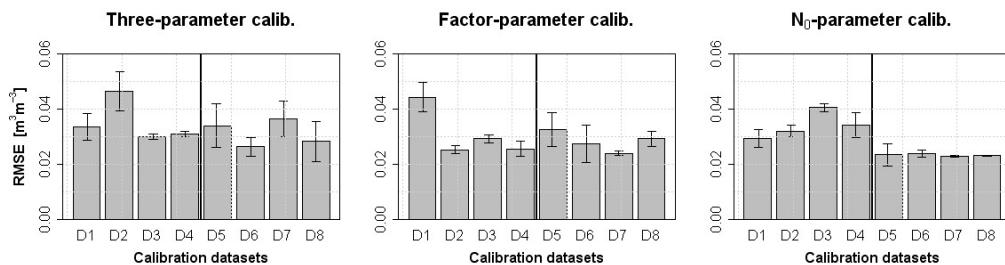
Figure 3.2: Comparison of the three calibration approaches in terms of root mean square error (RMSE, $\mathrm{m^3\,m^{-3}}$) for the three-parameter approach, factor-parameter approach, and N_0-parameter approach evaluated in eight crop seasons (Table 3.2) and with four calibration cases for depth integration (C1-C4). Notice that (i) the error bars are defined by one standard deviation computed from the calibration cases (i.e. different penetration depths), and (ii) RMSE corresponds to the validation period, outside of calibration window (split sampling).

than three-parameter approach (< 0.01 m^3 m^{-3}), but validation RMSE for three-parameter approach becomes double (~ 0.05 m^3 m^{-3}) than other two (< 0.029 m^3 m^{-3}). In this specific case study, a simple selection of one calibration fitting approach is not possible, since selection of calibration period (i.e. growing stage) becomes much more relevant for overall RMSE for entire season and two crops.

The effective depth for cases C2 and C4 ranged between 18 cm and 45 cm with the assumptions of $\tau = 0$. Introducing the measured value of lattice water 0.0012 g g^{-1}, penetration depth decreased down to 40 cm in dry periods. The real penetration depth may be slightly less than the range estimated here due to influence of vegetation cover but exact quantification was not possible in the present study. Cases with constant CRS depth (RMSE = 0.033$\pm$0.009 m^3 m^{-3}) and variable CRS depth (RMSE = 0.030 $\pm$ 0.007 m^3 m^{-3}) do not provide a statistical difference at the 5 % significant level based on Student's t-test. There was neither difference including or not a weighting function (cases C3 and C4) both with m^3 m^{-3}. Our observations of no need of weighting function are in agreement with Franz et al. (2012a) and Franz et al. (2012b), who evaluated a linear function for depth weighting. Therefore, neutron weighting scheme in depth may indeed not alter significantly performance of CRS soil moisture. However, it has to be noted that mean FDR soil moisture from 5 cm down to 40 cm is statistically comparable to weighted-mean FDR value according to z^* using Eq. (3.2). Therefore, we could not conclude on variable CRS penetration depth for other situations. Further research is required in this direction, e.g. with heterogeneous soil moisture profiles, in order to evaluate if CRS depth can be indeed simplified as constant or not.

Overall, different periods considered, the fitting approaches provided similar minimum RMSE (~ 0.02 m^3 m^{-3}). This range of RMSE is comparable to other studies such as Franz et al. (2012a) and Franz et al. (2012b). However, it is worthy to mention that these studies have performed CRS measurements in higher altitude locations, where CRS uncertainty decrease. Here, daily mean computations of soil moisture have been chosen to overcome low numbers of counts measured. Also, there are clearly pros and contra on the use of the different fitting approaches. For instance, the three-parameter approach requires a longer calibration period and with higher soil moisture dynamics in order to perform properly its nonlinear fitting. Clear advantage of this approach is however its high flexibility adapting to temporal variability of FDR soil moisture, compared to the one-parameter approach. On the contrary, both simple-parameter approaches can be calibrated with a few CRS data of soil moisture, e.g. at least 6 hrs–1 day at our experimental site. However, since entire time series of soil moisture relies on a single calibration

day, field conditions (especially incoming radiation and soil moisture) at the day of calibration become more important and weaken its representativeness to the rest of time series.

To better understand this behavior, the N_0- and f_{cal}- fitting approaches were then calculated also at daily time step. In general long term variability of RMSE was similar using daily or monthly computation. This reflects that few single-days soil samplings for calibration along the vegetative period are sufficient with a single parameter calibration (f_{cal} and N_0) as proposed in literature (Zreda et al., 2012). However, RMSE by choosing f_{cal} and N_0 at different days was highly variable in some cases. For instance, Figure 3.3 shows the variability of the calibrated parameters choosing a day at the middle stage of winter rye. The parameters strongly changed and, consequently, RMSE switched from 0.067 $m^3\,m^{-3}$ to 0.023 $m^3\,m^{-3}$ (N_0 approach) and from 0.206 $m^3\,m^{-3}$ to 0.022 (factor approach). This large overestimation was caused by calibrating one day in a week with very dry soil moisture (0.045 $m^3\,m^{-3}$), which coincided with maximum counting rate of the CRS probe. It has also to be noted that this variability corresponds also with a period a few days after the cosmic-ray event observed in world-wide neutron monitoring stations that, however, was not recorded at the station considered for the incoming neutron correction (e.g. Jungfraujoch and Kiel). Further research is required in order to investigate representativeness of neutron monitoring stations for corrections of CRS probe signal.

3.3.3. Effect of crop growing season on CRS soil moisture

From statistical analyses, we found a large variability of calibration performance (RMSE increased from 0.021 $m^3\,m^{-3}$ to 0.056 $m^3\,m^{-3}$) by choosing different calibration periods (D1-D8). Variability is more evident in the sunflower period than in the winter rye period from RMSE values (Figure 3.2). This is attributed to differences in soil moisture and crop characteristics during these two periods. Sunflower period covers entire plant growth, with similar stage lengths compared to winter rye period which has a long initial stage (with almost not vegetation, height < 10 cm), followed by a fast development.

Periods with minimum RMSE (for simple case C1) were identified in periods with crop cover of sunflower and winter rye. For instance, three-parameter and factor-parameter approaches reached minimum seasonal RMSE in maximum stage of sunflower. The N_0-parameter approach identified a minimum seasonal RMSE at period D7 and D8 with maximum stage of winter
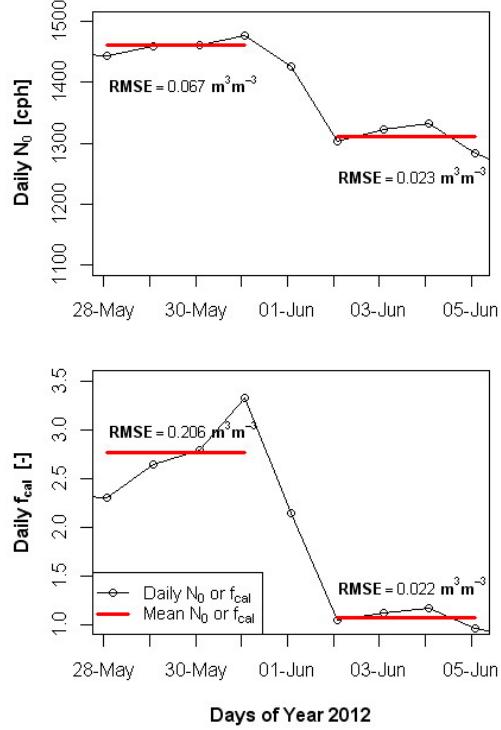
Figure 3.3: Daily computations of N_0 parameter (upper) and fcal parameter (lower) for a short period of middle stage of winter rye (D7). In both cases, red lines represent the mean values (four consecutive days). The RMSE between FDR soil moisture and CRS soil moisture for entire sunflower and winter rye periods is computed using mean values of N_0 and f_{cal} (red lines) in these short periods and presented in graph.

rye. In both periods, biomass and other crop characteristics are completely developed. Clearly, these results showed that CRS parameters calibrated at middle crop stage are also representative for others stages (with some deviation to FDR soil moisture, discussed later), because major extension of season is covered with vegetation, except initial stage (sunflower and winter rye).

Since minimum and maximum values of RMSE (Appendix B) depend on periods with or without significant vegetation cover, we focused this and next sections on a comparison of two periods: a period with significant higher vegetation influence (D3, middle sunflower season) and a period with significant lower vegetation influence (D1, initial stage of sunflower). CRS soil moisture with parameters from D3 and D1 periods for the three fitting approaches and constant penetration depth are shown in Figure 3.4. In general, periods of

68

CRS overestimation and underestimation to FDR profiles are associated to vegetation growing stages. For instance, using the period with low vegetation cover (i.e. low above- and below-biomass and its water content) provides a systematical overestimation of soil moisture for periods when crop reached its maximum stages. This overestimation was more evident in sunflower periods (D3-D4) than in winter rye periods (D6-D8).
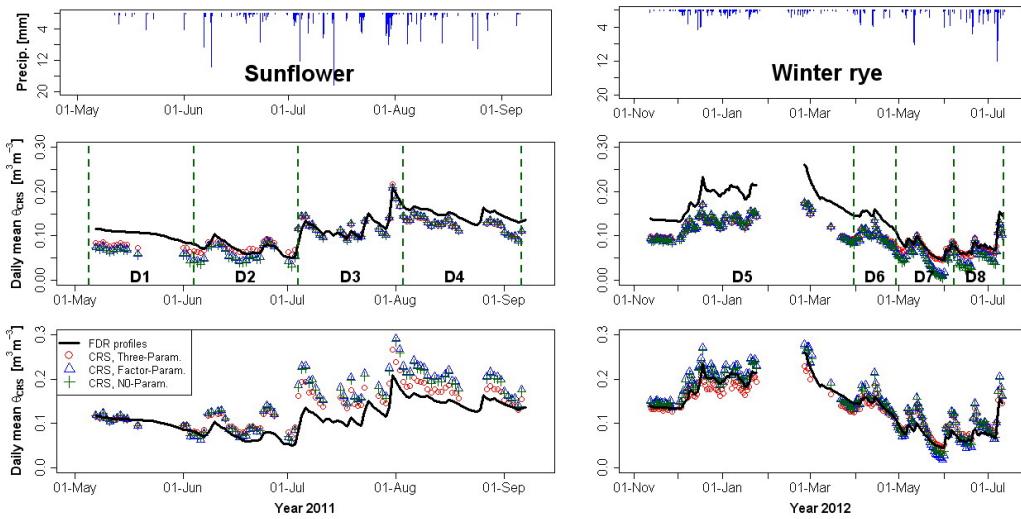
Figure 3.4: Time series of daily mean soil moisture during the sunflower period (left side) and winter rye period (right side); from top to bottom: (i) daily precipitation, (ii) FDR soil moisture and CRS soil moisture with calibration parameters from period D3, and (iii) FDR soil moisture and CRS soil moisture with calibration parameters from D1 period. No vegetation corrections are applied here.

Underestimation of soil moisture occurred using parameters from maximum sunflower development (D3) in other periods of sunflower (D1, D2 and D4) and winter rye (D5 and D6). For example in the drier period (May 2011, initial sunflower stage) with few precipitations and decrease of soil moisture by evapotranspiration, CRS underestimated the FDR soil moisture around $0.05 \ \mathrm{m^3 \, m^{-3}}$. Here, calibration parameters (D3) implicitly show already a crop influence (i.e. above and below biomass), but therefore they are hampered to predict precisely values of soil moisture in this period. At the end of winter rye season (D7-D8), D3 parameters performed better because biomass and crop water content increased according to crop stages. In both cases deviation was lower using the three-parameter approach compared to other two single-parameter approaches

69

Beside vegetation influence on CRS soil moisture, measurements are in good agreement with precipitation events, which is reflected by the good match to dynamics of FDR soil moisture (e.g. beginning and end of July 2011).

3.3.4. Neutron attenuation by vegetation and improvement of CRS soil moisture in cropped fields

Temporal variability of crop hydrogen-pools along season, as well spatial variability within the crop above- and below-ground biomass and root distribution, make it more challenging to interpretate the CRS signal in a cropped field. For instance, in the specific experimental site, fast neutrons decreased along the sunflower season (at least until its maximum stage) from 981-1104 counts per hour (initial stage with 5 cm height) up to 766-944 counts per hour (middle season with maximum height of about 150 cm). Thus, the relation between fast neutrons and soil moisture is not unique throughout the crop season. This behavior is shown in Fig. 3.5 with a scatter plot between soil moisture and relative neutrons (N/N_0). Calibration curve (high vegetation influence, e.g. D3 period and three-parameter approach) fitted well the datasets for the mid-season (D7) and late season (D8) of winter rye. In periods D7 and D8, fast neutrons may be similarly moderated than in period D3. This is because the two crops have its maximum development stage. In other periods deviations are larger due to vegetation changes.

To overcome these deviations, time series of neutrons were corrected by fitting a model for vegetation attenuation using values of N_{att} and Eq. (3.5) as shown in Figure 3.6. This allows to recalculate CRS soil moisture, to be illustrated subsequently. Vegetation-attenuated neutrons with calibration parameters from periods of high and low vegetation influence (periods D3 and D1, respectively) are shown for three fitting approaches, as discussed in previous section, (Figure 3.4). Values of N_{att} were fitted according to a piece-wise linear model following crop-development shape suggested by Allen et al (1998), as shown from Eq. (3.6) through Eq. (3.9). In general, values of N_{att} computed for three fitting approaches and with parameters of two periods (D1 and D3) follows very well proposed crop-development shape according to literature (Allen et al., 1998). At the period of calibration (D1 or D3), N_{att} is approximately zero and in other periods depends on crop stage during calibration period. Estimations with D3 parameters indicated a decrease of vegetation influence at periods D1, D2 and D4. During initial stage of winter rye (without vegetation), N_{att} is also negative, subsequently values of N_{att} for periods D7 and D8 are comparable to D3 period. This suggests that neu-
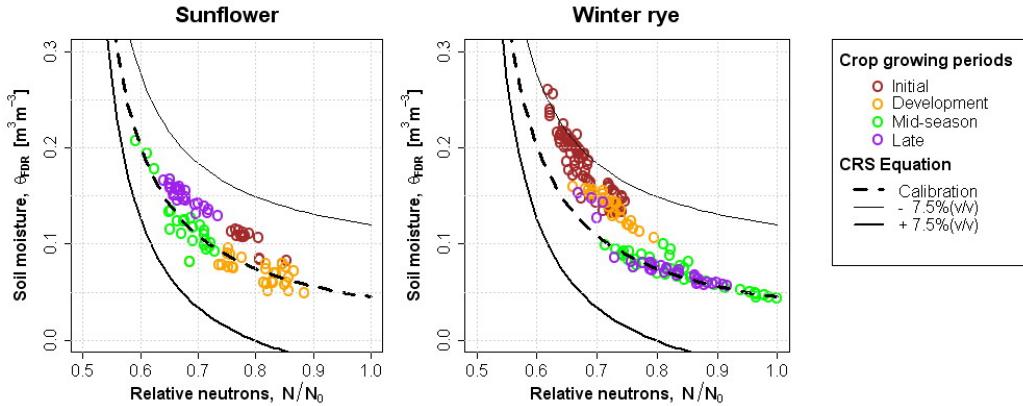
Figure 3.5: Relation between daily mean FDR soil moisture and daily mean relative fast neutrons (N/N_0) during sunflower and winter rye periods: CRS calibration curve (D3 period with high vegetation influence, constant penetration depth and three-parameter fitting approach) is plotted as the dashed black line and its readjustment by an increase ($+0.075$ $m^3\,m^{-3}$) or decrease (-0.075 $m^3\,m^{-3}$) of crop water content respect to calibration curve is plotted in continuous lines.

trons attenuated by vegetation are similar in maximum stages of sunflower and winter rye.

In the case of N_{att} computed with D1 period, values of N_{att} are general higher (positive) to periods when crops reached maximum stages (D2, D3, D4, D7 and D8). Periods with comparable neutron attenuation than D1 period have similar values of N_{att} ($\sim$ zero), e.g. D5 and D6 in winter rye. The fit cannot account for the sharp decrease of N_{att} (e.g. end of May 2012). The behavior observed in these few days is not attributed to vegetation changes or to rain and intercepted water (relatively dry period). Changes may be attributed to local variability of incoming radiation, which could not be corrected for using data from Jungfraujoch.

After vegetation correction (Figure 3.7), the CRS soil moisture clearly improved and the overestimation and underestimation attributed to parameters with periods of low and high developed vegetation (D1 and D3 respectively) significantly was minimized. The improvement of CRS soil moisture during sunflower period was comparable for three fitting approaches even if in the winter rye period, the three-parameter approach performed slightly better than other two approaches after corrections. RMSE decreases from 0.023 $m^3\,m^{-3}$ down to 0.012 $m^3\,m^{-3}$ using D1 parameters, and from 0.038 $m^3\,m^{-3}$ down to 0.015 $m^3\,m^{-3}$ using D3 parameters for the three-parameter approach.

The RMSE for factor-parameter approach reduced from 0.034 $m^3\,m^{-3}$ down to 0.023 $m^3\,m^{-3}$ (D1) and from 0.040 $m^3\,m^{-3}$ down to 0.015 $m^3\,m^{-3}$ (D3). The RMSE for N_0-parameter approach reduced after corrections from 0.031 $m^3\,m^{-3}$ down to 0.019 $m^3\,m^{-3}$ (D1), and from 0.041 $m^3\,m^{-3}$ down to 0.017 $m^3\,m^{-3}$ (D3). These final values of RMSE after corrections are well comparable to other studies with constant biomass (i.e. forest) or slow-changing biomass (Franz et al. 2010b).

The improvement of CRS soil moisture was substantially, though not all N_{att} values (daily resolution) fitted perfectly model according to crop development. Noise identified in time series of N_{att} is most substantial in winter rye period, when crop was in its maximum stage and it is not an expected fluctuation of N_{att} values. Moreover, this short-term variability of N_{att} may not be attributed to other dynamic hydrogen pools not considered like crop interception, since this period is relatively dry. Moreover, these discrepancies
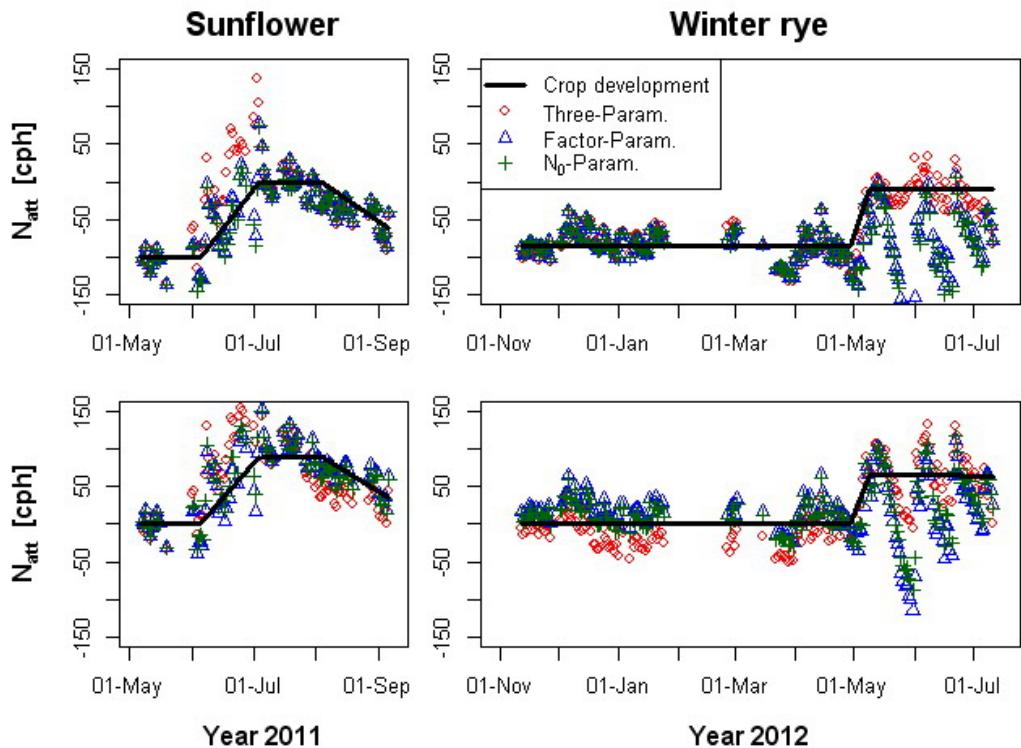
Figure 3.6: Vegetation-attenuated neutrons computed for period of high crop influence (D3, upper panel) and low crop influence (D1, lower panel) for three fitting approaches along sunflower and winter rye periods. Piecewise linear fitting proposed is according to crop development in literature (Allen et al 1998).
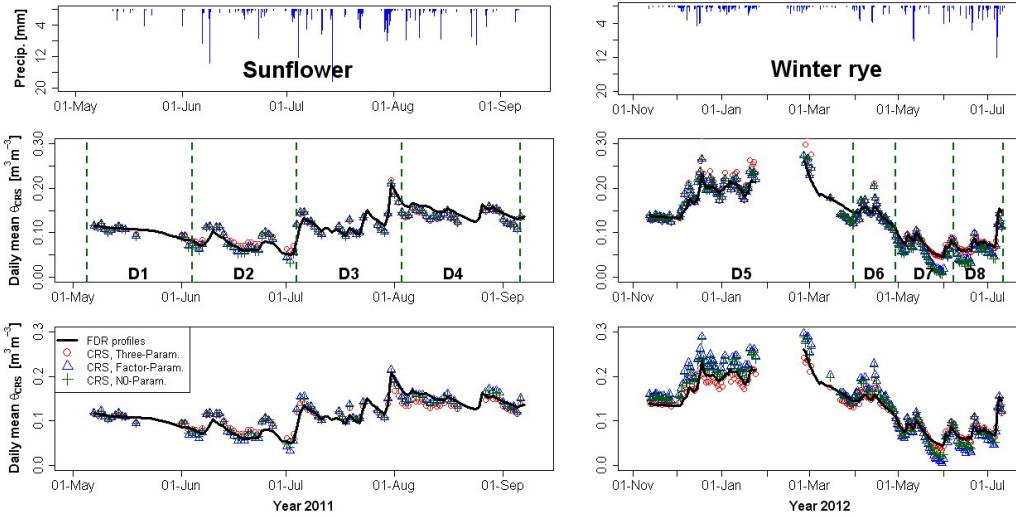
Figure 3.7: Improved CRS soil moisture estimation by correcting for crop development, for different calibration approaches. Time series of daily mean soil moisture during the sunflower period (left side) and winter rye period (right side), from top to bottom: (i) daily precipitation, (ii) FDR soil moisture and CRS soil moisture with calibration parameters from period D3, and (iii) FDR soil moisture and CRS soil moisture with calibration parameters from D1 period.

largely occurred in factor-parameter and N_0-parameter approaches, which are using same a_i parameters in Eq. (3.1). Also during this period, soil moisture conditions are approaching permissible limit of CRS parameters and equation (Desilets et al 2010). As discussed previously, an increase of incoming radiation, not corrected by the data from Jungfraujoch station cannot be discarded.

Finally, the neutron attenuation by vegetation is compared with the crop height (Figure 3.8). There is a clear relationship to crop height from initial through middle stage. However, we observed that crop height is not a well descriptor of vegetation-attenuated neutrons at the late part of sunflower and winter rye season. Here, crop height is slightly increased, but crop dries out significantly. Therefore, the relationship between absolute values of N_{att} and crop height is not anymore well defined. It can be speculated that other crop parameters, e.g. crop biomass and leaf area index (LAI) should be considered for an estimation of the vegetation correction in this late stage of the crop development.
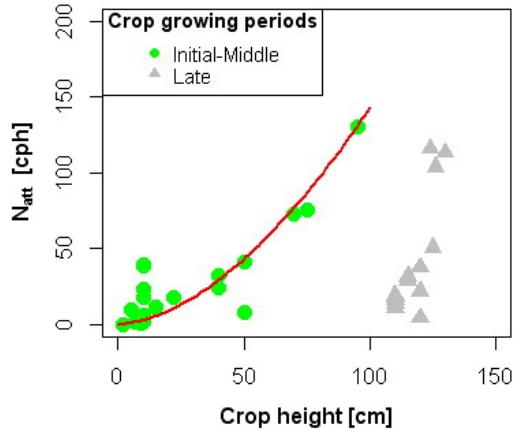
Figure 3.8: Correlation between vegetation-attenuated neutrons (N_{att}) and measured crop height of sunflower and winter rye. The two colors indicate periods from initial to middle stages (green) and late/senescence stage (gray) for the two crops. The red line is a fitted trend line for initial-middle stages.

3.4. Conclusions

This study evaluates the applicability of the cosmic-ray neutron sensing (CRS) method for field-scale soil moisture measurements in a farmland cropped with sunflower in 2011 and winter rye in 2012. The main conclusions are summarized as follow:

- In this specific case study, a simple selection of one best calibration fitting approach was not possible, because three approaches provided similar values of minimum RMSE ($\sim 0.02 \, \mathrm{m^3 \, m^{-3}}$). Analysis indicated that selection of calibration period (i.e. growing stage) becomes much more relevant than the manner how CRS equation is fitted. However, applicability and limitations between approaches arise mainly from practical aspects such as availability of relatively long time series of soil moisture for calibration (three-parameters fitting) and strong dependency on variability of neutron fluxes (single-parameter approaches);

- due to the relatively homogeneity of the soil layers and soil moisture profile at the experimental site, it was not possible to conclude differences in respect to handling penetration depth;

- CRS for soil moisture measurements in cropped fields is highly affected by vegetation along the growing season. For the specific case study,

74

deviations were quantified to reach 10.4 % of counting rates and approximately 0.11 $m^3 m^{-3}$ of soil moisture;

- deviations are time- and crop-dependent; however, the temporal dynamics of the vegetation–attenuated neutrons showed to be well related to crop growing stages (initial, development, middle, senescence);

- the minimum RMSE was achieved in periods of maximum crop development for all three different fitting approaches. This is a case-specific result because a major part of the season were covered with vegetation, except first weeks of initial stage of sunflower and major part of initial stage of winter rye;

- a time-variable neutron correction was successfully applied based on vegetation-attenuated neutrons (N_{att}). An improvement of CRS soil moisture was achieved with a single set of calibration parameters for entire growing season and two crops. This approach was tested for two calibration periods with low and high crop development. It is important to note that this result was independent from fitting approach and calibration period;

- crop height was well correlated with the vegetation-attenuated neutrons at beginning and middle of growing season, but showed large deviation during senescence stage. Further research should be focused on the evaluation of other vegetation parameters (e.g., LAI) and their correlation to attenuated neutrons, and the introduction of vegetation corrections.

Overall, this study successfully tested the applicability of the cosmic-ray neutron sensing in cropped fields. Cosmic-ray neutron sensing has the potential to provide reliable measurements of soil water mass storage between point scale and remote sensing scale also for cropped fields. However, practical ground-truthing approaches have to be applied and special attention should be taken on vegetation influence in cropped fields. Proceed for CRS vegetation corrections are an important step to improve applicability of the cosmic-ray neutron sensing in cropped fields and for agricultural water management.

Chapter 4

Inverse modelling of cosmic-ray soil moisture for field-scale soil hydraulic parameters

Abstract

We investigated inverse modelling of soil moisture measured via cosmic-ray neutron sensing (CRS) in order to estimate root zone soil hydraulic properties at the field scale. HYDRUS-1D model was calibrated with PEST (Parameter Estimation Software) using global optimizer Covariance Matrix Adaptation - Evolution Strategy (CMA-ES). Integral CRS measurements collected in a sunflower period in a farmland in Germany were considered in the study. The data were transformed to soil water storage, to allow a direct model calibration via HYDRUS soil-water balance. Effective parameters at the CRS scale were compared against local measurements and other inversely-estimated soil parameters from independent soil moisture profiles. Moreover, CRS-scale soil parameters were tested based on how these reproduce field soil moisture (vertical distribution) and soil water storage.

This framework provided good estimations of effective soil parameters at the CRS scale. Simulated soil moisture in different depths at the CRS scale was in agreement to field observations. Moreover, simulated soil water storage at the CRS scale is well comparable to calculations derived from point-scale profiles, despite their different support volumes. Soil hydraulic functions with CRS-scale parameters were contained within parameter variability identified from all inverse simulations at the local scale. This study

proves the potential of the CRS for inverse estimation of soil hydraulic properties.

4.1. Introduction

An adequate hydrological description of water flow and contaminant transport in the vadose zone relies on accurate estimate of the soil water retention and hydraulic conductivity functions (Vrugt and Dane, 2006). Moreover, the fact that soil properties may be highly variable in both horizontal and vertical directions increases the complexity to find a representative set of soil hydraulic properties for a specific scale. Moreover, this soil heterogeneity can be fully modeled in a deterministic way, because it would require too much data and computational effort (van Dam and Feddes, 1996). At the modelling scale, alternatively one could interpret the soil as an equivalent quasi-homogeneous medium with effective soil hydraulic properties (Gómez-Hernández and Gorelick, 1989; Zhu and Mohanty, 2003; Amor and Mohanty, 2008). Such properties could predict the average hydrological behavior at the scale of interest (Wildenschild and Jensen, 1999; Jhorar et al., 2004). For example, Mohanty and Zhu, (2007) estimated effective parameters based on matching the mean surface flux (evaporation or infiltration) irrespective of soil moisture and pressure profiles distribution. On the other hand, the existence of effective soil hydraulic properties at coarser scales is still an open question (Durner et al., 2008).

At the field and catchment scale, beside the upscaling approach (or bottom-up approach) of point-scale observations (e.g. soil cores and pedotransfer functions, Miller and Miller, 1956; Clausnitzer et al., 1992), the inverse modelling (Hopmans and Simunek, 1999; Vrugt and Dane, 2006; Durner et al., 2008) and assimilation techniques (Li and Islam, 1999; Pauwels et al., 2001; Heathman et al., 2003; Han et al., 2012; Yu et al., 2012) has become also an alternative for the estimation of soil hydraulic properties. In this study, we focused on the inverse modelling approach.

Inverse modelling is a frequently-employed approach to estimate effective parameters, at scales ranging from laboratory samples to regional applications. According to Vrugt and Dane (2006), inverse modelling research has been focused on (i) type of transient experiment and kind of prescribed initial and boundary conditions, (ii) investigation of different types of data (e.g, soil moisture, pressure, percolation, etc.) in several spatiotemporal scales for inverse simulations, (iii) appropriate model for representing soil hydraulic properties, (iv) adoption and development of Bayesian and multi-criteria techniques for uncertainty of estimated parameters, and (v) construction and

weighting of multiple sources of information in an objective function. From
all these research directions, two major groups also appear such as the fre-
quentist (classical) and Bayesian approaches. The first one is related to the
classical statistics considering fixed and unknown model parameters, and the
second treats model parameters as probabilistic variables (Vrugt and Dane,
2006). In this study, we focused on the understanding a new type of avail-
able soil moisture data (explained below) using a classical inverse modelling
approach.

Clearly, feasibilities of inverse modelling depend on algorithm used for
global search. Among others, some of these are the Shuffled Complex Evo-
lution (Duan et al., 1992), Annealing simplex methods (Pan and Wu, 1998),
Genetic algorithms (Takeshita et al., 2000), Grid sampling strategy (Ab-
baspour et al., 1997), Ant-colony methods (Abbaspour et al., 2001), and
Covariance Matrix Adaptation – Evolution Strategy (CMA-ES, Hansen et
al., 2003). It is worth to mention that this study does not focus on a deep
insight on algorithms; instead we are interested more in testing new kind
of available data for applicability of inverse modelling, as explained below.
Therefore for simplification, we chose one algorithm (CMA-ES) for this study,
which has been already tested in our modelling framework (cf. methodology
section).

One of the common state variables used in inverse modelling is soil mois-
ture. Due to measuring gap of soil moisture at the intermediate scale (Robin-
son et al., 2008), inverse modelling at large scale with field data is mainly
limited to the remote sensing scale (Feddes et al., 1993; Chang and Islam,
2000; Jhorar et al., 2004; Santanello Jr et al., 2007; Amor and Mohanty,
2008). In this case, parameter estimates and their uncertainty are also linked
to drawbacks of remote sensing such as limited time resolution (e.g. overpass
of 1-3 days by SMOS sensor or 46 days by ALOS sensor), lateral resolution
(e.g. ca. 40 km pixel of SMOS), near-surface observation depth (Santanello
Jr et al., 2007; Montzka et al., 2011); land cover and cloudiness (Jagdhu-
ber, 2012); etc. To overcome these limitations, in this study we investigate
the feasibility of recently-introduced measurement of soil moisture at the in-
termediate scale on the use of inverse modelling. The cosmic-ray neutron
sensing (CRS, Franz et al., 2012; Zreda et al., 2012; Rivera Villarreyes et
al., 2013a), as well named as ground albedo neutron sensing (Rivera Villar-
reyes et al., 2011), provides continuous measurements of field soil moisture
with a deeper penetration depth than remote sensing products; therefore, the
CRS approach is ideal to investigate effective soil hydraulic properties at the
root zone within the extension of small catchment scale or agricultural field
with inverse modelling. The CRS methodology is a ground-based approach
of soil moisture, successfully applied in several cropped fields in Germany

along different seasons (Rivera Villarreyes et al., 2011; 2013a). Likewise, the existing COSMOS Network using the CRS methodology provides soil moisture information at the continental USA (Zreda et al., 2012) and a few other locations worldwide. In this study, we present a simple approach for incorporating firstly the CRS methodology in a hydrological modelling framework, and secondly to derive inversely effective soil hydraulic properties using CRS soil moisture. To our knowledge, this is the first study presented yet on combination of cosmic-ray neutron sensing, inverse modelling and determination of soil hydraulic parameters. The main objectives of this study are:

- to adapt CRS soil moisture data in an inverse modelling framework

- to estimate effective soil hydraulic properties at the CRS measurement scale of about 27 ha

- to verify CRS effective soil hydraulic properties against local observations (soil moisture and saturated hydraulic conductivity)

4.2. Materials and methods

4.2.1. Field measurements and monitoring

The experimental site is located in a cropped field in Bornim (Brandenburg, Germany). It has an area of ca. 30 ha, well covering the horizontal footprint of a CRS probe (aproximately 600 m diameter, Desilets and Zreda, 2013). Soil texture is classified as loamy sand. Soil moisture at the local and field scale in different cropped conditions are measured since 2010 (see Rivera Villarreyes et al., 2011). Only the period with sunflowers (2011) is used in this current study because it constitutes a long time series and covers the complete crop season.

Precipitation is measured in-situ every 20 minutes with a rain gauge MD532 (Delta-T Devices Ltd., Cambridge, UK) (Figure 4.1, location A). The soil moisture measurements are based on a FDR (Frequency Domain Reflectometry) network and two cosmic-ray fast neutron detectors, CRS-1000 (Hydroinnova, Albuquerque, USA) installed within the field. The FDR network was implemented to observe soil moisture at 5 cm and 20 cm depths in five locations (A, B, C, D, and E in Fig. 4.1). Additionally, sensors were also installed at 40 cm depth in locations B and D (Figure 4.1). This FDR network was used as ground truth of soil moisture and for CRS calibration. The CRS probes (location A and D in Fig. 4.1) were mounted on a pole at

a height of 1.5 m above-ground. The neutron counter of the CRS probes
was set-up to record counts every 20 min; neutron counts were subsequently
integrated into one-hour time intervals.

The CRS principle for soil moisture determination is based on the inverse
correlation between of above-ground fast neutrons and hydrogen contained
in the soil (Zreda et al., 2012). Desilets et al. (2010) presented an equation
for relating fast neutrons and volumetric soil moisture as follows:

$$\theta_{\text{CRS}} = \frac{a_0}{\frac{N}{N_0} - a_1} - a_2 \tag{4.1}$$

where θ_{CRS} is the volumetric soil moisture [$L^3 L^{-3}$], N is the corrected
neutron counts per hour, N_0 is a reference neutron counts per hour over dry
soil conditions, and a_i are dimensionless fitting parameters [-]. Rivera Villar-
reyes et al. (2013a) evaluated several possibilities of CRS probe calibration
in the same experimental site considered in the present study (location A).
The calibration was evaluated by choosing different growing periods of sun-
flower and winter rye. An optimal probe calibration was achieved by fitting
a_0, a_1, and a_2, and by adopting N_0 parameter to the maximum observed
N, and with periods of mid-season sunflower and mid-season winter rye. In
the current study, all the computations of θ_{CRS} were carried out with CRS
parameters from winter rye period ($a_0 = 0.038$, $a_1 = 0.374$ and $a_2 = 0.024$
for $N_0 = 1330$ in Eq. 4.1). In this way, CRS and FDR measurements are
completely independent during sunflower period. For simplification, for the
second CRS probe (location D) of the same type we used the calibration
parameters from location A. For additional information about the experi-
mental design and the calibration approach we refer to Rivera Villarreyes et
al. (2013a).

Additionally to continuous measurements, two field campaigns were car-
ried out. In a first field campaign, two soil profiles in location B and D
(Figure 4.2) were drilled down to a depth of 150 cm for extracting 100 cm^3
soil cores (Ehlert and Partner, Niederkassel-Rheidt, Germany) with a sam-
pling resolution of ca. 10 cm. Subsequently, each sample was analyzed for
soil texture using the hydrometer method. In a second soil campaign, soil
samples were collected at 5 cm, 10 cm, 20 cm, 30 cm and 40 cm depths in
the five sensor locations. Each undisturbed soil sample (total number of 25)
was analyzed for saturated hydraulic conductivity by means of the constant
head permeameter method (Klute, 1986).
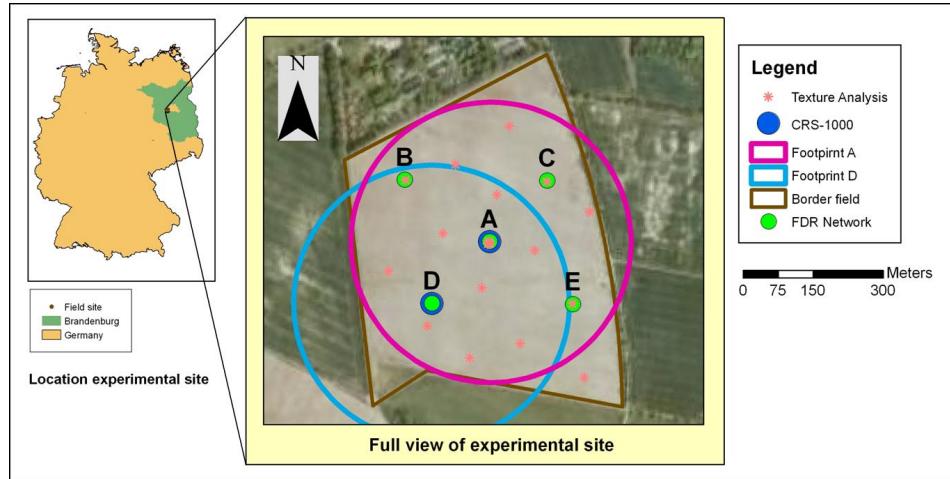
Figure 4.1: Monitoring setup at experimental site.

4.2.2. Numerical modelling of soil water dynamics

Governing flow equation

HYDRUS-1D model version 4.11 (Simunek et al., 2008) was used to simulate the hydrological processes in the experiment site. The simplification to a 1D domain goes along with the fact that the CRS probe does not provide either a horizontal nor a vertical resolution of soil moisture, instead an integral quantification in its entire support volume (Figure 4.1). Such an assumption has been adopted in similar cases with other measurement scales (Jhorar et al., 2004; Santanello Jr et al., 2007; Montzka et al., 2011). Moreover, the main objective is the determination of effective soil hydraulic properties under the assumption of single effective properties at the CRS measurement volume, which was placed already at a location with low variability of soil texture, vegetation, slope, organic matter content and agricultural management.

The model domain extended from the ground surface down to a depth of 1.5 m. The uniform water movement in the porous medium is described by a modified form of the Richards' equation (Simunek et al., 2008).

The root-water uptake model of van Genuchten (1987) was used in HYDRUS-1D, which assumed a potential water uptake equally distributed over the root zone and defined as the ratio between potential transpiration and root depth. A linear increase of sunflower root depth was assumed until a value of 1.15 m, according to the Food and Agriculture Organization (FAO). For root-water uptake model, water-stressed conditions are supplied using Vrugt's model (2001) defined by a fitting parameter with a typical value of $p = 3$ and

parameter h_{50}, which defines pressure at which 50 % of root-water uptake
reduction occurs. Value of h_{50} was optimized with a mean value of -3.7 m
(all modelling cases, cf. 2.3). This higher value of h_{50} is expected for coarse
soil textures (Vrugt et al., 2001). Moreover, h_{50} value seems to influence
negligibly soil moisture values for our model setup and monitoring period.
The main reason may be attributed to the continuous availability of tran-
spirable water for sunflower plants during monitoring season, precipitation
events occurred quite regular. Likewise, HYDRUS-1D simulations revealed
non water-stress conditions for sunflower, and the difference between actual
and potential evapotranspiration was almost negligible. Therefore, we con-
sidered a constant value of h_{50} in all simulation cases later.

The van Genuchten's soil hydraulic functions (1980) and the Mualem's
pore-size distribution (1976) were implemented to solve the Richards' equa-
tion in HYDRUS-1D. Here, residual soil moisture (θ_r) in [$L^3 L^{-3}$], satu-
rated soil moisture (θ_s) in [$L^3 L^{-3}$], saturated hydraulic conductivity (K_s)
in [$L\,T^{-1}$], and empirical parameters such as n [-] and α [L^{-1}] were opti-
mized with the inverse modelling framework (cf. section 4.2.3). The pore-
connectivity parameter (τ) in van Genuchten-Mualem model was assumed
to be 0.5 (Mualem, 1976).

Except the optimized layer 1, the material discretization in HYDRUS-
1D was defined from soil texture measurements (Figure 4.2). The dominant
class in the texture profiles was sandy loam. Layer definition for HYDRUS-
1D was based on a visual inspection how samples distribute on USDA soil
triangle. For instance, transition between layers 2 and 3 (Figure 4.2) is a
slight increase of clay content. In the transition between layers 3 and 4,
increase of clay content is more significant and samples are located in the
border between sandy loam to sandy clay loam. Layer 5 located within the
classification of sandy clay loam.

An initial estimation of soil parameters was carried out with the neural
network model ROSETTA (Schaap and Leiji, 1998). The CRS layer (0-40 cm
as discussed later) was assumed to be an average of 4 sample sets at 10, 20,
30 and 40 cm (cf. section 4.2.1) and two different locations (B and D). For
the rest of the soil profile (40-150 cm), a material distribution was assigned
based on observable changes of soil texture (Figure 4.2).

Boundary and initial conditions

An atmospheric boundary condition was set up in HYDRUS-1D as up-
per boundary condition. Run-off was assumed zero due to flat topography,
since run-off events were not observed after heavy precipitations. It is also
expected a high infiltration rate for Bornim soil (discussed later). The poten-
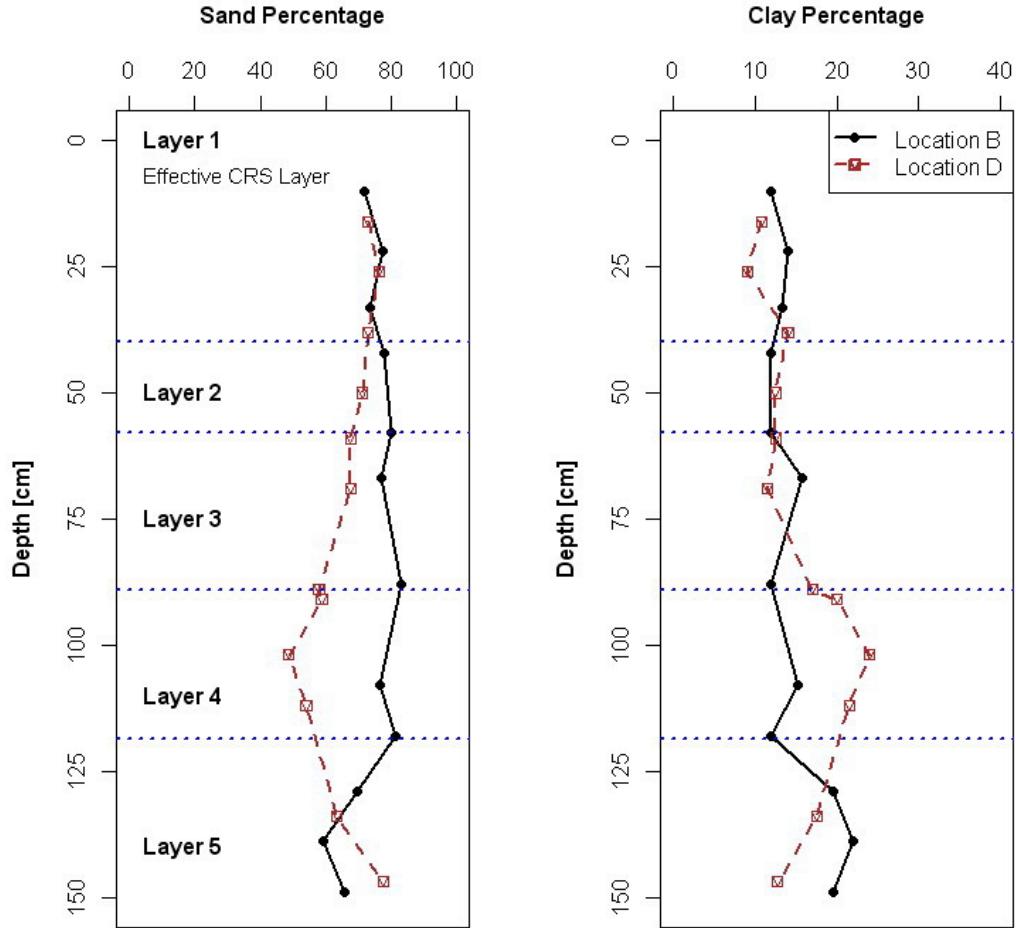
Figure 4.2: Measured soil texture distribution at locations B and D (cf. Figure 4.1): sand content on the left side and clay content on the right side. Horizontal lines indicate selected layer distribution for HYDRUS-1D model.

tial evapotranspiration for a reference crop (ET_o) was calculated using the FAO recommended Penman-Monteith equation (Allen et al., 1998). Computations were carried out with daily data from automatic weather station at the University of Potsdam (52.409° N 12.977° E), located at approximately 3.9 km distance from the experimental site. The potential sunflower evapotranspiration (ET_{sun}) was estimated assuming a single crop coefficient (Allen et al., 1998), which varied along the sunflower periods (0.35 at the initial and final stages, and 1.0 at the middle season of sunflower). The partitioning of potential transpiration and evaporation was based on the fraction of

incidence radiation not intercepted by the canopy (τ [-]),

$$\tau = e^{-k \cdot LAI} \tag{4.2}$$

where k is the extinction coefficient set as 0.398 (Ritchie, 1972), and LAI is the leaf area index, here derived from heat accumulation (Growing Degree Days, GDD) according to Mailhol et al. (1997). The GDD were estimated from air temperature data from a weather station. Range of LAI values were verified according to literature (Steer et al., 1993).

The lower boundary condition of the model domain was set as free drainage. A possible interaction of groundwater table was discarded due to its much deeper location (approximately 5 m below surface). The initial condition was assumed constant soil moisture profile defined from the FDR network. To allow for the relaxation of the initial soil moisture profile, we used a spin-up time of the first 30 days of the monitoring period.

4.2.3. Inverse simulations for CRS-scale effective soil hydraulic parameters

For the inverse simulations, CRS soil moisture was transformed to lengths of water (saturated depth) by multiplying with its effective depth (ED), $\mathrm{SWS_{CRS}} = \theta_{\mathrm{CRS}} \cdot \mathrm{ED}$, named here soil water storage (SWS). In HYDRUS-1D, the SWS is an output of the water balance for a defined soil region. The flow domain was split in two sub-regions (i) 0-40 cm and (ii) 40-150 cm. The first region corresponds to the thickness of the measurement volume of the CRS probe. The soil water storages in these regions are named here $\mathrm{SWS_1}$ and $\mathrm{SWS_2}$, respectively. During inverse simulations, residuals between modeled $\mathrm{SWS_1}$ and measured $\mathrm{SWS_{CRS}}$ were minimized, as described below in Eq. 4.3.

A constant CRS penetration depth of 40 cm was used to define CRS sampling volume in inverse simulations. According to Rivera Villarreyes et al. (2013a), this was a site-dependent characteristic concluded on the local soil properties (organic matter, lattice water, texture, etc.) and soil moisture profiles. However, as it has been addressed in Franz' study (2012a), penetration depth can vary strongly under other field conditions (i.e. hydrogen distribution in the system) and therefore, definition of CRS sampling volume becomes time-varying. Moreover under strong heterogeneous soil moisture profiles, integral values of CRS soil moisture are more sensitive to surface values with a decrease of sensitivity in depth (Franz et al., 2012a).

The Parameter Estimation software (PEST, Doherty, 2004) was implemented with the global optimizer Covariance Matrix Adaptation - Evolution

Strategy (CMA-ES) from Hansen et al. (2003) for the parameter optimiza-
tion. Applicability of CMA-ES with HYDRUS-1D for the estimation of soil
hydraulic properties has been already verified (Schelle et al., 2010; Durner
and Iden, 2011). Though, there may be other global algorithms that perform
similar or better than CMA-ES, the comparison between different algorithms
is not an objective here and readers can find further discussion in literature,
e.g. Hopmans and Simunek (1999) and Vrugt and Dane (2006). PEST was
coupled with HYDRUS-1D in the forward mode. It is worth to mention
that inverse modelling used least-square objective function, simplifying the
use of autocorrelation residuals as it has been applied in other hydrologi-
cal studies (Gottschalk et al., 2011; Li et al., 2011; Breinholt et al., 2012).
This optimization procedure minimizes the objective function implemented
as follows:

$$\Phi(q) = \sum_{i=1}^{N} [r_i(q)]^2 \tag{4.3}$$

where q denotes the vector of the parameters to be optimized, r_i are the
residuals, and the summation is carried out over the number of observations
N. Initially, the parameter vector q included the five soil hydraulic parame-
ters (θ_r, θ_s, K_S, n and α) and one water-uptake parameter (h_{50}). From first
optimization results, parameter h_{50} resulted to affect negligibly other five
parameters (cf. section 4.2.2). Therefore, h_{50} was set as constant, reducing
parameter vector q to only soil parameters.

The uncertainty of each optimized parameter q_j, $j = 1, \cdots$, was deter-
mined from the diagonal elements of the parameter covariance matrix $C(q)$
(Kool and Parker, 1988; Hopmans and Simunek, 1999), evaluated for the
final parameter set q^*. This value represents the estimate of the standard
deviation ($s_j = \sqrt{C(q^*)_{jj}}$). The uncertainties of the two soil hydraulic func-
tions and the uncertainty of the model predictions were calculated by linear
error propagation (Omlin and Reichert, 1999). The goodness of the fit ob-
tained from the inverse simulations was defined by the root mean square
error (RMSE).

Inverse simulations used SWS$_{CRS}$ measured at locations A and D (Fig-
ure 4.1). The footprint of D partially overlaps footprint of A and also in-
cludes partly other nearby sunflower fields and a relatively small number of
tree bordering the experimental site. Therefore, similarity in soil hydraulic
parameters from inverse modelling with these two datasets (A and D) is not
necessarily expected.

4.2.4. Verification of CRS-scale effective soil hydraulic parameters

The soil hydraulic parameters at the CRS scale were compared against also inversely-derived parameters from five single FDR profiles and one FDR profile with mean values of previous five. All six FDR inverse simulations used same initial and boundary conditions as CRS inversion. However, in this case, HYDRUS model was forced to mimic FDR soil moisture at 5 cm, 20 cm and 40 cm depths, instead of matching the soil water storage down to 40 cm (CRS simulations). Material layering for simulations was same as CRS inverse simulations for layers 2-5 (Figure 4.2). First CRS layer (0-40 cm) was split in three sub-layers accounting for the measurement thickness of each FDR sensor. Here, the layer transition does not necessarily mimic the field reality, but it could provide an idea of the vertical parameter variability. Indeed during sensor installation, a natural layer located between 25 cm and 30 cm depth was identified visually. If soil hydraulic properties are not significantly different in these three layers, final optimized parameters are expected to be similar.

4.3. Results and discussions

4.3.1. Soil hydraulic properties at the CRS scale

Inverse determination of the effective properties at the field scale employed time series of hourly SWS_{CRS}. The monitoring period was wetter than the mean annual precipitation (591 mm $\pm$ 96 mm, from 1983 to 2011, German Weather Service), we can presume possible broader range of field soil moisture used for inverse simulations. Without a long-term historical record of soil moisture, we can only take range of measured precipitation amounts and soil moisture as proxy for the natural range of soil moisture at which effective soil hydraulic properties need to be estimate.

Values of non-optimized parameters (Layers 2-5 in Fig. 4.2) and final optimized parameters (Layer 1 in Fig. 4.2) are presented in Table 4.1 and Table 4.2, respectively. Optimized retention and hydraulic conductivity functions are shown in Figure 4.3. Differences between optimized soil parameters from locations A and D were minimal with variations of only 0.01 m^3 m^{-3} for θ_r, 0.002 m^3 m^{-3} for θ_s and 0.017 m^{-1} for α as shown in Table 4.2. Therefore, effective retention curves and hydraulic functions were almost invariant for the range of field soil moisture (Figure 4.3), as reflected in very similar values of RMSE (0.034 m^3 m^{-3} and 0.036 m^3 m^{-3}) from these two datasets.

Table 4.1: Initial parameters derived from soil texture information (Figure 4.2) and ROSETTA (Schaap and Leiji, 1998). Notice that layers 2-5 were not optimized with PEST.

Layer	Depth [m]	θ_r [m^3 m^{-3}]	θ_s [m^3 m^{-3}]	α [m^{-1}]	n [-]	K_s [m d^{-1}]	τ [-]
1	$0.00 - 0.40$	0.049	0.380	3.42	1.466	0.48	0.5
2	$0.40 - 0.60$	0.048	0.381	3.41	1.440	0.46	0.5
3	$0.60 - 0.90$	0.051	0.380	3.27	1.412	0.38	0.5
4	$0.90 - 1.20$	0.057	0.384	2.84	1.358	0.22	0.5
5	$1.20 - 1.50$	0.057	0.381	2.97	1.362	0.24	0.5

A higher value of parameter n from inverse simulations implies a steeper water retention curve and an unsaturated conductivity function in which values decreases rapidly with decreasing matric potential (Yakirevich et al., 2009), as shown in Figure 4.3.

Table 4.2: Van-Genuchten Mualem parameters inversely estimated with CRS soil water storage (locations A and D). Values in brackets indicate the standard deviation (s_j) of the estimated parameter. The root mean square error is presented for the calibration (RMSE$_c$) and verification (RMSE$_v$). Value of RMSE$_v$ was calculated between simulated HYDRUS soil moisture with CRS-scale soil parameters and FDR mean measurements at 5 cm, 20 cm and 40 cm depths.

Case	θ_r [m^3 m^{-3}]	θ_s [m^3 m^{-3}]	α [m^{-1}]	n [-]	K_s [m d^{-1}]	RMSE$_c$ [mm]	RMSE$_v$ [m^3 m^{-3}]
CRS-A	0.053 (0.002)	0.404 (0.004)	3.987 (0.048)	2.357 (0.048)	9.054 (2.577)	4.010	0.034
CRS-D	0.043 (0.002)	0.406 (0.004)	4.004 (0.056)	2.284 (0.056)	6.857 (1.456)	3.978	0.036

Confidence interval of K_s parameter was relatively higher compared to other optimized parameters. Uncertainty computed from final covariance

matrix and expressed as standard deviation (s_j) was 2.577 (location A) and
1.456 (location D). The inverse simulations estimated K_s values much higher
compared to PTF value for Bornim soil. From inverse simulations, these
values were estimated for field range of soil moisture and value of pore-
connectivity set as τ (non-optimized). According to Schuh and Cline (1990),
τ could vary from -8.73 to 14.80, differing from Mualem's range (1976) from
-1 to 2.5. Moreover, Yakirevich et al. (2010) suggested a possible effect of τ
on K_s. Thus, the obtained K_s values from inverse simulations have a great
deal of uncertainty and especially are less valid to simulate conditions close
to saturation.

For further investigation on the use of the CRS method for inverse mod-
elling, soil hydraulic parameters were also derived using a daily time res-
olution of SWS$_{\text{CRS}}$ (result not shown). In this case, uncertainty of CRS
measurements is decreased by integrating counts (N in Eq. 4.1) in a longer
time step. The major parameter difference between hourly and daily esti-
mations occurred in values of θ_s. For instance, θ_s was 0.40 m^3 m^{-3} using
hourly SWS$_{\text{CRS}}$ compared to a value of 0.30 m^3 m^{-3} using daily data. This
discrepancy could be attributed to time resolution (i.e. accuracy of CRS), as
well as lack of CRS observations near saturation values, leading to the same
discussion as for K_s above. Also at daily time step, results of inverse simula-
tions using CRS data from locations A and D did not differ significantly in
terms of effective retention curve and effective hydraulic conductivity func-
tion. Therefore for simplification, further discussion in next sections is only
based on parameters derived at location A with CRS data at the hourly res-
olution. More discussion of their differences to local-scale parameters (FDR,
PTF and measurements) is presented in section 4.3.2.

4.3.2. Comparison of soil hydraulic parameters at the CRS scale versus local scale

Results of soil texture at the CRS observation thickness suggested a soil
classification as sandy loam (USDA) with sand amounts from 71.6 % to
78.0 % and clay amounts from 9 % to 14 %. Predictions of soil hydraulic
parameters based on PTFs are presented in Table 4.1 (first row) and its
hydraulic functions in Figure 4.3. In general, PTF-predicted retention curve
suggests higher values of soil moisture than those from CRS-inverse soil pa-
rameters at the same matric potential. Moreover, PTF hydraulic conductiv-
ity function predicted values of K_s significantly lower than those predicted
by inverse simulations with SWS$_{\text{CRS}}$ data.

Soil hydraulic properties derived with FDR inverse simulations (six cases)
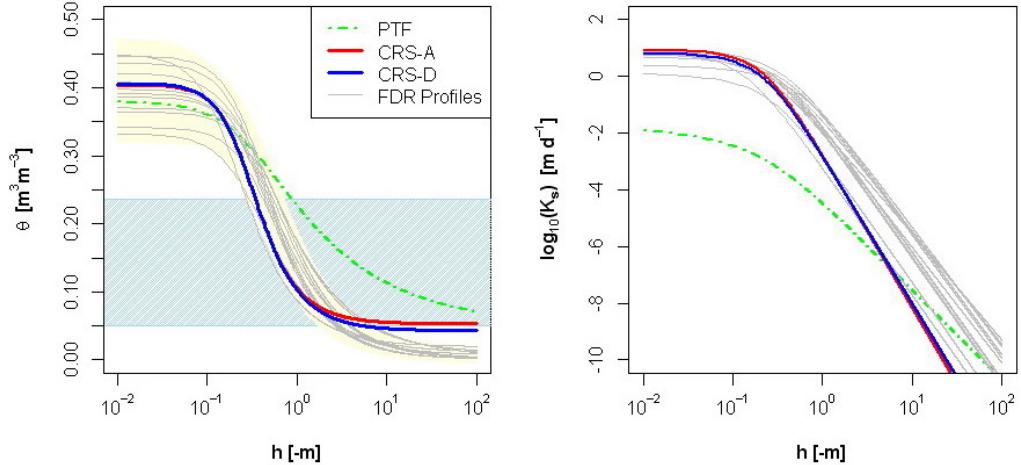
Figure 4.3: Optimized parameters with hourly SWS_{CRS} and FDR soil moisture in objective function: retention curve (Left) and hydraulic conductivity function (Right). Blue shadow area indicates the range of measured soil moisture in the field. Yellow shadow area represents the confidence bounds of all FDR inverse simulations (cf. Table 4.3). A $\log_{10}$-transformation for K_s was used in the right plot. Horizontal axes are in logarithmic scale.

are shown in Table 4.3. Whereas significant variability between retention curves at FDR scale was observed, variability bounds (95 % confidence interval) contain still retention curve at CRS scale. Slope of retention curves with field (CRS) and local (FDR) scale parameters is very similar within measurement range of soil moisture. This confirms the validity of the CRS-based soil parameters, since FDR-data inverse simulations use a different approach by minimizing objective function with soil moisture at 5 cm, 20 cm and 40 cm depths, instead of matching water balance at the CRS scale simulations. Some discrepancies are mainly observed outside of observed range of soil moisture, i.e. high uncertainty of porosity value.

In the case of hydraulic conductivity functions, as previously discussed, discrepancies between two scales may be due to model assumptions and lack of data near saturation. From field data, saturated hydraulic conductivity was measured as 2.62 ± 1.63 m d^{-1} on undisturbed soil cores by means of the permeameter method. This value is significantly lower than 9.05 ± 2.56 m d^{-1} from inverse simulations with SWS_{CRS}.

Different reasons may explain the discrepancies between effective CRS-scale parameters and local optimized parameters (or measurements). The first and probably most relevant is the scaling problem (Blöschl and Sivapalan, 1995). In this study, the scale differences are obvious in terms of

Table 4.3: Van-Genuchten Mualem parameters inversely estimated with FDR soil moisture at 5 cm, 20 cm and 40 cm depth. Values in brackets indicate the standard deviation (s_j) of the estimated parameter.

Case	Depth [m]	θ_r $[m^3\,m^{-3}]$	θ_s $[m^3\,m^{-3}]$	α $[m^{-1}]$	n [-]	K_s $[m\,d^{-1}]$	RMSE$_c$ $[m^3\,m^{-3}]$
FDR-A	5	0.001 (0.004)	0.409 (0.015)	3.272 (0.539)	1.832 (0.047)	6.808 (0.791)	0.030
FDR-A	20	0.001 (0.004)	0.386 (0.015)	2.817 (0.224)	2.000 (0.052)	8.483 (0.659)	0.039
FDR-B	5	0.001 (0.005)	0.436 (0.017)	3.198 (0.342)	2.000 (0.081)	1.255 (1.327)	0.021
FDR-B	20	0.001 (0.005)	0.392 (0.016)	3.012 (0.370)	2.000 (0.086)	7.678 (0.87)	0.035
FDR-B	40	0.008 (0.006)	0.342 (0.022)	2.555 (0.438)	2.000 (0.111)	5.074 (0.753)	0.037
FDR-C	5	0.001 (0.005)	0.370 (0.018)	2.123 (0.264)	1.936 (0.064)	6.065 (0.926)	0.033
FDR-C	20	0.001 (0.004)	0.365 (0.017)	2.263 (0.348)	1.931 (0.063)	9.908 (0.631)	0.041
FDR-D	5	0.001 (0.004)	0.447 (0.013)	3.131 (0.318)	2.000 (0.062)	7.938 (0.780)	0.025
FDR-D	20	0.019 (0.005)	0.449 (0.015)	6.347 (0.771)	1.994 (0.063)	9.151 (0.812)	0.018
FDR-E	5	0.010 (0.005)	0.398 (0.017)	2.696 (0.857)	1.796 (0.076)	8.765 (0.857)	0.022
FDR-E	20	0.004 (0.005)	0.422 (0.019)	3.339 (0.834)	1.699 (0.078)	8.308 (0.816)	0.033
FDR-E	40	0.011 (0.005)	0.332 (0.016)	3.618 (0.931)	1.888 (0.078)	2.535 (0.851)	0.038
FRD-Mean	5	0.001 (0.005)	0.445 (0.017)	2.836 (0.417)	2.000 (0.071)	10.000 (0.739)	0.017
FDR-Mean	20	0.001 (0.005)	0.360 (0.017)	2.597 (0.386)	2.000 (0.081)	7.981 (0.846)	0.024
FDR-Mean	40	0.001 (0.006)	0.319 (0.020)	2.594 (0.485)	1.939 (0.087)	2.447 (0.847)	0.040

data used for inverse simulations (local FDR profiles vs. field-scale CRS). Moreover, laboratory measurements of K_s were carried out on 100 cm^3 soil cores (open-ended columns), compared to model optimizations with a flow domain down to 1.5 m depth. In addition, K_s measurements in general depend strongly on the estimation method (Reynolds et al., 2000) and size of soil cores (Mallants et al., 1997). For instance, considering that CRS estimated parameters refer to a control volume of several cubic meters, it is reasonable that the permeability averaged over such volume accounts for macro-pores that may easily increase permeability of one order of magnitude. Moreover, inverse-estimated permeability may change even keeping invariant the scale of interest, but modifying the macro-pore density (Arora et al., 2011). Additionally, since some of the measurement uncertainty relates to the methodological uncertainty as well as the true spatial variability makes complex a direct comparison of permeability between scales. Further discussion related to scale and methodology issues on permeability estimation can be found on Chappell et al., 1998 and Chappell et al., 2007.

Another possible reason is whether the CMA-ES reached the true minimum value of the objective function. On the one hand, CMA-ES being a global optimizer allows certain confidence that global optimum was found in inverse simulations. On the other hand, inverse data contains uncertainty from FDR network and CRS probe calibrations (Rivera Villarreyes et al., 2013a). Especially in case of the latter, its signal is highly influenced by biomass and other crop characteristics along the growing period (Franz et al., 2013; Hornbuckle et al., 2012). Moreover, CRS assumptions of constant penetration depth and homogenous sensitivity in depth (Rivera Villarreyes et al., 2013a) may include an additional uncertainty that should be evaluated in further studies with different field conditions.

A last possible reason is related to the uncertainty inherent in simulations due to: (i) input uncertainty (e.g. precipitation and evapotranspiration) and (ii) model conceptualization. For instance, evapotranspiration fluxes included several simplifications and assumptions related to crop coefficient, LAI, root depth, root-water uptake model, etc. Therefore, this may influence parameter optimization and differences of fitted to measurements of K_s. In the model conceptualization, hysteresis was not considered during wetting and drying cycles. No data is available to estimate hysteresis parameters in HYDRUS-1D. Therefore, this process can be only incorporated indirectly, if it is accounted for in the optimization, meaning an increase of parameter uncertainty (Mertens et al., 2005).

4.3.3. Simulated CRS soil water storage

A further evaluation of the CRS-scale parameters is based on how these parameters reproduce field soil moisture and field soil water storage, comparing HYDRUS results using CRS-scale soil parameters and field data. Simulated values of SWS_1 (0-40 cm) mimicked very well measured SWS_{CRS} in terms of dynamics and absolute values with and between simulated and observed SWS from CRS probe (Figure 4.4). It should also notice that simulated SWS_1 become much more uncertain with increasing CRS soil moisture (Data not shown). Certainly, this is attributed to CRS performing better at high neutron counting rates, i.e. low values of field soil moisture. This is due to Poisson counting statistics to which CRS method based on (Zreda et al., 2012). Experimental sites situated at lower elevations (e.g. Bornim), therefore lower neutron counts, are subjected to higher uncertainty compared to mountain altitudes.

Also an important point in this discussion is the real value of CRS penetration depth. Based on Bornim field conditions penetration depth was simplified as a fixed value (further details in Rivera Villarreyes et al., 2013a), however this assumption may be not fully valid in other field conditions, for instance soil profiles with strong vertical variability. In other sites with significant changes of atmospheric humidity, uncertainty may arise in the CRS footprint (i.e. decrease in diameter of 40 m for every 0.01 kg kg^{-1} increase of humidity). In this case, dependency on soil moisture is small and lateral footprint is determined mainly by the properties of air (Desilets et al., 2013).

Additionally, uncertainty of CRS calibration parameters (Eq. 4.1) varies along sunflower season (Rivera Villarreyes et al., 2013a). Moreover, SWS_1 is in agreement with temporal dynamics of precipitation. Since other components of the water balance such as percolation and actual evapotranspiration were not measured, we can not verify value of soil water storage (SWS) directly from optimization results (e.g. RMSE and objective function). Therefore, future studies should consider other integral information at the large scale (e.g. evapotranspiration fluxes from eddy covariance towers, discharge, etc.) in order to constrain inversion results at the CRS scale, reduce uncertainty of input variables, and therefore reduce uncertainty on CRS-scale soil hydraulic parameters.

For further verification of simulated SWS at the CRS scale, we compare its value to SWS computed from FDR soil moisture. For calculation of SWS from FDR network, boundaries of each FDR measurement thickness were located at middle point between sensors. The SWS calculated from FDR soil moisture and simulated with soil parameters at CRS scale are well comparable, beside their different support scales (Figure 4.4, lower graph). Cer-
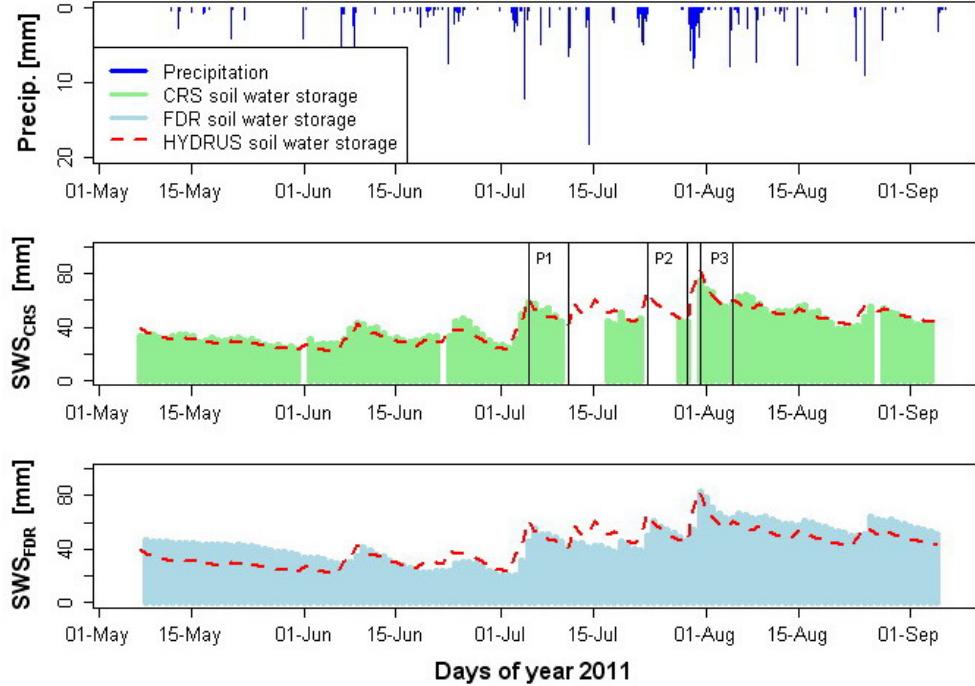
Figure 4.4: Soil water storage (SWS) during monitoring period: (upper) precipitation, (middle) measured SWS at the CRS scale and (lower) calculated SWS from the FDR network. Notice that SWS at the CRS probe was used for inverse simulations and determination of effective soil parameters. Periods P1, P2 and P3 are evaluated in Fig. 4.6

tainly, CRS-scale parameters overestimated the SWS calculated from FDR network at the beginning and end of monitoring period. Such behavior is not attributed to an optimization problem or HYDRUS setup, however it is related to CRS probe calibration and its relation with crop biomass (Rivera Villarreyes et al., 2013a).

4.3.4. Simulated soil moisture profile with field-scale parameters

Simulated soil moisture at the CRS scale is presented in Figure 4.5. Simulated soil moisture based on effective parameters and FDR observations can be expected to not match perfectly. This is on one hand because effective parameters are adjusted to match the integral soil water storage (SWS), irrespective of soil moisture and pressure profiles. On the other hand, the point-based FDR network will not perfectly represent the average profile in

the CRS footprint. However, in the specific field conditions, model results predicted acceptable field soil moisture. For instance, simulated values at 5 cm depth are in very good agreement with FDR network with RMSE = 0.022 $m^3 m^{-3}$ and $r^2 = 0.704$. At the 20 cm depth, model predictions followed well observations and its temporal variability is still contained within FDR uncertainty bands. Simulated values at the lowermost depth responded more significantly to heavy precipitation events (e.g. from June until July 2010) than FDR sensors, producing an overestimation of field soil moisture (RMSE = 0.036). This overestimation may be attributed to the influence of the layer distribution in HYDRUS-1D.

To further analyze this behavior, comparison between simulated soil moisture profiles at the CRS scale and FDR measurement profiles (Figure 4.6) was carried out for three specific time periods (P1, P2 and P3 from Fig. 4.4). These periods covered short times from peaks of SWS_{CRS} until day when soil percolation tends to its base value ($\sim$ steady-state). For instance, the SWS varied from 61 mm to 43 mm (P1), from 67 mm to 46 mm (P2), and from 83 mm to 55 mm (P3) at the beginning and end of selected periods, respectively. Approximately, the peak of SWS in all the cases decreased after approximately 5 days, giving an idea of a soil percolation rate of about 4.5 ± 1.0 mm d^{-1}. Moreover, vertical variability of soil moisture is expected to be higher within these three periods due to infiltration process and soil moisture redistribution.

Simulated profiles at CRS scale did not show a complex vertical variability compared to FDR profiles (Figure 4.6). This is due to layer discretization and way how CRS data was incorporated into the PEST-HYDRUS interface (cf. section 4.2.3). Hourly variability of FDR profiles was larger from 5 cm to 20 cm depths compared to variability simulated by HYDRUS with soil parameters at the CRS scale, especially in periods of lower precipitation events, i.e. lower changes of SWS (e.g. P1). Likewise, mean hourly FDR in P1 was outside of the simulated range. On the other hand, CRS simulated profiles become a better representation of field variability of soil moisture with increasing SWS, e.g. from P1 to P3.
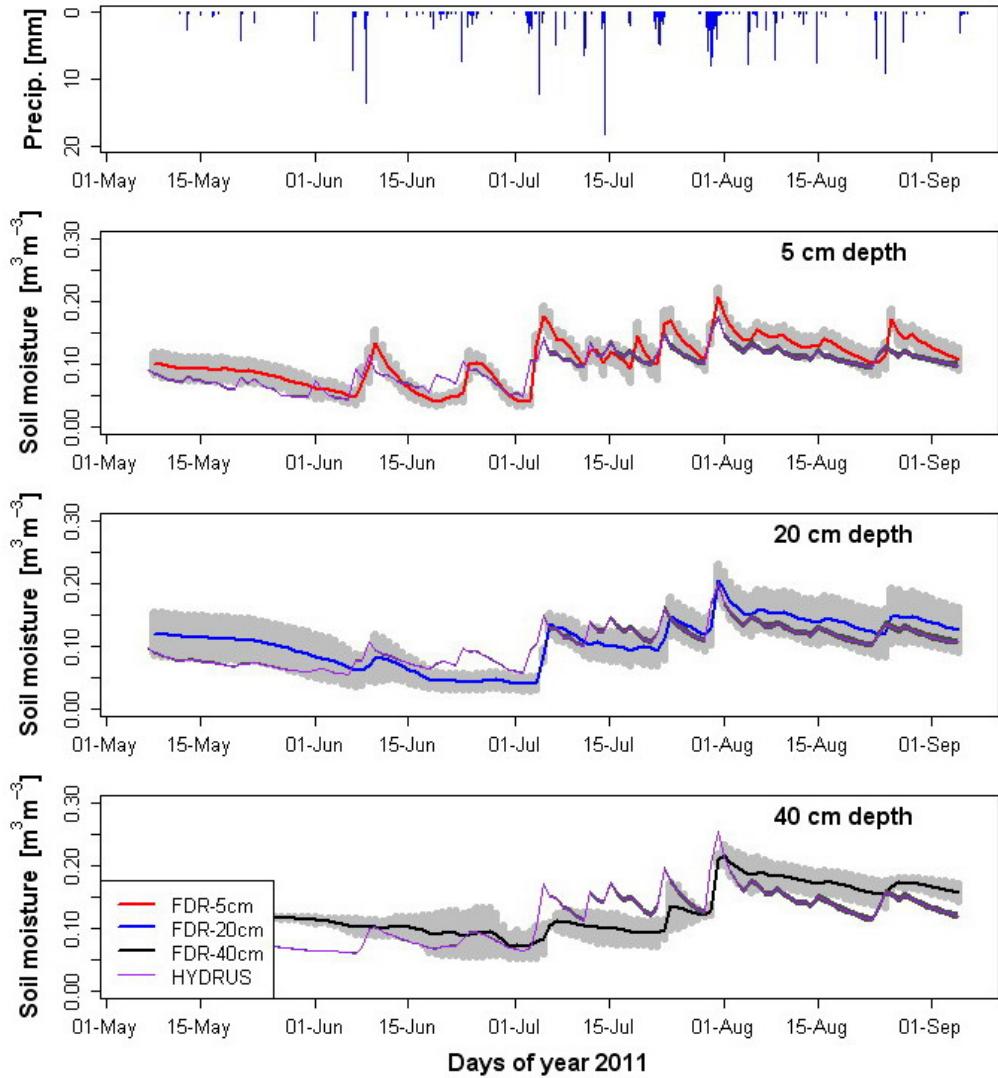
Figure 4.5: Time series of soil moisture at 5 cm, 20 cm and 40 cm from HY-DRUS simulations using effective parameter at the CRS scale vs. FDR field measurements of soil moisture. Notice that uncertainty bands are plotted in gray and dark gray for FDR and HYDRUS, respectively. Comparison of SWS from FDR network and simulated with CRS parameters (Lower graph).

4.4. Conclusions

This study proves the potential of cosmic-ray neutron sensing (CRS) and inverse modelling for the determination of soil hydraulic parameters at the scale between point and remote sensing observations. Integral quantifications
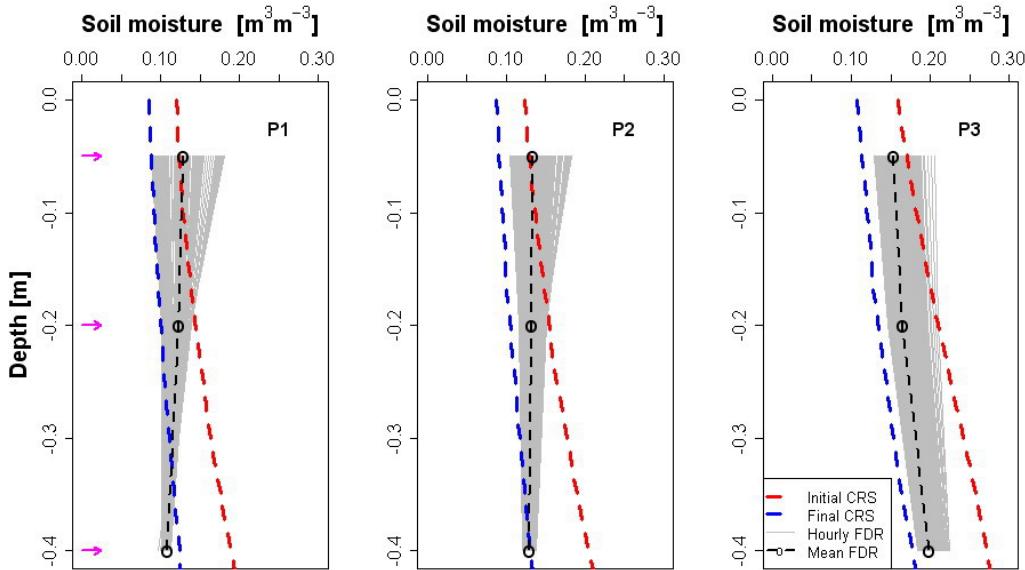
Figure 4.6: Comparison of HYDRUS soil moisture profiles derived with effective parameters at CRS scale against hourly measured FDR profiles. Each graph corresponds to one of three different short periods (Figure 4.4). Mean value of FDR soil moisture for each period is indicated in black dots. Horizontal arrows are the sensor locations.

of soil moisture at the CRS support volume were transformed to soil water storage (saturation length) for a direct calibration of the soil-water balance in HYDRUS-1D. Clearly, inversely-estimated parameters are effective for the soil water storage, but not necessarily to soil moisture and pressure profiles. However, our modelling approach provides acceptable results for simulating soil moisture in different depths at the CRS scale, in comparison to time series of FDR soil moisture and FDR soil water storage, beside different support scales (field vs. local). Additionally, this modelling approach could be addressed to retrieve a vertical discretization of CRS measurements in similar conditions as those evaluated here, i.e. sandy loam soil and absence of strong vertical soil layering. Moreover, we observed that simulated soil moisture profiles with effective CRS parameters covered hourly variability of FDR profiles better after heavy precipitation events.

Future work should include other large-scale measurements such as evapotranspiration fluxes from eddy covariance towers in order to constrain inversion results at the CRS scale and therefore, reduce uncertainty on estimated parameters. These additional data can be also used to close the soil water balance at the CRS scale. More data at the local scale should be also

included such as in-situ tensiometers (complementing FDR profiles used in inverse problem) and measured saturation-pressure curves in laboratory in order to validate field-scale CRS soil hydraulic properties.

Soil hydraulic parameters at the CRS scale were in agreement to parameters from inverse simulation with FDR soil moisture profiles. However, since other fluxes in the water balance were not measure, it is not possible to identify which scale provides better estimations. On the other hand, effective soil hydraulic functions at CRS scale were contained within the parameter variability derived from FDR inverse simulations. This confirms the validity of CRS-scale parameters, since FDR-scale inverse simulations use a different approach by minimizing objective function with soil moisture at 5 cm, 20 cm and 40 cm depths, instead of matching water balance at the CRS-scale inverse simulations.

The fact that the cosmic-ray neutron sensing provides an integral observation of soil moisture at the field scale with a deeper penetration than remote sensing products, has a great potential for model parameterization in different contexts such as hydrology, climatology, ecohydrology at the intermediate scale (e.g. field scale or small catchment scale). Further research could address this issue in other modelling frameworks, e.g. data assimilation with data input from CRS probe, inverse simulations with time-varying CRS support volume and with changes of sensitivity based on local soil moisture profiles, etc.

Chapter 5

The benefits of the cosmic-ray neutron sensing for measuring integral soil and snow water storages at the small catchment scale

5.1. Introduction

Major hydrological processes controlling the catchment state are directly linked to spatio-temporal variability of soil moisture and snow cover. Soil moisture is a key state variable controlling hydrological and energy fluxes at different spatio-temporal scales, e.g. influencing the partition of rainfall into infiltration and run-off, and the partition of net radiation into sensible heat and latent heat fluxes (Robinson et al., 2008; Vereecken et al., 2008). Among others, soil moisture also influences a variety of ecohydrological processes related to plant growth, ecological patterns and agricultural production within the catchment (Rodriguez-Iturbe and Porporato, 2005). In catchments with seasonal presence of snow, catchment hydrology is strongly governed by snow cover on the ground in snow-covered areas (Whitaker et al., 2008). Snow accumulation and ablation processes considerably affect stream water quality as well as water run-off (Woli et al., 2008). Areas seasonally covered by snow are among the most sensitive areas to the recent climate change, e.g. snow melt season in mountain areas is occurring progressively earlier (Rango, 1995) and reduction in snow melt contribution to stream flow (Piechota et al., 2004).

The knowledge of soil moisture is very important to assess the hydrological response of a catchment. Especially, run-off generation is directly linked to antecedent variability of soil moisture previous to the rainfall event (Graeff et al., 2009). To characterize this variability even for a small catchment, remote sensing data should be used (Pietroniro and Prowse, 2002). However its temporal resolution is unsuitable for flood prediction and for observing fast catchment responses, and its spatial resolution sometimes is larger than area of interest, requiring some downscaling techniques (Piles et al., 2011). On the opposite to remote sensing, wireless sensor networks (Bogena et al., 2010) are promising approaches for characterizing catchment soil moisture at a very fine spatio-temporal resolution, however it requires an invasive installation of point-scale sensors and its support area is limited to number of devices, i.e. cost-dependent factor.

Snow, as well as soil frost and thawing, is of importance in mid-latitudes and mountain catchments. Spring snow melt or frequent melting periods during winter are responsible for annual run-off, erosion rates and matter transport (Ollesch et al., 2005; Ollesch et al., 2006; Ollesch et al., 2008a). For instance, surface run-off generation in winter at the Schaefertal catchment (low mountain range) in Germany causes higher erosion rates than summer events. Suspended sediment concentration after snow melt event in combination with soil frost can reach 40 times higher amounts than for a run-off event without frozen soil (Ollesch et al., 2005). Similar picture is observed in other catchments, e.g. Yamagata catchment (280-618 m a.s.l.) in Japan presents 60 % of the annual sediment load during the snow-melting period (Iida et al., 2012).

Research on snow characterization has been intensively evaluated along different spatio-temporal scales from point-scale snow cores (Watson et al., 2006) to remote sensing (Matson, 1991; Gao et al., 2010; Paudel and Andersen, 2011; Zhou et al., 2013) with large footprints (e.g. from 500 m to 0.25° footprint, and from swath to daily, to 8-day to monthly in MODIS). Snow monitoring is carried out with a broad branch of physical methods such acoustic wave propagation (Albert et al., 2008), infrared radiation method (Domine et al., 2006; Gergely et al., 2010), pressure pillow method (Sorteberg et al., 2001), optical observation techniques (Frei and Lee, 2010; Metsämäki et al., 2012; Wiebe et al., 2013), cosmic-ray neutrons (Kodama, 1980), and others.

In this chapter the benefits of the cosmic-ray neutron sensing (CRS) for monitoring soil moisture and snow water equivalent at the small catchment scale are presented. Detailed physics and methodology about CRS for soil moisture measurements has been presented in previous chapters. In the case of snow monitoring, Kodama (1975); Kodama et al. (1979) and Kodama

(1980) presented the first research of cosmic-ray neutrons for measurements of snow water equivalent, using the so-called cosmic-ray snow gauge. For instance, Kodama (1975) identified an inverse correlation between cosmic-ray neutrons and snow water equivalent up to values of 30 cm. Furthermore, Desilets et al. (2010) recently quantified snow water equivalent from fast neutrons measured aboveground. Later, Rivera Villarreyes et al. (2011) observed significant attenuation of fast neutrons and, therefore, rise of total water content in periods of snow cover in Bornim (Chapter 2).

In this dissertation section, I presented the state of the art of a network of four cosmic-ray neutron sensors at the Schaefertal catchment (Harz, Germany). Such as network was implemented in the framework of the dissertation in order to monitor integral temporal changes of soil moisture and snow water equivalent. Here, a close overview on understanding how secondary cosmic-ray neutrons (thermal and fast) responded to snow events is evaluated. CRS signal and CRS products (snow and soil moisture) are treated as an integral measure at the catchment level and in a remote-sensing manner.

For instance, CRS soil moisture in previous chapters has been always compared to ground truth FDR sensors; however, such facilities were not available in the Schaefertal catchment and therefore, use of ancillary data (e.g. weather station) was applied as simple proxy for verifying measurements. The main objectives of this chapter are described as follows:

- to present data collected in long-term monitoring of cosmic-ray neutrons in Schaefertal catchment

- to investigate possible calibrations of the cosmic-ray neutron sensing approach

- to analyse soil moisture and snow effect on the cosmic-ray neutron sensing approach

The analysis presented in this chapter is corroborated based on weather data. Further steps will be conducted for a deeper interpretation.

5.2.   Materials and methods

5.2.1.   Experimental site

The experimental site is the Schaefertal catchment at the Eastern part of the Harz Mountains (NE Germany) and approximately 150 km south-west of Berlin (Figure 1). The headwater catchment is a small, average mountain

catchment with an area of 1.44 km^2 (51º 39$'$ N, 11º 03$'$ E). The Schaefertal catchment is highly characterized by pronounced hill-slopes, total elevation difference up to 80 m and the catchment outlet is at an elevation of 392 m a.s.l. The land-use on the valley bottom is pasture and hill-slopes are intensively used for agriculture (Ollesch et al., 2006; Ollesch et al., 2008b; Graeff et al., 2009). Major crops are winter grain and rape in a rotation of various lengths (Table 5.2). The use of Tricale Talento has become important in last years. Sowing dates of main crops fluctuates between last week of September and first week of October. Harvesting dates are approximately middle of August. The total biomass at the harvesting date in entire catchment rose up to 1.73 kg m^{-2} (years 2010 and 2011). The Eutric Gleysols and Dystric Gleysols soils at the valley bottom are utilized for pasture or meadow. The soil profiles are in general Luvisols and Cambisols, as presented in Figure 2 (Ollesch et al., 2005). The average annual rainfall is approximately 640 mm; the annual average temperature is 6.8º C, ranging from -1.8º C in January to 15.5º C in July (German weather station Harzgerode).

Currently, the Schaefertal catchment is one of the intensive test sites of the Terrestrial Environmental Observatories (TERENO), the Harz/Central German Lowland Observatory (TERENO - UFZ). The main goal of the TERENO project in Schaefertal is the development of methods for the quantification and prediction of water fluxes at the small catchment scale (Zacharias et al., 2011). In the framework of the TERENO project, monitoring activities with CRS probes were initiated in 2011, as described in next section.
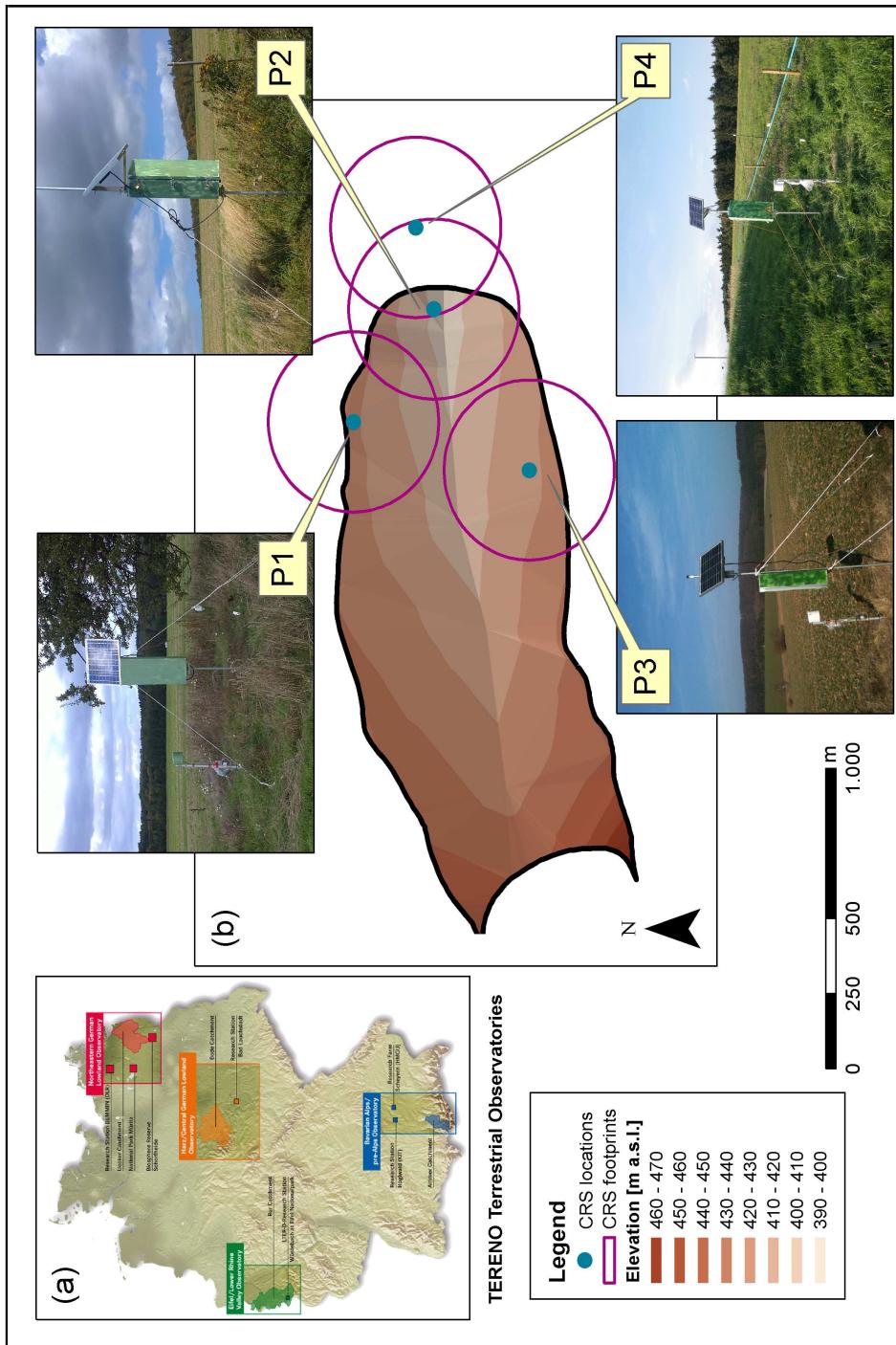
Figure 5.1: Network of cosmic-ray neutron sensors at the Schaefertal catchment: (a) Distribution of terrestrial observatories (TERENO Project) in Germany and (b) location of four cosmic-ray neutron sensors with its expected maximum footprint.

Table 5.1: Number of sensors and local conditions at position of cosmic-ray neutron sensors

Location	Exposition	CRS counter	Other sensors
P1	South	Moderated	Rain-gauge FDR profile (5 and 20 cm) RH and Temp. at 2 m height
P2	North and south	Bare Moderated	FDR profile (5 and 20 cm) RH and Temp. at 2 m height
P3	North	Bare Moderated	Rain-gauge RH and Temp. at 2 m height
P4	South	Moderated	Rain-gauge RH and Temp. at 2 m height
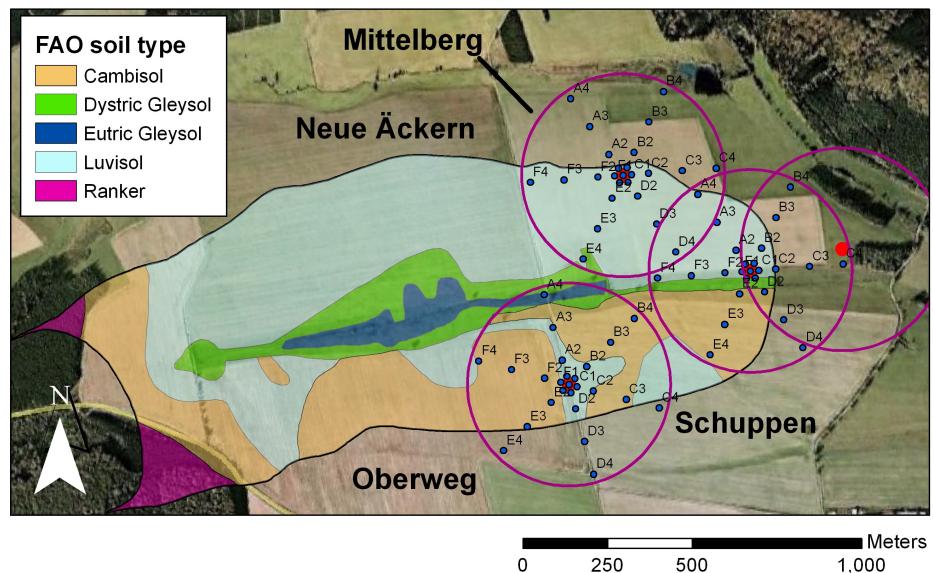
Figure 5.2: Soil types (FAO classification) and sampling design for CRS calibration (soil moisture and snow water equivalent)

5.2.2. Field instrumentation

Four cosmic-ray neutron sensing (CRS) probes from Hydroinnova (Model
CRS-1000, Albuquerque, NM) were placed at the catchment according to
Figure 5.1. The CRS probes measures natural neutrons (fast and thermal
level), atmospheric local pressure, relative humidity and air temperature.
The CRS probes were set-up with a telemetry option for data transmission
to an email server. Two probes (P1 and P3) were placed in opposite hill-
slopes with exposition to north and south. Other two probes (P2 and P4)
were located near to the valley. Probes P1 and P2 started monitoring on
June 3rd 2011, probe P3 on March 14th 2012 and probe P4 on August 17th
2012.

The CRS support volume is defined in the soil by a cylinder of 335 m
radius and depth according to soil moisture (Franz et al. 2012a). Influence of
other hydrogen pools, beside soil moisture, on penetration depth is discussed
later in section 5.2.4. In the atmosphere, this volume is conformed by a
hemisphere of 335 m radius.

The horizontal footprints of probes P1 and P3 are mainly contained inside
of agriculture fields. Footprint of probe P2 contains partially arable lands
exposed to the north and south, and a pasture area located in the valley.
Footprint of probe P4 covers similar land-use than probe P3 and additionally
a small part of forest (East direction).

Fast neutrons and thermal neutrons were measured in probes P2 and
P3, and fast neutrons only in probes P1 and P4 in a 20 minutes interval.
Subsequently, neutron counts were integrated in the post-processing at hourly
resolution. Additionally, local reference of soil moisture was placed at the
top (P1) and bottom (P2) of northern hill-slope. Two Frequency Domain
Reflectometry (FDR, Delta-T Devices Ltd., Cambridge, UK) sensors were
installed at 5 cm and 20 cm depths in each location. Rain-gauges MD532
(Delta-T Devices Ltd., Cambridge, UK) were placed in locations P1, P3 and
P4. A summary of all measurement sensors is in Table 5.2.

Data of two weather stations, part of German national network (Deutscher
Wetterdienst, DWD), was available. Stations Harzgerode-Güntersberge (51.648º
N, 10.983º E and 420 m a.s.l.) and Harzgerode (51.653º N, 11.138º E and
404 m a.s.l.) were located in less than 3 km and 6 km, respectively.

5.2.3. Neutron-derived soil moisture and probe calibra-tion

Fast neutrons were corrected by pressure, incoming radiation (Zreda et
al. 2012) and water vapour (Rosolem et al. 2013). Details of pressure

Table 5.2: Different crops registered from 2010 until 2013 in Schaefertal catchment. Location refers to sections of the catchment: Oberweg (57.4 ha), Neue Äckern (64.5 ha), Schuppen (48.7 ha) and Mittelberg (35.5 ha), as indicated in Figure 5.2

Year	Location	Main crop
2010	Oberweg	Tricitale Talentro
2010	Neue Äckern	Rape
2010	Schuppen	Winter wheat
2010	Mittelberg	Rape
2011	Oberweg	Summer wheat
2011	Neue Äckern	Winter wheat
2011	Schuppen	Tricitale Talentro
2011	Mittelberg	Winter wheat
2012	Oberweg	Winter wheat
2012	Neue Äckern	Winter wheat
2012	Schuppen	Winter rape
2012	Mittelberg	Winter wheat
2013	Oberweg	Rape
2013	Neue Äckern	Tricitale Talentro
2013	Schuppen	Winter wheat
2013	Mittelberg	Tricitale Talentro

corrections are presented in Eq. 2.3. Neutron correction of incoming radiation was computed using neutron monitoring stations Kiel and Jungfraujoch, as explained in Chapter 2 and Chapter 3. Neutron corrections of water vapour considered the following equation:

$$CWV = 1 + 0.0054 \cdot (\rho_v^0 - \rho_v^{ref}) \tag{5.1}$$

where CWV is the scaling factor for temporal changes of cosmic-ray intensity as a function of changes in atmospheric water vapour, ρ_v^0 (g cm^{-3}) is the actual air density at 2 m height, and ρ_v^{ref} (g cm^{-3}) is the air density at a reference condition (here dry air, $\rho_v^{ref} = 0$).

Fast neutrons were transformed to soil moisture measurements following Desilets' approach (2010), which has been previously applied in other studies (Rivera Villarreyes et al., 2011; Franz et al., 2012b; Rivera Villarreyes et al.,

2013a):

$$\theta_{\mathrm{CRS}} = \frac{0.0808}{\frac{N}{N_0} - 0.372} - 0.115 \qquad (5.2)$$

where θ_{CRS} is the volumetric areal mean soil moisture [$\mathrm{m^3\,m^{-3}}$], N is the corrected neutron counting rate [-], and N_0 is defined as the corrected neutron counting rate over dry soil under the same reference conditions used for N. Values of 0.0808, 0.372 and 0.115 correspond to the calibration parameters a_0, a_1 and a_2, defined previously using neutron transport simulations in Desilets et al. (2010).

The parameter N_0 was fitted according to mean values of soil moisture using two single-day calibrations on May 5th 2013 and May 21th 2013 for probes P1 and P2, respectively. The sampling approach for calibration was based on a modified procedure suggested in literature (Zreda et al., 2012). Twenty-four sampling locations were selected, instead of recommended 18 positions, based on the sensitivity areas of the CRS probe. This approach distributes sampling points in three recommended sensitivity rings (25 m, 75 m and 175 m) and one additional ring of 225 m radius. This extra sampling ring would include also soil moisture observations at the upper parts of the hill-slope (e.g. in probe P2). In these locations, values are expected to be much drier than locations near the valley. Such additional samples would take into account possible topography-dependence soil moisture patterns.

The soil samples in first campaign were taken by opening small trenches (approximately an area of 0.35 m x 0.35 m) and subsequently taking 100 cm^3 undisturbed soil cores up to 30 cm depth in intervals of 5 cm. In the second campaign, a split-tube sampler (Eijkelkamp Agrisearch Equipment, The Netherlands) was used for extracting undisturbed soil cores up to a 40 cm length. Subsequently, long soil cores were split in intervals of 5 cm. In both campaigns, wet soil samples were weighted directly in the field. Each individual sample was analysed for gravimetric water content, bulk density, lattice water, organic matter and soil texture. In total dataset consisted in 144 and 192 soil samples for first and second campaign, respectively.

5.2.4. Snow water equivalent and neutron signal

A CRS calibration for snow water equivalent (SWE) is not straightforward compared to case of soil moisture. It is not clear which part of the neutron energy spectrum (fast neutrons, thermal neutrons or a combination of these) provide better insights to monitor snow. Previously, Rivera Villarreyes et al. (2011) observed a very good correlation of fast neutrons and snow accumulation in Bornim farmland (Brandenburg, Germany), as described in Chapter

2. Here, CRS total water content significantly increased in snow periods. Moreover, a field neutron ratio was identified (N_f, in Eq. 2.6, Rivera Villarreyes et al., 2011) in order to observe different field conditions (cropped field, bare field and snow-covered field) and identify periods of snow accumulation and snow melting.

Fast neutrons and thermal neutrons respond different to snow water. For instance, Desilets et al. (2010) observed a sharp increase of thermal neutrons in the first 3 cm SWE, followed by a decrease. This behaviour is contrarily to fast neutrons, which decrease monotonically from the beginning of the snow accumulation. Increase of thermal neutrons is related to its rapid production from fast neutrons highly moderated by snow water, although production rate does not decline, however new thermal neutrons are not able any more to escape the snow layer.

In the case of a calibration with fast neutrons only, the contribution of soil moisture is still present and this needs to be eliminated for a estimation of SWE only. However under most field conditions with snow cover, soil is frozen and soil moisture temporal variability is minor. In such situation, attenuation of soil moisture to fast neutrons during periods of snow cover can be considered as a constant background.

In Schaefertal catchment, three different relationships between neutrons and SWE were evaluated: (i) fast neutrons, (ii) thermal neutrons and (iii) field neutron ratio N_f. Snow data included daily measurements of SWE at weather station (November 2012 - April 2013). It is worthy to note that none of these three relationships were used as calibration curves. Only objective here is to understand which part of the neutron energy spectrum (thermal-fast) is more subjected to variations due to snow fall and accumulation. As discussed later, only snow calibration is applied using universal calibration function (Franz et al., 2013a).

5.2.5. Effective sensor depth under snow cover periods

During periods of snow cover, the CRS signal is moderated by the snow water, soil moisture (either from a frozen layer, unfrozen layer or both) and other constant pools (lattice water and hydrogen contained in organic matter). In the following framework, the CRS effective depth (Franz et al., 2012a) is slightly modified to account for the contribution of snow water, as well as for other water pools.

The two e-folding depth of the CRS sensor is defined as the volume within 86 % of the detected neutrons above the surface originate. Such point is called the effective depth of the sensor and defined by the 86 % cumulative

sensitivity contour ($\varphi(z)$, Franz et al. 2012a) as follows:

$$\varphi(z) = 5.8 - 0.0829 \cdot z \qquad (5.3)$$

where z is the vertical distance in soil, positive downward [cm]. All hydrogen pools affecting the CRS effective depth are quantified in lengths of water as follows and the sum of all is equal to the the 86 % cumulative sensitive contour (Eq. 5.3)

$$5.8 - 0.0829 \cdot z = W_{snow} + W_{pond} + W_{veg} + W_{lattice} + W_{SOC} + W_{pore} \quad (5.4)$$

Contributions from lattice water, soil organic carbon and pore water can be expressed in terms of bulk density (ρ_b , $g\,cm^{-2}$), lattice water (τ, $g\,g^{-1}$), soil organic carbon (SOC, $g\,g^{-1}$) and soil moisture (θ, $m^3\,m^{-3}$) as follows:

$$5.8 - 0.0829 \cdot z = W_{snow} + W_{pond} + W_{veg} + \int_0^{z^*} [\rho_b \cdot (\tau + SOC) \cdot z^* + \theta(z)] \cdot dz \quad (5.5)$$

Values of lattice water and SOC in depth can be assumed constant, since they correspond to mean values from sampling campaigns. Also note that value W_{veg} is considered outside of the integral, since this equation would be only applied in snow periods with negligible (or none) vegetation. Under other conditions W_{veg} is time variable. Evaluating Eq. (5.5) at z^* and reorganizing terms, the penetration depth of CRS probe (z^*) is defined as follows:

$$z^* = \frac{5.8 - W_{snow} - W_{pond} - W_{veg}}{\rho_b \cdot (\tau + SOC) + \theta + 0.0829} \qquad (5.6)$$

Note that $\theta(z)$ during winter periods can be separated in frozen and unfrozen compartments for a better quantification. Here an averaged value in the soil profile is considered for simplification. This value can be an independent soil moisture measurement (e.g. soil moisture networks) or a CRS measurement (Zreda et al. 2012). The contribution of ponded water (W_{pond}) is not relevant in all CRS footprints in Schaefertal. In the case of small stream (Schaeferbach) partially contained inside footprint P2 and P4, this covers approximately 0.2 % of the total catchment area (Ollesch, 2008b). Water contribution from vegetation in winter crops under snow cover is mainly provided by the root system. For instance, winter wheat can reach maximum root depths down to 30 cm (initial growing stage) with values of root

biomass up $100\,\mathrm{g\,m^{-2}}$ and root water content ($> 90\,\%$), according to Thorup-Kristensen et al. (2009). Thus, the contribution of root water during winter periods can be approximately to $0.09\,\mathrm{mm}$. A further discussion of hydrogen from vegetation water is provided in results section. Finally, CRS effective depth in Eq. (5.6) during winter periods is mainly controlled by constant hydrogen pools (τ and SOC), and time-varying hydrogen pools (soil moisture and SWE). It is noteworthy that SOC was not directly measured in soil samples, instead analyses of organic matter (OM) were performed. Estimates of OM from loss-on-ignition (LOI) method are transformed to SOC usually assuming that 58 % of OM is composed by carbon (Ball, 1964).

5.2.6. Universal calibration function for measurements of snow water equivalent

The universal calibration function (UCF, Franz et al. 2013a) relates hydrogen molecular fraction (HMF) and fast neutrons observed by the CRS sensor. The approach presented in the following lines is designed for the estimation of snow water equivalent. The UCF requires a complete knowledge of all hydrogen pools inside CRS footprint at the day of calibration, i.e. vegetation aboveground, soil moisture, lattice water, organic matter, snow water, etc. Therefore, a convenient calibration period in an agricultural catchment is during short periods of bare soil or snow periods, when time-varying hydrogen pools are reduced to only one (i.e. soil moisture and snow). Opposite situation occurs for example, during the crop vegetative season with time-varying hydrogen contributions from soil moisture and crop water. Therefore, a calibration was opted during winter period (explained below). The UCF is defined as follows:

$$\frac{N}{N_S} = 4.486 \cdot e^{(-48.1 \cdot HMF)} + 4.195 \cdot e^{(-6.181 \cdot HMF)} \tag{5.7}$$

where N is the corrected neutron counts and N_S is the corrected saturated neutron count observed in an infinitely deep layer of water beneath the sensor (i.e. opposite to N_0 in Eq. 5.2) or calibrated with field observations, and $HMF = \sum H_i / \sum A_i$ is the hydrogen molecular fraction [$\mathrm{mol\,mol^{-1}}$], defined as follows:

$$HMF = \tag{5.8}$$

$$\frac{H_\tau + H_{SOC} + H_\theta + H_{SWE} + H_{VEG}}{NO + SiO_2 + H_2O_\tau + H_2O_{SOC} + H_2O_\theta + H_2O_{SWE} + C_6H_{10}O_5 + H_2O_{VEG}}$$

where H_i is the sum of hydrogen moles from lattice water (H_τ), soil organic carbon water equivalent (H_{SOC}), soil moisture (H_θ), snow water equivalent (H_{SWE}) and vegetation (H_{VEG}) inside the CRS support volume, and A_i is the sum of all moles from air NO (assumed 79 % N and 21 % O by mass), soil SiO_2, lattice water ($H_2O)_\tau$, soil organic carbon water equivalent $(H_2O)_{SOC}$, soil moisture $(H_2O)_\theta$, snow $(H_2O)_{SWE}$ and biomass ($C_6H_{10}O_5$) inside the CRS support volume. Franz et al. (2013a) verified the simplification of SiO_2 soil composition, instead of real chemical composition, with excellent agreements in 50 COSMOS sites in USA. Recently, Franz et al. (2013b) used UCF to separate hydrogen contribution from soil moisture and above-ground biomass for a maize field and a forest site. Contribution of lattice water and SOC is constantly as presented in Eq. (5.6) and Eq. (5.8).

The hydrogen contribution from the atmosphere is not included in Eq. 5.8, since neutrons have been previously corrected due to changes of water vapour using a reference condition of dry air (ρ_v^{ref}). The CRS support volume is defined as a hemisphere in the atmosphere and a cylinder (radius of 335 m and height equal to CRS effective depth from Eq. 5.6) in the soil (Franz et al., 2013a). Note that CRS effective depth should also consider contribution of snow.

The calibration of parameter N_S in Eq. (5.7) was carried out using the snow campaign in winter period 2012-2013. The snow campaign consisted in measurements of snow height, snow density and snow water equivalent inside footprint P3 on April 2nd 2013. Sampling approach followed same number of locations as soil moisture campaigns, 24 locations were distributed in six angles and four sensitivity rings of radius 25 m, 75 m, 175 m and 225 m. Snow density and snow water equivalent was measured from snow cores with a plastic cylinder ($\sim$ 6.1 cm diameter). In this approach, only single average values of snow density for each snow core at each sampling location are possible. The 24 locations within footprint P3 covered a good range of field conditions with different expositions on the hill-slope, e.g. different topographical features (valley, intermediate hill-slope and upper hill-slope) and two land uses (pasture and agricultural field). During sampling day, snow layer covered completely catchment area and there was no vegetation aboveground inside CRS footprint. From average SWE measured at day of calibration and Eq. (5.6), contribution of soil moisture to the CRS support volume become negligible ($z^* \sim 0\,\text{cm}$). In that situation, UCF is only controlled by SWE, therefore allows its direct estimation.

5.3. Results and discussions

5.3.1. Neutron counts at the Schaefertal catchment

Corrected fast neutrons in the Schaefertal catchment fluctuated from 727 cph to 1348 cph (P1 location), from 644 cph to 1204 cph (P2 location), from 681 cph to 1392 cph (P3 location) and from 671 cph to 1056 cph (P4 location). The mean neutron counting rate in the catchment varied from 720 cph to 1168 cph. In general, these numbers are relatively low compared to sites from COSMOS network (Zreda et al., 2012). This is due to the differences in elevation. For instance, counting rates at COSMOS site Mt. Lemmon at 2745 m a.s.l. varied from 1800 cph to 3600 cph. In Schaefertal, the CRS sensors located at the upper hill-slopes (P1 and P3) reported higher counting rates than probes located near the valley or bottom hill-slope. Correlations between four individual probes and their mean value are very high ($0.88 \leq r^2 \leq 0.93$, Figure 5.3) using hourly integration times. The CRS neutron noise decreases strongly at daily time intervals, as presented in gray color. Thus, to overcome high signal-noise ratio from low number of neutron counts, daily average of neutron counts was considered in further analysis.

Temporal variability of the neutron counts was evaluated comparing daily relative differences of counts at each probe in respect to the mean neutron count. In general, average relative difference for entire monitoring period was less than 5.8 %. Probes at locations P2 and P4 (downhill) indicated higher values than mean counting rate in -3.3 % and -5.8 %, respectively. Probes P1 and P3 (uphill) indicated lower counts than mean counting rate in 4.5 % and 5.0 %, respectively. Obviously, these deviations are due to wetter and drier soil moisture spots (i.e. near stream and uphill, respectively) located within each footprint. Changes of land-use may play a role on the counting rate as well. For instance, footprint P4 containing a small area covered by forest, presented the lowest counting rates. Although tree biomass and its water content was not quantified, it is presumable that this small area of forest may contribute to the high neutron moderation, as it has been observed in other studies (Bogena et al. 2013).

5.3.2. Calibration of soil moisture equation and universal function

The CRS calibration for soil moisture was carried out following standard calibration procedure (Zreda et al., 2012). Two sampling campaigns inside footprint P1 and P2 with mean soil moisture values of 0.284 $m^3\,m^{-3}$ and 0.245 $m^3\,m^{-3}$, respectively were used for calibration. The standard de-
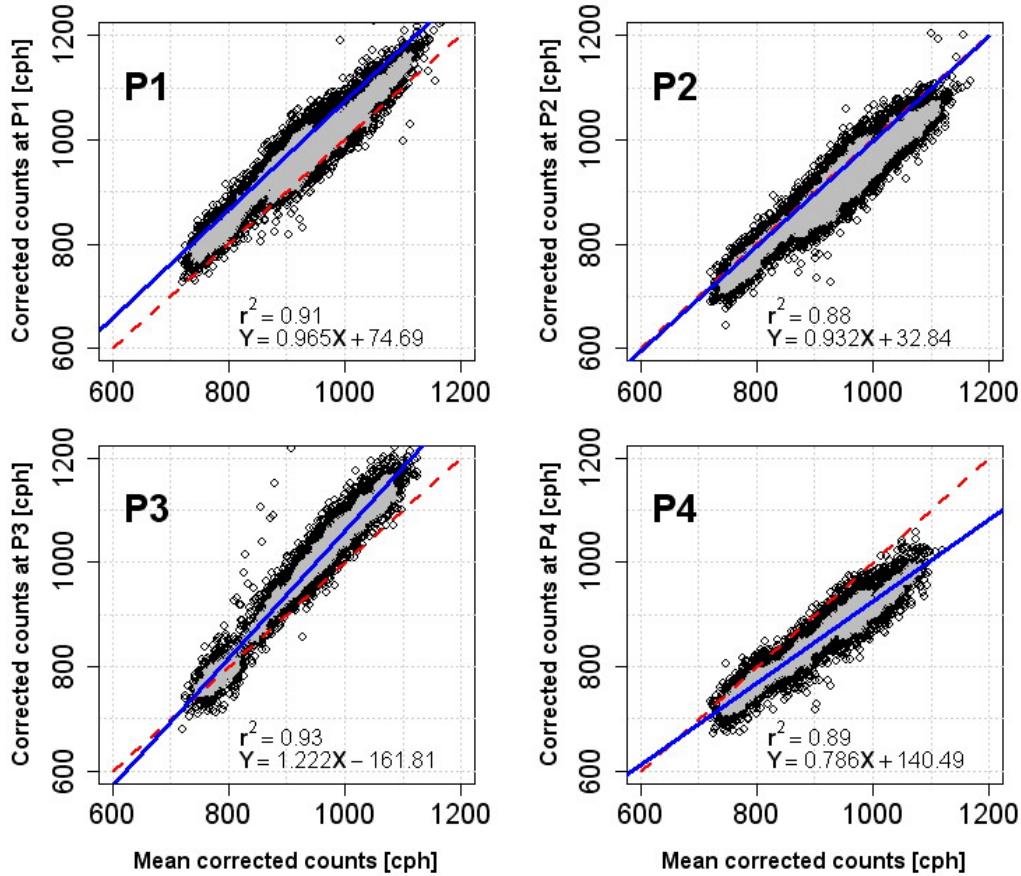
Figure 5.3: Correlation graph between neutron counts in each CRS location (P1-P4) and mean neutron count: Black and gray dots represent hourly and daily integration times, respectively. Blue solid line is the best linear fitting (equation shown in graph) and red dash is the line $1-1$. Neutron corrections of pressure, incoming radiation and water vapour were applied to all datasets.

viation was computed as 0.009 $m^3 m^{-3}$ and 0.023 $m^3 m^{-3}$ for P1 and P2, respectively. Variability in second campaign was larger because the footprint P2 covers partially four different soil types in the Schaefertal, compared to footprint P1 which is mainly located in Luvisols region (Figure 5.2). Although differences in soil types, intensive sampling indicated similar values of lattice water ($\tau = 0.0103 \pm 0.003\,g\,g^{-1}$) and soil organic carbon ($SOC = 0.044 \pm 0.014\,g\,g^{-1}$) between two campaigns (28 samples), which covers large part of Schaefertal. Since only limitation to transfer CRS calibration parameters to different field sites is τ and SOC, a unique calibration curve for entire Schaefertal catchment can be proposed.

Soil moisture from two sampling campaigns, as well as lattice water and SOC, indicated values of penetration depth of 13 cm and 15 cm, respectively. The weighted means of soil moisture down to penetration depth were 0.278 $m^3\,m^{-3}$ and 0.299 $m^3\,m^{-3}$, which were subsequently used for calibration.

Probe P2 was selected for calibration in following analysis. This probe presented lower deviation of neutron counts in respect to mean counting rates during monitoring period, as discussed previously in section 5.3.1. Also, probe P2 contains longer time series (less data gaps because of battery failures). It is worthy to mention that this is a simplification, which is mainly hold on low variability of lattice water and soil organic matter observed in collected samples. A more detailed evaluation will require intensive mapping of these variables in the Schaefertal catchment in order to evaluate the need of individual CRS probe calibration.

The parameter N_0 calibrated at P2 was subsequently transferred to and tested by probe P1, which provides maximum counting rates and differs significantly from P2. The Eq. (5.2) was calibrated with a value of $N_0 = 1428$ ± 38 counts per hour. Transferring this value to probe P1, provides an overestimation of approximately 0.025 $m^3\,m^{-3}$, partially due to differences in vegetation crop between time of campaigns (from $\sim 2\,cm$ to $\sim 15\,cm$ height) and differences of lattice water and organic matter. This deviation is very similar to the soil moisture variability observed between two sampling campaigns and is within calibration error presented in literature (Rivera Villarreyes et al., 2011; Franz et al., 2012b; and Zreda et al., 2012) and in cropped fields (Chapter 3). For practical reasons, a single soil moisture calibration is assumed for all CRS probes.

The third sampling campaign, consisting in observations of SWE inside footprint P3, was used to calibrate parameter N_S in Eq. (5.7). The mean value of SWE equivalent was 85 mm ± 10 mm. This number is well comparable with SWE value at same day in weather station. Observed SWE corresponded to a hydrogen molecular fraction (HMF) of approximately 0.20 $mol\,mol^{-1}$. The best fit in the UCF was identified with N_S equal to 654 ± 26 counts per hour. Such value of N_S is relatively low compared to that identified in previous studies (Franz et al. 2013a and Franz et al. 2013b), i.e. $N_S > 1000$ counts per hour. This discrepancy is clearly attributed to low range of fast neutron in Schaefertal.

Calibrated UCF with single campaign of SWE was subsequently validated with the two soil moisture campaigns in spring 2013 as shown in Figure 5.4. The estimations of HMF from soil moisture campaigns fitted very well UCF. Neutron counts estimated solving Eq. (5.7) for known HMF from soil moisture campaigns were 1010 cph and 899 cph, respectively. These estimates of N indicated only a deviation of 47 cph and 25 cph in respect to real counts

measured at calibration days. Thus, such a deviation corresponds to the natural variability of fast counts ($St. Dev. = \sqrt{N}$).

5.3.3. Spatio-temporal variability of CRS water content

Daily soil moisture via CRS approach is presented in Figure 5.4. Temporal variability in all CRS sensors responds consistently with the daily amounts of precipitations. The temporal variability of soil moisture in all CRS sensors follows the same dynamics. CRS sensors fluctuate from 0.10 $\mathrm{m^3\,m^{-3}}$ and 0.30 $\mathrm{m^3\,m^{-3}}$ outside of snow-covered periods. Also, dynamics of field-scale soil moisture (CRS probe) and local-scale profiles (FDR at locations P1 and P2) were observed very similar, except in periods of snow cover or soil frozen conditions (e.g. from December until April), when these techniques behave differently due to their contrast on physical basis. Furthermore, variability of CRS soil moisture between probes is within the variability of local soil moisture (soil cores or split tube) at the day of calibration. For instance, mean values of two soil moisture campaigns (July 2011) at the near-surface within footprint P1 agree well to CRS soil moisture, which has a deeper observation into the soil. In these two campaigns, soil moisture was 0.069 ± 0.014 (n = 249) and 0.110 ± 0.018 (n = 177), respectively. Comparable results are not surprisingly because field conditions (e.g. lattice water, SOC and soil moisture) can reduce significantly CRS penetration depth to a value $z^* < 0.15\,\mathrm{m}$, which is just two-fold value of FDR rods ($\sim 6\,\mathrm{cm}$) used in campaigns.

Dynamics of CRS soil moisture correspond well to temporal variability of HMF computed using universal calibration function. For instance, both curves (soil moisture and HMF) showed sharp increases in periods of snow cover, e.g. winter 2012-2013, however this is more pronounced in Desilets' calibration. Here, time series of HMF indicated a systematically increase of hydrogen pool, causing a decrease of neutron counting rates, and therefore an unrealistic increase of soil moisture with Desilets' equation. A further discussion of snow and CRS signal is presented later in this chapter.

Since no ground-truthing soil moisture was available during the monitoring period to contrast CRS soil moisture in all four probes, discussion of the spatio-temporal variability of CRS water content is based on ancillary data only. First, the spatial variability is evaluated based on local information within the CRS footprint and how CRS probes differ to each other. Second, the temporal variability is addressed at the seasonal scale.

Although four CRS sensors were placed with a large footprint overlap, patterns of soil moisture at the CRS scale could been identified. For instance, CRS sensor at P2 located at the valley (blue dots in Fig. 5.4) present con-
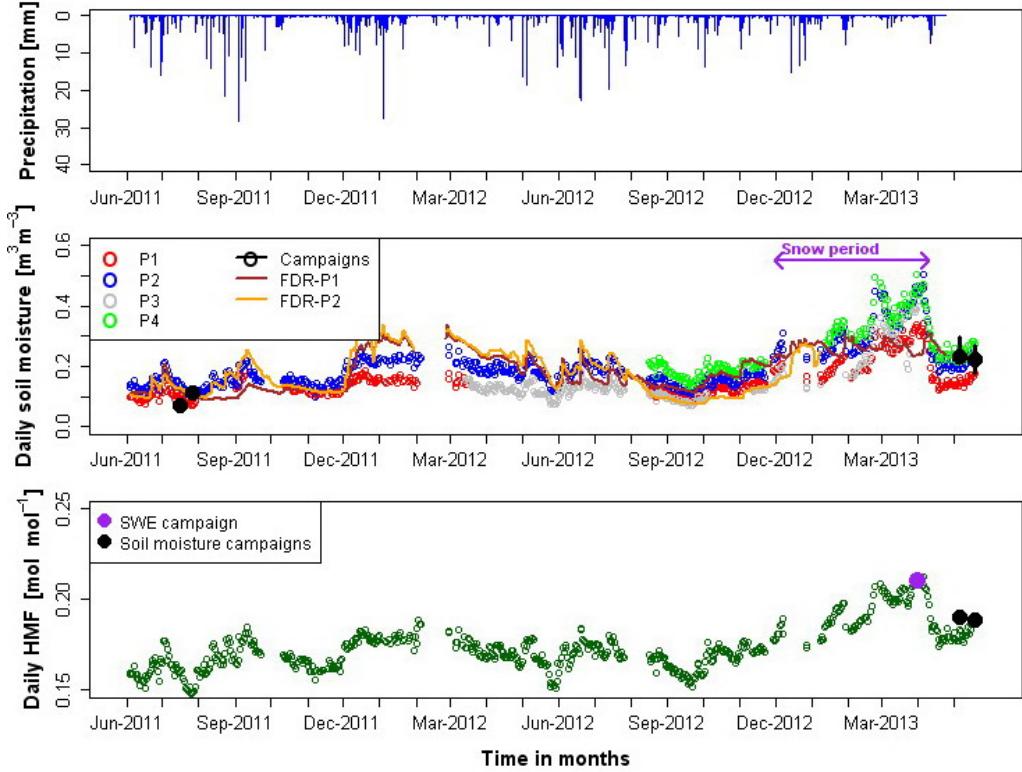
Figure 5.4: Time series of daily precipitation (upper panel), daily CRS soil moisture in four different CRS locations (middle panel) and daily mean hydrogen molecular fraction (HMF) in Schaefertal catchment. The HMF is defined as the ratio between total hydrogen moles and total moles inside CRS footprint. Continues solid lines correspond to mean local soil moisture (5 cm and 20 cm) at locations P1 and P2. Black dots in July 2011 correspond to surface sampling campaign (only footprint P1) and black dots in April 2013 corresponds to calibration campaigns inside footprint P1 and P2. The HMF was computed from calibrated UCF and values correspond to daily mean from four CRS sensors.

stantly higher soil moisture values than CRS sensor at P1 located at the top of hill-slope (red dots in same figure). In similar manner, probe P4 indicated maximum values of soil moisture, slightly higher than probe P2. Here the lower neutron counts of probe P4 is a mixture from wetter areas closer to the stream and neutron moderation by the forest. This spatio-temporal variability of soil moisture in Schaefertal is assumed to be dominated by topographical features, as it has been demonstrated in other hill-slope catchments. An interpretation of wetter and drier areas indicated by CRS approach was based

on the topographic wetness index (TWI, Beven and Kirkby 1979), computed
using a digital elevation model of 5 m resolution. The TWI, which combines
information of the local up-slope contributing area and slope, is commonly
used to quantify topographic control on hydrological processes (Sorensen et
al., 2006) and observe the degree of spatial organization within a catchment
(Green and Erskine, 2004). In Schaefertal, TWI verified observations from
the CRS approach, topographic-induced wetter areas are in general situated
in the vicinity of probe locations P2 and P4, which indicated lower counting
rates (cf. section 5.3.1). Areas near to stream showed maximum values of
TWI, and although these are not so large compared to total CRS footprint,
however these small areas coincided with CRS area of higher sensitivity (i.e.
radius of ~ 25 m, Zreda et al. 2012).

Although it has not been addressed in this chapter, the use of topo-
graphical features in Schaefertal can be a valuable information for further
research in (i) downscaling approaches of CRS soil moisture, (ii) addressing
issue of CRS horizontal footprint and (iii) initial validation of future CRS
rover-approach in Schaefertal.

Furthermore, the spatial organization of soil moisture at the CRS scale
may be evaluated from soil moisture maps using the rover-approach of the
CRS (e.g. Chrisman and Zreda, 2013). A simplified methodology was to
correlate CRS mean and standard deviation from four stationary probes in
Schaefertal, as shown in Figure 5.5. As first results, soil moisture variability
at the CRS scale (~ 600 m) increased constantly with increasing mean soil
moisture from $0.05 \, \text{m}^3 \, \text{m}^{-3}$ to $\sim 0.25 \, \text{m}^3 \, \text{m}^{-3}$. Similar trend was also observed
in literature, e.g. Famiglietti et al. (2008) at scales of 800 m, 1600 m and
50 km. However, empirical trend identified here should be carefully verified
with more measurements in future research.

This knowledge of the spatial variability can improve the predictive skills
of hydrologic, weather prediction, and general circulation models, includ-
ing processes such as evapotranspiration and run-off (Famiglietti and Wood,
1994) in the Schaefertal catchment. For instance, understanding variability
of soil moisture within a remote sensing pixel by using the CRS approach
may provide better insight for validation of remote sensing products and
approaches.

As it has been already discussed in literature, methodologies with large
integral observations of water storage (e.g. gravimeter or CRS) are promising
to understand (i) connection between hydrological process and water storage
(Creutzfeld et al., 2013), and (ii) water storage response to climate change
or hydrological extremes (Creutzfeld et al., 2012). In this study, temporal
variability of the CRS water content, i.e. without distinction between soil
moisture and snow water equivalent, was computed at the monthly time
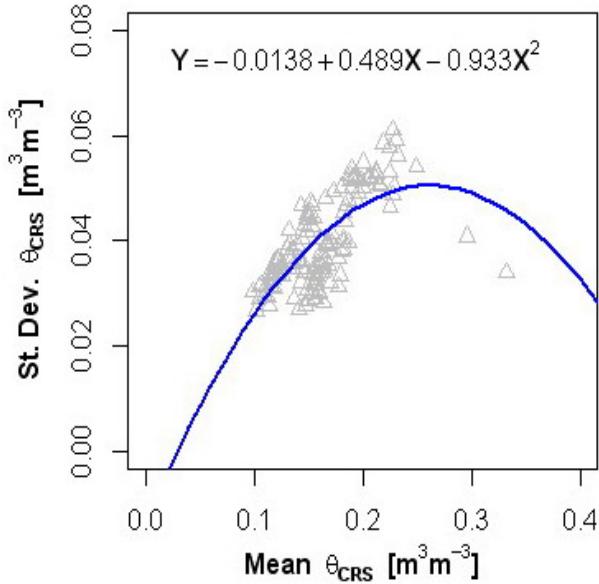
Figure 5.5: Relationship between mean CRS soil moisture (θ_{CRS} , $m^3\,m^{-3}$) and standard deviation for four CRS sensors in the Schaefertal catchment. Computations of θ_{CRS} are based on average daily corrected neutron counts. Note that plot does not consider snow periods.

scale and compared to weather records. Time series of monthly precipitation (P), potential evapotranspiration (PET) and temperature are presented in Figure (5.6). Potential evapotranspiration was computed using Thornthwaite method with temperature records. Remote-sensed leaf area index (LAI) from MODIS satellite mission, which is weekly available, was also included for discussion.

The monitoring period in Schaefertal along two years indicated that daily variability of CRS water content within a month is in general similar, as shown in the distribution of box plots and its components, except winter period from December 2012 until April 2013 with significant snow amounts. Historical records in weather stations reveal that region where Schaefertal catchment is located has previously experienced extreme snow events in the past, for instance winter periods 2009-2010 with 67 cm and 2010-2011 with 112 cm of snow height (weather station). Beside winter periods, anormal daily variability of CRS water content can be also attributed to variability of vegetation cover within a month. For instance, higher variability of CRS water content within June 2012 was correlated to fast increase of LAI during this month. Here, vegetation water is quickly increased, as observed in increase of LAI, therefore CRS water content is also affected in this period.
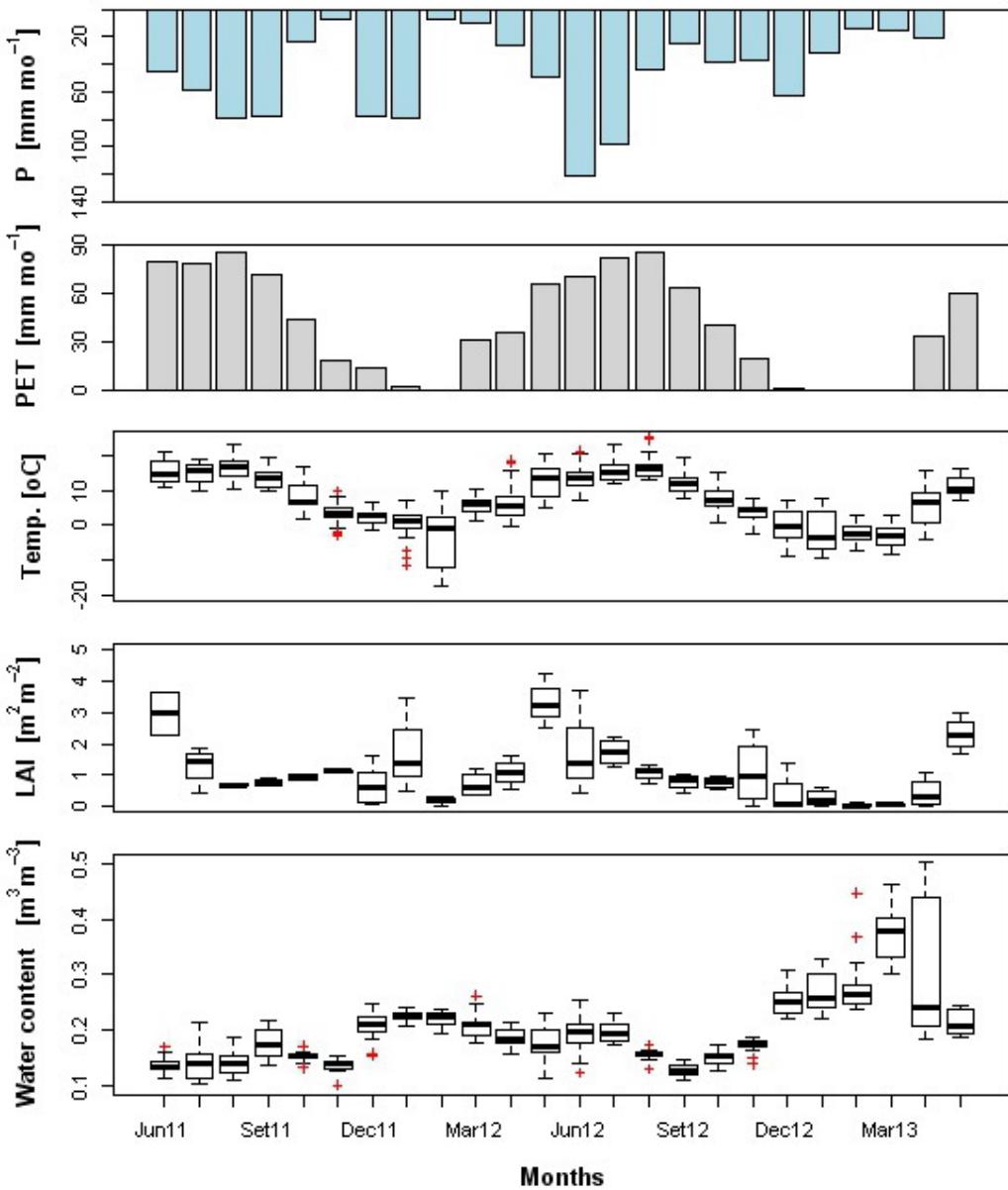
Figure 5.6: Time series of monthly precipitation (P), potential evapotranspiration (PET), temperature (Temp.), satellite leaf area index (LAI) and CRS water content.

A comparison between CRS water content and two seasonal weather variables (P and PET) is presented in Figure 5.7 for further discussion. In general, the response of the CRS probe is well dominated by $P - PET$ at the monthly time resolution for drier and wetter conditions. Furthermore, it
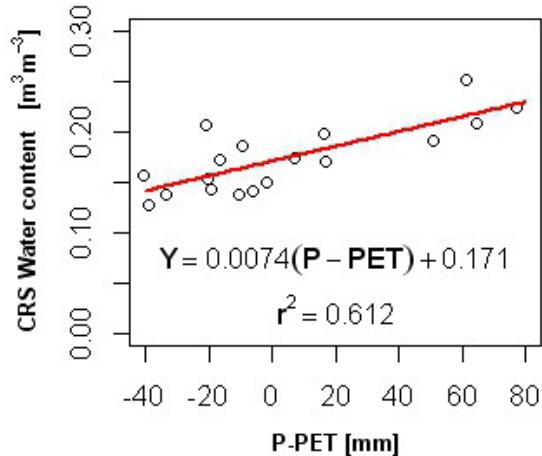
Figure 5.7: Relationship between monthly CRS water content and P-PET. Empirical linear fit is presented. Note that months with snow records were not included in analysis.

seems to exist a minimum CRS storage ($\sim$ 0.14 m^3 m^{-3}) for normal years (e.g. not extremely dry period), which may be related to the water content at field capacity. The correlation coefficient between CRS storage and $P-PET$ was found $r^2 = 0.612$, which is considered relatively higher for this kind of comparison (Creutzfeld et al., 2012). Part of the variability of CRS water storage not accounted by $P - PET$ may be due to uncertainty of PET (i.e. using only temperature for calculations). Obviously, clear deviation in this comparison is also due to other important components of the water balance such as groundwater, soil percolation and catchment discharge, which were not considered (not available at time of analysis). Therefore, a further step in this analysis should take into account this information to close the water balance.

5.3.4. Hydrogen pools in Schaefertal catchment

As discussed previously, time series of HMF (Figure 5.4) follows very well dynamics of soil moisture. In the case of snow periods, HMF becomes a mixture of soil moisture and SWE (discussed later). The fact that Schaefertal is mainly an agricultural catchment (83.6 % arable land, 11.6 % grassland and 3.1 % forest), it is expected that vegetation influences the CRS signal during spring and summer seasons, as observed in previous studies (Rivera Villarreyes et al., 2013a). In this study, corrections of attenuated neutrons due to vegetation (Chapter 3) are not applied, since independent soil moisture mea-

surements during crop development were not available. Alternatively, CRS
deviations at maximum and minimum vegetation stages can be quantified.
Hydrogen percentages for different ranges of wet biomass under Schaefertal
conditions of lattice water and organic matter were computed using UCF.
For the final harvested amount in year 2010-2011 of $1.73\,\mathrm{kg\,m^{-2}}$, vegetation
contribution to total hydrogen pool was only 3.8 % and 2.9 % for dry (0.05
$\mathrm{m^3\,m^{-3}}$) and wet ($0.35\ \mathrm{m^3\,m^{-3}}$) conditions, respectively. The contribution of
hydrogen from vegetation is more reliable at higher amounts of biomass. A
biomass of about 20 $\mathrm{kg\,m^{-2}}$ (e.g. forest) can contribute up to 30.3 % and
25.1 % of the total hydrogen under drier and wetter soil conditions, respec-
tively. In the Schaefertal catchment only 3.1 % of the area is forest, which
is partially inside footprint P4. This situation justifies lowest counting rates
observed at this probe, as discussed in section 5.3.1. Additionally, the contri-
bution of hydrogen from vegetation may also decrease the CRS penetration
depth. However, such quantification requires knowledge of vegetation water
content. In other studies, for instance, Franz et al. (2013b), biomass con-
tent of a maize field was estimated using fast neutrons, independent values
of soil moisture and universal calibration. Although, influence of vegetation
water on penetration depth was completely neglected, estimates of biomass
and biomass water content were acceptable in comparison to independent
measurement.

Snow contributes significantly to the total hydrogen pool. During moni-
toring period in Schaefertal, maximum values of SWE were recorded in the
winter 2012-2013. In this period, weather station reported values from 8.8
mm up to 88.8 mm. From Eq. (5.6), z^* was estimated ~ 20 cm depth without
snow presence and for an average CRS soil moisture of ~ 0.20 $\mathrm{m^3\,m^{-3}}$. An
increase of SWE only up to 40 mm, a reduction of z^* occurs down to ~ 6 cm.
Therefore, influence of snow on penetration depth was considered in further
analysis of SWE measurements via CRS approach and UCF.

The hydrogen contribution of snow water can be similar or higher than
soil moisture contribution. However, soil moisture contribution, a difference
of snow water, can be assumed as constant. This is under the assumption that
soil moisture dynamics are reduced significantly. In Schaefertal, for instance,
level of soil moisture in period December 2012 until April 2013 was in general
similar without significant temporal changes, as shown in two FDR profiles
(Fig. 5.4) installed at upper and lower part of the hill-slope, in a network of
local-scale soil moisture (40 nodes at 5, 25 and 50 cm depths) placed partially
within footprint P4 (Martini et al., 2013). The major hydrogen contribution
in winter period 2012-2013 was observed to come from SWE, according to
scatter plot HMF vs. SWE in Figure 5.8. Here, most of the variability
of HMF during winter period was attributed to SWE with a $r^2 = 0.874$.
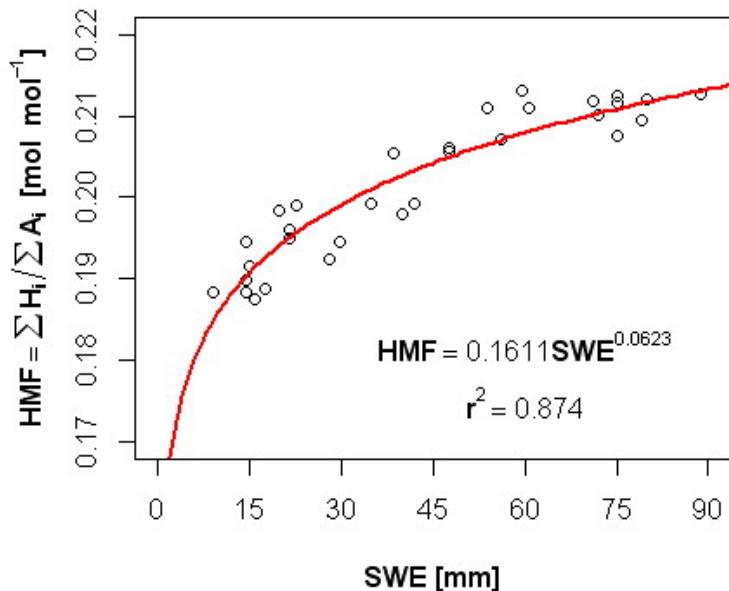
Figure 5.8: Contribution of snow water equivalent (SWE, mm) to the hydrogen molecular fraction (HMF, $\mathrm{mol\,mol^{-1}}$) in the universal calibration function (UCF, Franz et al. 2013a). An empirical fit is presented.

The rest of the variability is explained by the soil moisture contribution to HMF and representativeness of snow measurements from weather station to Schaefertal catchment (discussed in next section).

5.3.5. CRS signal during snow periods

The correlation between fast neutrons, thermal neutrons and N_f ratio against SWE is presented in Figure 5.9 and Table 5.3. Fast neutrons (N_{Fast}) and thermal neutrons (N_{Th}) indicated the best and worst correlation with SWE, respectively. Combining neutrons at the thermal and fast energy level, expressed as the N_f neutron field ratio (Eq. 2.6), correlation coefficient was 0.721. Time series of fast neutrons and thermal neutrons showed different behaviour during snow period (Figure 5.10). On the one hand, thermal neutrons increased sharply at the first snowfall with a SWE peak of 28 mm, followed by a fast decrease until returning to level before snowfall (i.e. mean value of 530 counts per hour). On the other hand, fast neutrons monotonously decrease during snowfall. The significant production of thermal neutron at first snowfalls is stopped when thermal neutrons are not any more able to escape from the snow layer. Furthermore, this behaviour of thermal neutrons is the cause of slight decrease in $r^2 = 0.721$ between N_f and SWE. The root
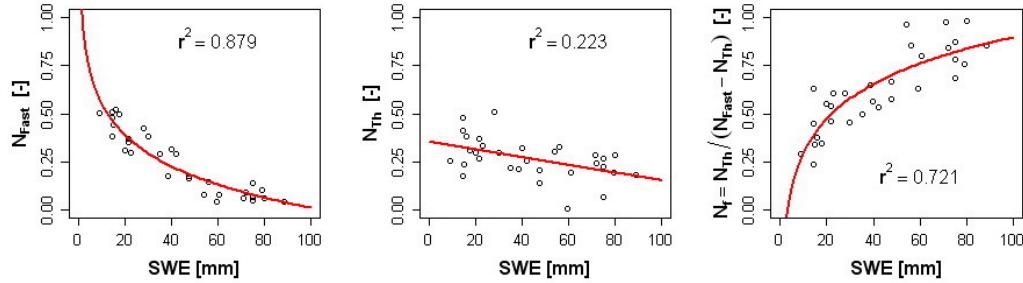
Figure 5.9: Correlation between snow water equivalent (SWE, mm) and (i) fast neutrons (N_{Fast}) on the left, (ii) thermal neutrons (N_{Th}) on the middle, and (iii) field neutron ratio (N_f, Rivera Villarreyes et al. 2011) on the right. Notice that vertical axes in all cases are normalized respect to corresponding minimum and maximum values.

Table 5.3: CRS calibration for snow water equivalent (SWE, mm) based on fast neutrons and neutron field ratio (N_f). Mathematical form of the CRS model is $\mathrm{SWE_{CRS}} = K_1 \cdot X^{K_2}$, where X is either fast neutrons [cph] or N_f [-].

Model	Coefficient K_1	Coefficient K_2	RMSE	r^2
	[-]	[-]	[mm]	[-]
Fast neutrons	$2.81 \cdot 10^{34}$	-11.352	9.3	0.933
N_f	1.9561	4.084	14.2	0.822

mean square error was computed as 9.3 mm for the fast neutrons and 14.2 mm for the N_f ratio.

Snow water equivalent estimated via CRS (SWE$_{\mathrm{CRS}}$) was derived using Eq. (5.6) through Eq. (5.8). These two equations are controlled by changes of soil moisture and snow water equivalent within the Schaefertal catchment. From previous analysis, HMF in Eq. (5.8) is highly dominated from SWE (cf. section 5.3.4 and Fig. 5.7). Moreover, soil moisture dynamics at soil moisture network (SoilNet, Martini et al. 2013) indicated low variability during snow periods. Based on these two observations, SWE_{CRS} was computed assuming $\theta \approx 0.15$ m^3 m^{-3} ($\sim$ average soil moisture before first snowfall).

The SWE$_{\mathrm{CRS}}$ calculated with the UCF is presented in Figure 5.10 (lower panel). Estimations of SWE$_{\mathrm{CRS}}$ followed quite well dynamics of snow water equivalent and snow height from weather stations. However, SWE$_{\mathrm{CRS}}$ indicated higher absolute values than weather station, e.g. peak of SWE
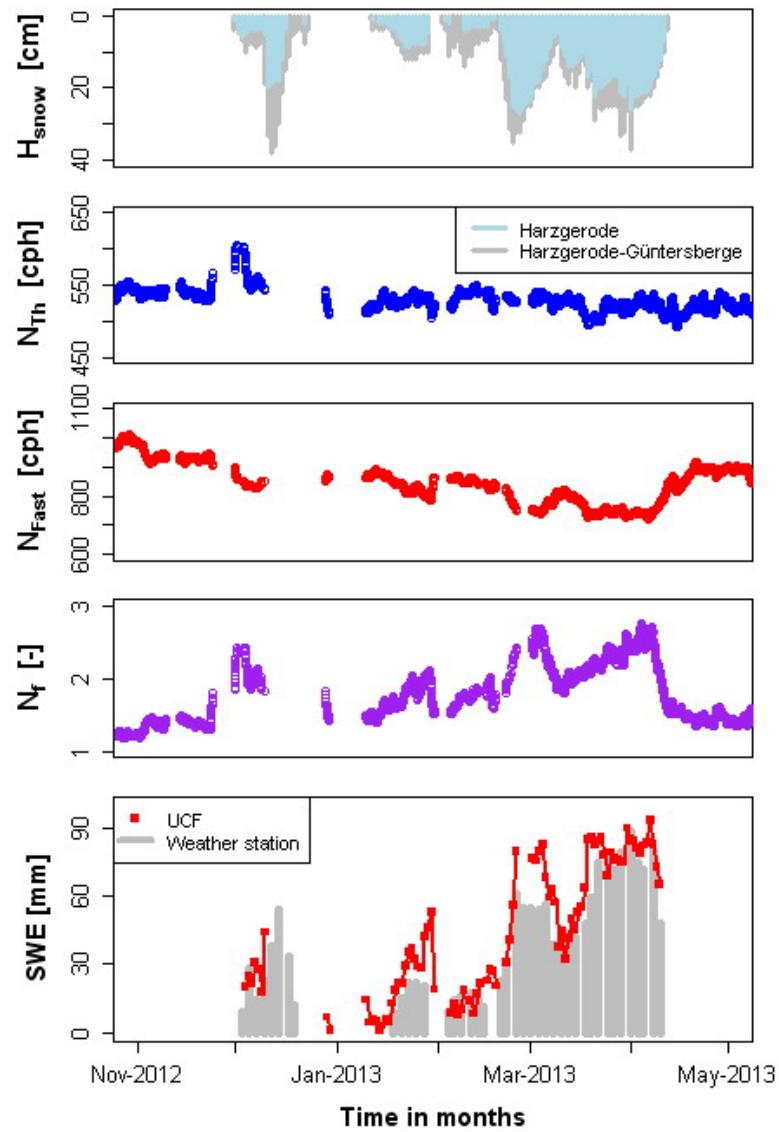
Figure 5.10: Response of CRS sensor during winter season (Nov. 2012 – April 2013): From top to bottom: (i) time series of daily snow height from two weather stations, (ii) time series of daily averaged thermal neutrons, (iii) time series of daily averaged fast neutrons mean daily, (iv) time series of daily averaged field neutron ratio (N_f, Rivera Villarreyes et al. 2011), and (v) measured SWE (gray bars) and estimated SWE with CRS approach.

at beginning of March 2013. Large discrepancy is attributed to variability of snow height and SWE inside catchment, which can not be significantly represented by local snow measurements at weather station. For instance, during snow sampling campaign, large snow accumulation were identified primarily at the hill-slope exposed to north direction. Furthermore, there is a clear scale difference between field-scale CRS probe and point-scale snow cores from weather station. Therefore, further research should be addressed to quantify accuracy of SWE estimations using the CRS probe and universal calibration function.

5.4.   Conclusions

The analysis evaluated in this chapter demonstrated several benefits of using the cosmic-ray neutron sensing (CRS) for catchment monitoring. Two CRS equations (Desilets et al., 2010 and Franz et al., 2013) were calibrated for soil moisture and snow water equivalent, respectively. It is worthy to notice that universal calibration (Franz et al., 2013) is also able to compute soil moisture, however this requires knowledge of a time-varying CRS penetration depth for the signal disaggregation (i.e. snow-free periods). In the case of winter periods with high snow accumulation, universal calibration is highly capable to compute snow water, since contribution of soil moisture is negligible (penetration depth ~ 0 cm). Additionally, three empirical relationships between snow water equivalent and neutrons (thermal, fast and their ratio) were discussed for understanding neutrons behaviour under snow fall and accumulation.

The specific conclusions of this study are summarized in the following points:

- The temporal variability of CRS water content at the monthly resolution correlated well with monthly precipitation and potential evapotranspiration ($r^2 = 0.612$), although other water balance components were not included in analysis (groundwater, soil percolation and catchment discharge).

- Snow water affects significantly to the CRS signal and its penetration depth into the soil. The average CRS penetration depth in Schaefertal catchment was estimated ~ 20 cm for specific values of lattice water and soil organic carbon. Considering an average SWE of 40 mm, observed in weather station and estimated by CRS probe, penetration depth is reduced down to ~ 6 cm.

- This study also proves the potential of using the universal calibration function in winter periods. Moreover, the use of a calibration/validation procedure in two seasons (winter and spring) with information from a snow sampling campaign and two soil moisture campaigns.

Chapter 6

General discussion and final conclusions

6.1. Summary of achievements

Using the specific case studies of Bornim farmland and Schaefertal catchment, this section summarizes briefly the major research achievements and complements the previous discussion in respect to main objectives.

This dissertation evaluates the use of the cosmic-ray neutron sensing (CRS) approach in cropped fields. The important scientific contribution here is the continuous monitoring, evaluation and discussion of the CRS approach in Bornim farmland with three different crops (Chapters 2 and 3, Rivera Villarreyes et al., 2011 and 2013a). So far, these are first study cases carried out in agriculture fields with important time-varying biomass and crop water content (both above- and below-ground). Thus, insights found in these publications provide first knowledge of the CRS approach in cropped fields.

Here, the applicability of the CRS in cropped fields was demonstrated. Important "take home" message is that transferability of CRS calibration parameters to different crop seasons requires further evaluation of field condition changes (vegetation, CRS characteristics, etc.) in respect to the calibration period. For instance, CRS calibration parameters from "corn" period with near-surface ground-truthing soil moisture provided a large overestimation (RMSE ~ 0.143 m^3 m^{-3}) in sunflower and winter rye periods now using soil moisture profiles as ground-truthing.

The issue of the CRS penetration depth underestimation has arisen in this context. In the corn period, assumption of 5 cm of CRS observation depth was discarded with new calculations revealing a more realistic value of 20 cm depth in sunflower and winter rye periods. It is also important to

127

mention that the alteration of ground-truthing soil moisture from 19 near-surface locations to 5 profiles contributed only with ~ 0.02 m^3 m^{-3} in the overall overestimation. Therefore, major discrepancy between CRS approach and ground-truthing in sunflower and winter rye periods cannot be attributed to the reference network, but to other variables such as vegetation characteristics (water content, biomass, etc.).

Another crucial point not taken into account in the calculation of CRS penetration depth is the water contribution from above- and below-ground biomass. Similar to framework used in section 5.2.5 for snow in Schaefertal, influence of vegetation on the CRS depth should be addressed in further studies. However, continuous measurements of crop water content is limited because of technical challenges.

In terms of calibration approaches for CRS soil moisture, three different ways of fitting the CRS equation (Desilets et al., 2010), four ways of integrating the ground-truthing soil moisture in depth and eight calibration periods (crop stages of sunflower and winter rye) were tested, analysed and interpreted in Chapter 3. The main conclusion from all this calibration effort was that selection of a calibration period within the crop development is much more relevant than manner how calibration equation is fitted. Certainly here, exists a validation error depending on the period which has been used for calibration. However in all cases, calibration window with high development of vegetation was well representative to the rest of crop stages, with some discrepancies in first weeks of crop season.

In Chapter 3, further steps of the typical CRS calibration were provided. A methodology for correction of attenuated-neutrons due to vegetation influence is presented. A linear piecewise model for time-varying neutron corrections was formulated based on classical model of crop development (Allen et al., 1998). The concept of attenuated neutrons follows a combination of the physical definition of neutrons (increase of hydrogen content slows down more neutrons) and conceptual definition of crop development.

This vegetation correction was successfully applied to three fitting approaches and two periods with high and low vegetation characteristics (initial and middle crop stages) for sunflower and winter rye. A significant improvement of RMSE was achieved (~ 0.015 m^3 m^{-3}) which was comparable to other studies without vegetation contribution (e.g. Franz et al., 2012a and 2012b).

Knowledge from intensive field work in Bornim farmland (soil characteristics, weather variables, vegetation, etc.) was used to set-up a simple HYDRUS-1D model to simulate the soil-water fluxes. Model set-up repre-

sented the support scale of the cosmic-ray neutron probe and main objective was to inversely estimate soil hydraulic properties at the CRS scale (Chapter 4). The monitoring period with sunflower crop (Chapter 3) was used. An automatic model calibration with Parameter Estimation Software (PEST) was combined with HYDRUS-1D.

Although CRS probe was simplified to a case of constant depth in modelling framework, this approach provided acceptable results for inversely estimate of soil hydraulic properties at the CRS scale, when comparing to reference values. As discussed previously and in detail in Chapter 3, soil moisture profiles in Bornim did not show strong vertical variability. Therefore, there was neither statistical difference in cases of variable and constant penetration depth during CRS calibration (Chapter 3). Thus, CRS simplification accounted in HYDRUS-1D were realistic and provided good estimates of soil hydraulic properties. However, this assumption was to be verified under other field conditions, i.e. heterogeneous soil layering.

Soil hydraulic properties at field-scale (CRS probe) and local-scale (FDR profiles) were well comparable. Since other fluxes within the water balance (e.g. evapotranspiration or soil percolation) were not directly measured, it was not possible to identify which scale provides better estimations. Therefore, further studies will need to include additional information at the large scale, e.g. evapotranspiration fluxes from Eddy covariance towers, in order to constrain inverse problem and validate model fluxes at the CRS scale.

As discussed in previous chapters, the CRS approach provides only an integral quantification of the total soil water storage, without knowledge of spatial variability inside the CRS support volume. In Chapters 2 and 3, CRS approach was mainly compared to the mean vertical value from ground-truthing soil moisture. In Chapter 4, comparison between model-based CRS vertical profiles and measured soil moisture profiles was carried out. Approach of CRS vertical disaggregation should be further investigated under other field conditions and using vertical weighting functions to account for more realistic the sensitivity of CRS in depth.

In Chapter 5, the state-of-the-art of current measurements in Schaefertal catchment using CRS probes is presented. Analysis presented here has been limited by the use of ancillary data (e.g. weather data) for verifying and analysing CRS measurements. From preliminary analysis, variability of neutron counts in four CRS probes is well related to their locations within the catchment. Variability of neutrons is related to dry (top hill-slope) and wet (valley) areas as product of topographic patterns. Further analysis requires to investigate the spatial structure of soil moisture at the CRS scale, for instance mapping soil moisture in entire catchment with CRS rover-approach.

A simple analysis of temporal variability at the monthly resolution indicated that CRS measurements are well correlated to weather variables such as precipitation (P) and potential evapotranspiration (PET). The 61.2 % of the CRS monthly variance is explained by $P - PET$. The variability of LAI from MODIS within a month can be used to track also large variability of CRS water content within same month. This last one is presumable due to redistribution of hydrogen in the environment, specifically due to vegetation within CRS support volume. As observed and analysed in Bornim dataset, CRS soil moisture is highly influenced by fast changes of vegetation. Further analysis requires to incorporate measurements of other water balance components (groundwater, soil percolation and catchment discharge) in order to verify CRS storage measurements in Schaefertal.

A further evaluation of the snow analysis presented in Bornim (Chapter 2) was carried out using Schaefertal data. The response of the CRS signal (thermal and fast neutrons) was analysed during snow periods. Moreover, an approach to estimate the real CRS penetration depth under snow cover was presented. Subsequently, using universal calibration function, the snow contribution was separated from the total hydrogen pool (soil moisture, snow, lattice water and soil organic matter) for the estimation of snow water equivalent with the CRS approach.

6.2. Discussion, outlook and final conclusions

Practical limitations have arisen to this dissertation in terms of CRS accuracy due to altitude at which probes were placed. Low neutron counting rates, especially in Bornim farmland, reflect large uncertainty in CRS soil moisture. Partially, this has been accounted for using moving average or daily mean calculations in the analysis. Alternatives to overcome CRS noise problems is the technical development of new probes for the detection of fast neutrons with large neutron detectors. This is a special issue for incoming CRS applications such as the cosmic-ray rover (Chrisman et al., 2013).

It has been also observed that neutron monitoring stations used for corrections of incoming radiations in some occasions were not adequate to describe the incoming neutron intensity at the CRS location. For example, a large deviation of CRS soil moisture during winter rye period (Chapter 3) was attributed to an anomaly of incoming radiation neither observed in station Jungfraujoch nor Kiel. Although, physics and measurement techniques of incoming cosmic rays and secondary neutrons are well understood (Hess, 1936), scientific community in Nuclear Physics pays important attention to clarify spatial variability of cosmic-rays anomalies. For purposes of this dissertation,

possibly a scaling correction factor due to geomagnetic-latitude on cosmic rays (e.g. Zreda et al., 2003) could have improved neutrons measurements at the ground level. However, this approach is unpractical for hydrological applications, since it requires deep knowledge of cosmic-ray astrophysics.

The calibration analysis presented in Chapter 2 and Chapter 3 could not address two main issues (i) representativeness of CRS field-scale soil moisture in respect to the "real" soil moisture and (ii) incompatibility of the support volumes of point measurements and the cosmic-ray neutron sensing. It is worthy to mention that any bridging-approach (upscaling or downscaling) was not provided to none of the soil moisture time series (CRS and FDR). Always CRS approach was calibrated (or validated) based on the mean values from FDR sensors (using either a specific time or part of time series).

Partially, mean value from five FDR profiles (Chapter 3) was verified using previous time series and soil information. Indeed, a deviation of mean soil moisture used for calibration was identified when comparing to high-dense soil moisture campaigns. However, this deviation becomes important at high soil moisture situations only. The main limitation to validate the representativeness of CRS soil moisture in cropped fields is due to practical aspects. On the one hand, large monitoring networks of soil moisture (e.g. Bogena et al., 2010) disturbs farmer's field activities and can not be placed permanently. On the other hand, field sampling campaigns with soil cores or manual FDR sensors (e.g. Chapter 3) can be applied, but these are tedious and with limitations in time. Here also, the definition of "representativeness" plays an important role. CRS observes indeed more water pools than soil moisture from classical instruments or campaigns. Therefore, this makes it difficult to elucidate if CRS soil moisture is really deviated from truth soil moisture because of a scale problem and not due to anything else.

In the case of scaling approaches, a downscaling approach of the CRS soil moisture is definitively a promising future research direction. This will make more reliable using the CRS methodology in fine resolution case studies (e.g. modelling or field comparison of spatial variability with monitoring networks). However, firstly issue of horizontal sensitivity has to be addressed with exact weighting functions in the radial distance. At the moment, spatial-varying CRS signal sensitivity is considered indirectly in the sampling approach for calibration (e.g. Schaefertal calibration), as recommended by Zreda et al. (2012). However, this sampling approach in COSMOS sites (108 total samples collected at each site at 6 depths, 0-30 cm every 5 cm, and 18 horizontal locations, 0-360° every 60°, and radii of 25, 75, and 200 m) is mainly focused on reducing CRS standard error. Furthermore, such sampling approach for CRS calibration should be varied in much complex field conditions, e.g. spatial variability of crop covers.

In this dissertation, a further and important step on the use of CRS approach in cropped fields was the development of the piecewise linear model to correct attenuated-neutrons due to vegetation presence. Although significant improvement in final CRS soil moisture was achieved after corrections, other crop measurements (besides crop height) were not analysed to understand the dynamics of the vegetation-attenuated neutrons. In Chapter 3, correlation between crop height and vegetation-attenuated neutrons decreased substantially at the late period of crop development. Further analysis is suggested for correlating attenuated neutrons with leaf area index or biomass. Although verification of the piece-wise linear model of attenuated neutrons with other crops is also important, as well as the verification of absolute value of neutron attenuation per stage and per crop. In this sense, function of vegetation correction can be completely generalized for summer and winter crops, and corrections can be applied in a direct manner.

A promising application of the CRS approach is the computation of the water balance with field measurements or in a modelling framework. This has been partially investigated in this dissertation within Chapter 4 and Chapter 5. However, it was not completely addressed because of lack of knowledge in other components of the water balance. For instance, inverse modelling in Bornim site could have been used to identify if field-scale parameters (CRS) or local-parameters (FDR profiles) drive better quantifications of soil percolation to groundwater. In the case of Schaefertal, use of groundwater level and catchment discharge is necessary to fully understand monthly variability of CRS water content and to close the water balance at the catchment level. In definitive, knowledge of water storage at intermediate measuring scale (i.e. field or small catchment) is a valuable information to improve knowledge of climate change and hydrological extremes (Creutzfeldt et al., 2012), and to understand the integral response of a system (e.g. catchment, Creutzfeld et al., 2013). Thus, the cosmic-ray neutron sensing is a valuable approach for these applications.

The use of cosmic-ray neutron sensing for measurements of snow water equivalent is promising and has not been fully explored. In the Schaefertal catchment, time series of neutrons (thermal neutrons, fast neutrons and proposed neutron field ratio in Chapter 2) were analysed to understand the CRS signal response to snow events. The fast neutrons and neutron field ratio indicated very high correlations to dynamics of snow measurements in weather station, although there were differences in support volume. Further research is recommended to derive new calibration functions for measurements of snow water equivalent via the CRS approach. Instead, the universal calibration function (Franz et al., 2013a) was applied in Schaefertal to disaggregate signal of snow and soil moisture. Here, main advantage was that soil moisture had

low variability during winter period in Schaefertal. No continuous independent measurements of soil moisture were carried out in this dissertation, but range of soil moisture was known from network of local devices placed in the catchment (Martini et al., 2013). Though this simplification and limitation, CRS estimations of snow water equivalent corresponded well to variability observed in weather station. Snow variability was a research question not addressed in this study, but it may play an important role in Schaefertal due to varied topographical features (Ollesch et al. 2006). Therefore, this should be taken into consideration for a further verification of proposed framework in Chapter 5.

Similar methodology of hydrogen separation was applied to measure biomass water content via CRS approach (Franz et al., 2013b). The universal calibration function has promising capabilities, which has not been fully explored yet, to disaggregate different hydrogen pools (vegetation, snow and soil moisture) from the total CRS signal.

This dissertation explored the use of cosmic-ray neutron sensing (CRS) approach to measure field-scale soil moisture in cropped fields. A simple model for neutron corrections due to vegetation was presented, as well as CRS deviation in cropped fields was quantified. A first framework to adapt the CRS water storage in soil hydrological modelling was presented. Subsequently, an inversely-estimation of effective soil hydraulic properties at the CRS support volume was evaluated against local scale soil properties. The current state of monitoring activities at the Schaefertal catchment was presented. In this catchment, CRS water content was well correlated to monthly variability of precipitation and potential evapotranspiration. Furthermore, here also a framework to separate snow and soil moisture signal from total hydrogen pool was developed, which allowed indirect estimations of snow water equivalent at the CRS scale.

Bibliography

[1] Abbaspour, K.C., Schulin, R. and van Genuchten, M.T.: Estimating unsaturated soil hydraulic parameters using ant colony optimization, Advances in Water Resources, 24, 827-841, 2001.

[2] Abbaspour, K.C., van Genuchten, M.T., Schulin, R. and Schläppi, E.: A sequential uncertainty domain inverse procedure for estimating subsurface flow and transport parameters. Water Resources Research, 33, 1879-1892, 1997.

[3] Albergel, C., Calvet, J. C., de Rosnay, P., Balsamo, G., Wagner, W., Hasenauer, S., Naeimi, V., Martin, E., Bazile, E., Bouyssel, F., and Mahfouf, J.F.: Cross-evaluation of modelled and remotely sensed surface soil moisture with in situ data in southwestern France, Hydrology and Earth System Sciences, 14, 2177-2191, DOI: 10.5194/hess-14-2177-2010, 2010.

[4] Albergel, C., de Rosnay, P., Gruhier, C., Muñoz-Sabater, J., Hasenauer, S., Isaksen, L., Kerr, Y., and Wagner, W.: Evaluation of remotely sensed and modelled soil moisture products using global ground-based in situ observations, Remote Sensing of Environment, 118, 215-226, 2012.

[5] Albert, D. G., Decato, S. N., and Carbee, D. L.: Snow cover effects on acoustic sensors, Cold Regions Science and Technology, 52, 132-145, 2008.

[6] Allen, R.G., Pereira, L.S., Raes, D. and M., S.: Crop-evapotranspiration (guidelines for computing crop water requirements), FAO Irrigation and drainage paper No 56. FAO - Food and Agriculture Organization of the United Nations, 1998.

[7] Amor, I.V.M. and Mohanty, B.P.: Near-surface soil moisture assimilation to quantify effective soil hydraulic properties under different hydro-climatic conditions. Vadose Zone Journal, 7, 39-52, 2008.

[8] Arora, B., Mohanty, B. P., and McGuire, J. T.: Inverse estimation of parameters for multidomain flow models in soil columns with differ-

ent macropore densities, Water Resources Research, 47, W04512, doi: 10.1029/2010wr009451, 2011.

[9] Bachelet, F., Balata, P., Drying, E., and Iucci, N.: Attenuation Coefficients of the Cosmic-Ray Nucleonic Component in the Lower Atmosphere, IL Nuovo Cimento, XXXV, 1, 1965.

[10] Barker R, Moore J. 1998. The application of time-lapse electrical tomography in groundwater studies. The Leading Edge 17: 1454–1458.

[11] Baumhardt, R. L., Lascano, R. J., and Evett, S. R.: Soil Material, Temperature, and Salinity Effects on Calibration of Multisensor Capacitance Probes 1 The mention of trade or manufacturer names is made for information only and does not imply an endorsement, recommendation, or exclusion by the USDA-ARS, Soil Sci. Soc. Am. J., 64, 2000.

[12] Baup, F., Mougin, E., de Rosnay, P., Timouk, F., and Chênerie, I.: Surface soil moisture estimation over the AMMA Sahelian site in Mali using ENVISAT/ASAR data, Remote Sensing of Environment, 109, 473-481, 2007a.

[13] Baup, F., Mougin, E., Hiernaux, P., Lopes, A., De Rosnay, P., and Chenerie, I.: Radar Signatures of Sahelian Surfaces in Mali Using ENVISAT-ASAR Data, Geoscience and Remote Sensing, IEEE Transactions on, 45, 2354-2363, 2007b.

[14] Barrett, B. W., Dwyer, E., and Whelan, P.: Soil Moisture Retrieval from Active Spaceborne Microwave Observations: An Evaluation of Current Techniques, Remote Sensing, 1, 210–242, doi:10.3390/rs1030210, 2009.

[15] Beverwijk, A.: Particle size analysis of soils by means of the hydrometer method, Sedimentary Geol., 1, 403–406, 1967.

[16] Binley, A., Henry-Poulter, S., and Shaw, B.: Examination of Solute Transport in an Undisturbed Soil Column Using Electrical Resistance Tomography, Water Resources Research, 32, 763-769, 1996.

[17] Blöschl, G. and Sivapalan, M. 1995. Scale issues in hydrological modelling: A review. Hydrological Processes, 9, 251-290.

[18] Bogena, H. R., Huisman, J. A., Oberdörster, C., and Vereecken, H.: Evaluation of a low-cost soil water content sensor for wireless network applications, Journal of Hydrology, 344, 32-42, 2007.

[19] Bogena, H. R., Herbst, M., Huisman, J. A., Rosenbaum, U., Weuthen, A., and Vereecken, H.: Potential of wireless sensor networks for measuring soil water content variability, Vadose Zone J., 9, 1002–1013,

2010.

[20] Bogena, H. R., Huisman, J. A., Baatz, R., Hendricks Franssen, H. J., and Vereecken, H.: Accuracy of the cosmic-ray soil water content probe in humid forest ecosystems: The worst case scenario, Water Resources Research, 49, 5778-5791, doi: 10.1002/wrcr.20463, 2013.

[21] Braun, J., C. Rocken, and R. Ware (2001), Validation of line-of-sight water vapor measurements with GPS, Radio Science, 36, 459–472.

[22] Breen, S. J., Carrigan, C. R., LaBrecque, D. J., and Detwiler, R. L.: Bench-scale experiments to evaluate electrical resistivity tomography as a monitoring tool for geologic CO_2 sequestration, International Journal of Greenhouse Gas Control, 9, 484-494, 2012.

[23] Breinholt, A., Møller, J.K., Madsen, H. and Mikkelsen, P.S.: A formal statistical approach to representing uncertainty in rainfall–runoff modelling with focus on residual analysis and probabilistic output evaluation – Distinguishing simulation and prediction. Journal of Hydrology, 472–473, 36-52, 2012.

[24] Brevik, E., Fenton, T., and Lazari, A.: Soil electrical conductivity as a function of soil water content and implications for soil mapping, Precision Agric, 7, 393-404, 2006.

[25] Brocca, L., Melone, F., Moramarco, T., Wagner, W., Naeimi, V., Bartalis, Z., and Hasenauer, S.: Improving runoff prediction through the assimilation of the ASCAT soil moisture product, Hydrology and Earth System Sciences, 14,1881-1893, doi: 10.5194/hess-14-1881-2010, 2010.

[26] Calamita, G., Brocca, L., Perrone, A., Piscitelli, S., Lapenna, V., Melone, F., and Moramarco, T.: Electrical resistivity and TDR methods for soil moisture estimation in central Italy test-sites, Journal of Hydrology, 454–455, 101-112, 2012.

[27] Callegary, J.B., T.P.A. Ferré, and R.W. Groom. 2007. Spatial sensitivity of low induction-number frequency-domain electromagnetic induction instruments. Vadose Zone J. 6:158–167.

[28] Chang, D.-H. and Islam, S.: Estimation of Soil Physical Properties Using Remote Sensing and Artificial Neural Network. Remote Sensing of Environment, 74, 534-544, 2000.

[29] Champagne, C., McNairn, H., and Berg, A. A.: Monitoring agricultural soil moisture extremes in Canada using passive microwave remote sensing, Remote Sensing of Environment, 115, 2434-2444, 2011.

[30] Chappell, N. A., Franks, S. W., and Larenus, J.: Multi-scale permeability estimation for a tropical catchment, Hydrological Processes, 12,

1507-1523, 1998.

[31] Chappell, N. A., and Lancaster, J. W.: Comparison of methodological uncertainties within permeability measurements, Hydrological Processes, 21, 2504-2514, 2007.

[32] Choi, M., and Jacobs, J. M.: Soil moisture variability of root zone profiles within SMEX02 remote sensing footprints, Advances in Water Resources, 30, 883-896, 2007.

[33] Chrisman, B., and Zreda, M.: Quantifying mesoscale soil moisture with the cosmic-ray rover, Hydrology and Earth System Sciences Discussions, 10, 7127-7160, 2013.

[34] Christiansen, L., Lund, S., Andersen, O. B., Binning, P. J., Rosbjerg, D., and Bauer-Gottwein, P.: Measuring gravity change caused by water storage variations: Performance assessment under controlled conditions, Journal of Hydrology, 402, 60-70, 2011.

[35] Clausnitzer, V., Hopmans, J.W. and Nielsen, D.R.: Simultaneous scaling of soil water retention and hydraulic conductivity curves. Water Resources Research, 28, 19-31, 1992.

[36] Collow, T. W., Robock, A., Basara, J. B., and Illston, B. G.: Evaluation of SMOS retrievals of soil moisture over the central United States with currently available in situ observations, Journal of Geophysical Research: Atmospheres, 117, D09113, doi: 10.1029/2011jd017095, 2012.

[37] Creutzfeldt, B., A. Guntner, T. Klugel, and H. Wziontek.: Simulating the influence of water storage changes on the superconducting gravimeter of the Geodetic Observatory Wettzell, Germany, Geophysics, 73, WA95, 2008.

[38] Creutzfeldt, B., Güntner, A., Thoss, H., Merz, B., and Wziontek, H.: Measuring the effect of local water storage changes on in situ gravity observations: Case study of the Geodetic Observatory Wettzell, Germany, Water Resources Research, 46, W08531, doi: 10.1029/2009wr008359, 2010a.

[39] Creutzfeldt, B., Güntner, A., Vorogushyn, S., and Merz, B.: The benefits of gravimeter observations for modelling water storage changes at the field scale, Hydrology and Earth System Sciences, 14, 1715-1730, 2010b.

[40] Creutzfeldt, B., Ferré, T., Troch, P., Merz, B., Wziontek, H., and Güntner, A.: Total water storage dynamics in response to climate variability and extremes: Inference from long-term terrestrial gravity measurement, Journal of Geophysical Research: Atmospheres, 117, D08112,

doi: 10.1029/2011jd016472, 2012.

[41] Creutzfeldt, B., Troch, P. A., Güntner, A., Ferré, T. P. A., Graeff, T., and Merz, B.: Storage-discharge relationships at different catchment scales based on local high-precision gravimetry, Hydrological Processes, doi: 10.1002/hyp.9689, 2013.

[42] Daily, W., Ramirez, A., LaBrecque, D., and Nitao, J.: Electrical resistivity tomography of vadose water movement, Water Resources Research, 28, 1429-1442, 1992.

[43] Daily, W., Ramirez, A., Binley, A., and LeBrecque, D.: Electrical resistance tomography, The Leading Edge, 23, 438-442, 2004.

[44] Davis, J. L., and Annan, A. P.: Ground-Penetrating radar for high-resolution mapping of soil and rock stratigraphy, Geophysical Prospecting, 37, 531-551, 1989.

[45] Desilets, D., Zreda, M., and Ferré, T. P. A.: Nature's neutron probe: Land surface hydrology at an elusive scale with cosmic rays, Water Resour. Res., 46, W11505, doi: 10.1029/2009WR008726, 2010.

[46] Desilets, D., and Zreda, M.: Footprint diameter for a cosmic-ray soil moisture probe: Theory and monte carlo simulations, Water Resources Research, 49, 3566-3575, doi: 10.1002/wrcr.20187, 2013.

[47] Doherty, J.: PEST: Model independent parameter estimation. Fifth edition of user manual., Brisbane, Australia: Watermark Numerical Computing, 2004.

[48] Domine, F., Salvatori, R., Legagneux, L., Salzano, R., Fily, M., and Casacchia, R.: Correlation between the specific surface area and the short wave infrared (SWIR) reflectance of snow, Cold Regions Science and Technology, 46, 60-68, 2006.

[49] Dorigo, W. A., Wagner, W., Hohensinn, R., Hahn, S., Paulik, C., Xaver, A., Gruber, A., Drusch, M., Mecklenburg, S., van Oevelen, P., Robock, A., and Jackson, T.: The International Soil Moisture Network: a data hosting facility for global in situ soil moisture measurements, Hydrology and Earth System Sciences, 15, 1675-1698, 2011.

[50] Driscoll, W. C.: Robustness of the ANOVA and Tukey-Kramer statistical tests, Computers & Industrial Engineering, 31, 265-268, 1996.

[51] Duan, Q., Sorooshian, S. and Gupta, V.: Effective and efficient global optimization for conceptual rainfall-runoff models. Water Resources Research, 28, 1015-1031, 1992.

[52] Durner, W. and Iden, S.C.: Extended multistep outflow method for the accurate determination of soil hydraulic properties near water sat-

uration. Water Resources Research, 47, W08526, 2011.

[53] Durner, W., Jansen, U. and Iden, S.C.: Effective hydraulic properties of layered soils at the lysimeter scale determined by inverse modelling. European Journal of Soil Science, 59, 114-124, 2008.

[54] Entekhabi, D., Njoku, E. G., O'Neill, P. E., Kellogg, K. H., Crow, W. T., Edelstein, W. N., Entin, J. K., Goodman, S. D., Jackson, T. J., Johnson, J., Kimball, J., Piepmeier, J. R., Koster, R. D., Martin, N., McDonald, K. C., Moghaddam, M., Moran, S., Reichle, R., Shi, J. C., Spencer, M. W., Thurman, S. W., Tsang, L., and Van Zyl, J.: The Soil Moisture Active Passive (SMAP) Mission, P. IEEE, 98, 704–716, 2010.

[55] Entin, J. K., Robock, A., Vinnikov, K. Y., Hollinger, S. E., Liu, S., and Namkhai, A.: Temporal and spatial scales of observed soil moisture variations in the extratropics, Journal of Geophysical Research: Atmospheres, 105, 11865-11877, doi: 10.1029/2000jd900051, 2000.

[56] Famiglietti, J. S., Ryu, D., Berg, A. A., Rodell, M., and Jackson, T. J.: Field observations of soil moisture variability across scales, Water Resources Research, 44, W01423, doi: 10.1029/2006wr005804, 2008.

[57] Feddes, R.A., Menenti, M., Kabat, P. and Bastiaanssen, W.G.M.: Is large-scale inverse modelling of unsaturated flow with areal average evaporation and surface soil moisture as estimated from remote sensing feasible? Journal of Hydrology, 143, 125-152, 1993.

[58] Fernández-Gálvez, J.: Errors in soil moisture content estimates induced by uncertainties in the effective soil dielectric constant, International Journal of Remote Sensing, 29, 3317-3323, 2008.

[59] Franz, T. E., Zreda, M., Ferre, T. P. A., Rosolem, R., Zweck, C., Stillman, S., Zeng, X., and Shuttleworth, W. J.: Measurement depth of the cosmic ray soil moisture probe affected by hydrogen from various sources. Water Resour. Res., 48, W08515, 10.1029/2012wr011871, 2012a.

[60] Franz, T.E., Zreda, M., Rosolem, R. and Ferre, T.P.A. Field Validation of a Cosmic-Ray Neutron Sensor Using a Distributed Sensor Network. Vadose Zone Journal, 11, 2012b.

[61] Franz, T. E., Zreda, M., Rosolem, R., and Ferre, T. P. A.: A universal calibration function for determination of soil moisture with cosmic-ray neutrons, Hydrology and Earth System Sciences Discussions, 17, 453-460, 2013a.

[62] Franz, T. E., M. Zreda, R. Rosolem, B. Hornbuckle, S. Irvin, H. Adams, T. Kolb, C. Zweck, and W. J. Shuttleworth.: Ecosystem scale mea-

surements of biomass water using cosmic-ray neutrons. Geophysical Research Letters, doi:10.1002/grl.50791, 2013b.

[63] Frei, A., and Lee, S.: A comparison of optical-band based snow extent products during spring over North America, Remote Sensing of Environment, 114, 1940-1948, 2010.

[64] French, H., and Binley, A.: Snowmelt infiltration: monitoring temporal and spatial variability using time-lapse electrical resistivity, Journal of Hydrology, 297, 174-186, 2004.

[65] Garre, S., Javaux, M., Vanderborght, J., Pages, L., and Vereecken, H.: Three-Dimensional Electrical Resistivity Tomography to Monitor Root Zone Water Dynamics, Vadose Zone J., 10, 412–424, 2011.

[66] Gao, Y., Xie, H., Lu, N., Yao, T., and Liang, T.: Toward advanced daily cloud-free snow cover and snow water equivalent products from Terra–Aqua MODIS and Aqua AMSR-E measurements, Journal of Hydrology, 385, 23-35, 2010.

[67] Gaur, N., and Mohanty, B. P.: Evolution of physical controls for soil moisture in humid and subhumid watersheds, Water Resources Research, doi: 10.1002/wrcr.20069, 2013.

[68] Gebbers, R., Lück, E., Dabas, M., and Domsch, H.: Comparison of instruments for geoelectrical soil mapping at the field scale, Near Surf. Geophys., 9, 179–190, 2009.

[69] Geoff Wang, G.: Use of understory vegetation in classifying soil moisture and nutrient regimes, Forest Ecology and Management, 129, 93-100, 2000.

[70] Gergely, M., Schneebeli, M., and Roth, K.: First experiments to determine snow density from diffuse near-infrared transmittance, Cold Regions Science and Technology, 64, 81-86, 2010.

[71] Giménez, D., Perfect, E., Rawls, W. J., and Pachepsky, Y.: Fractal models for predicting soil hydraulic properties: a review, Engineering Geology, 48, 161-183, 1997.

[72] Gómez-Hernández, J.J. and Gorelick, S.M.: Effective groundwater model parameter values: Influence of spatial variability of hydraulic conductivity, leakance, and recharge. Water Resources Research, 25, 405-419, 1989.

[73] Gottschalk, L., Leblois, E. and Skøien, J.O.: Correlation and covariance of runoff revisited. Journal of Hydrology, 398, 76-90, 2011.

[74] Graeff, T., Zehe, E., Reusser, D., Lück, E., Schröder, B., Wenk, G., John, H., and Bronstert, A.: Process identification through rejection

of model structures in a mid-mountainous rural catchment: observations of rainfall–runoff response, geophysical conditions and model inter-comparison, Hydrological Processes, 23, 702-718, 2009.

[75] Graeff, T., Zehe, E., Schlaeger, S., Morgner, M., Bauer, A., Becker, R., Creutzfeldt, B., and Bronstert, A.: A quality assessment of Spatial TDR soil moisture measurements in homogenous and heterogeneous media with laboratory experiments, Hydrology and Earth System Sciences, 14, 1007–1020, 2010.

[76] Graham Milledge, D., Warburton, J., N. Lane, S., and J. Stevens, C.: Testing the influence of topography and material properties on catchment-scale soil moisture patterns using remotely sensed vegetation patterns in a humid temperate catchment, northern Britain, Hydrological Processes, 27, 1223-1237, 2013.

[77] Greaves, R., Lesmes, D., Lee, J., and Toksöz, M.: Velocity variations and water content estimated from multi-offset, ground-penetrating radar, Geophysics, 61, 683-695, 1996.

[78] Greco, R.: Soil water content inverse profiling from single TDR waveforms, Journal of Hydrology, 317, 325-339, 2006.

[79] Greco, R., and Guida, A.: Field measurements of topsoil moisture profiles by vertical TDR probes, Journal of Hydrology, 348, 442-451, 2008.

[80] Grippa, M., Kergoat, L., Frappart, F., Araud, Q., Boone, A., de Rosnay, P., Lemoine, J. M., Gascoin, S., Balsamo, G., Ottlé, C., Decharme, B., Saux-Picart, S., and Ramillien, G.: Land water storage variability over West Africa estimated by Gravity Recovery and Climate Experiment (GRACE) and land surface models, Water Resources Research, 47, W05549, doi: 10.1029/2009wr008856, 2011.

[81] Grote, K., Anger, C., Kelly, B., Hubbard, S., and Rubin, Y.: Characterization of Soil Water Content Variability and Soil Texture using GPR Groundwave Techniques, Journal of Environmental and Engineering Geophysics, 15, 93-110, doi: 10.2113/JEEG15.3.93, 2010.

[82] Güntner, A.: Improvement of Global Hydrological Models Using GRACE Data, Surveys in Geophysics, 29, 375 - 397, doi: 10.1007/s10712-008-9038-y, 2008.

[83] Hajnsek, I., Jagdhuber, T., Schon, H., and Papathanassiou, K. P.: Potential of Estimating Soil Moisture Under Vegetation Cover by Means of PolSAR, IEEE Transactions on Geoscience and Remote Sensing, 47, 442-454, 2009.

[84] Han, E., Merwade, V. and Heathman, G.C.: Implementation of surface soil moisture data assimilation with watershed scale distributed hydrological model. Journal of Hydrology, 416–417, 98-117, 2012.

[85] Hansen, N., Müller, S.D. and Koumoutsakos, P.: Reducing the Time Complexity of the Derandomized Evolution Strategy with Covariance Matrix Adaptation (CMA-ES). Evolutionary Computation, 11, 1-18, 2003.

[86] Hassanein, R., Lehmann, E., and Vontobel, P.: Methods of scattering corrections for quantitative neutron radiography, Nuclear Instruments and Methods in Physics Research Section A: Accelerators, Spectrometers, Detectors and Associated Equipment, 542, 353-360, 2005.

[87] Heathman, G.C., Starks, P.J., Ahuja, L.R. and Jackson, T.J.: Assimilation of surface soil moisture to estimate profile soil water content. Journal of Hydrology, 279, 1-17, 2003.

[88] Hess, W. N., Canfield, E. H., and Lingenfelter, R. E.: Cosmic-Ray Neutron Demography, J. Geophys. Res., 66, 665–677, 1961.

[89] Hillel, D.: Environmental soil physics: Fundamentals, Applications, and Environmental Considerations, Ed. 1, Elsevier, London, 1998.

[90] Hopmans, J.W. and Simunek, J.: Review of inverse estimation of soil hydraulic properties. In: van Genuchten, M.Th., Leiji, F.J., Wu, L., Characterization and Measurement of the Hydraulic Properties of Unsaturated Porous Media, pp. 643-659, University of California, Riverside, CA, 1999.

[91] Horsley, A.: Neutron cross sections of hydrogen in the energy range 0.0001 eV–20 MeV, Nucl. Data Sheets, 2, 243–262, doi: 10.1016/S0550-306X(66)80005-8, 1966.

[92] Hornbuckle, B., Irvin, S., Franz, T. E., Rosolem, R., and Zweck, C.: The potential of the COSMOS network to be a source of new soil moisture information for SMOS and SMAP, in: Proc. Geoscience and Remote Sensing Symposium (IGARSS), 22–27 July 2012, Munich, Germany, IEEE International, 1243–1246, doi:10.1109/IGARSS.2012.6351317, 2012.

[93] Hubbard, S., Grote, K., and Rubin, Y.: Mapping the volumetric soil water content of a California vineyard using high-frequency GPR ground wave data, The Leading Edge, 21, 552-559, 2002.

[94] Huisman, J. A., Sperl, C., Bouten, W., and Verstraten, J. M.: Soil water content measurements at different scales: accuracy of time domain reflectometry and ground-penetrating radar, Journal of Hydrology, 245,

48-58, 2001.

[95] Huisman, J. A., Hubbard, S. S., Redman, J. D., and Annan, A. P.: Measuring Soil Water Content with Ground Penetrating Radar: A Review, Vadose Zone J., 2, 476–491, 2003.

[96] Hydroinnova: Technical Document 01-07: Soil Water Content Measurements with Cosmic Rays, Albuquerque, New Mexico, 2010.

[97] Jagdhuber, T.: Soil Parameter Retrieval under Vegetation Cover Using SAR Polarimetry. Doctoral thesis, University of Potsdam, Potsdam, Germany, 2012.

[98] Jhorar, R.K., Dam, J.C.v., Bastiaanssen, W.G.M. and Feddes, R.A.: Calibration of effective soil hydraulic parameters of heterogeneous soil profiles. Journal of Hydrology, 285, 233-247, 2004.

[99] Kerr, Y. H., Waldteufel, P., Wigneron, J.-P., Martinuzzi, J., Font, J., and Berger, M.: Soil moisture retrieval from space: the Soil Moisture and Ocean Salinity (SMOS) mission, IEEE T. Geosci. Remote, 39, 1729–1735, 2001.

[100] Klute, A.: Water retention: laboratory methods. In: Methods of Soil Analysis. Part I. Physical and Mineralogical Methods (ed. Klute, A.), 1986.

[101] Koster, R. D., Mahanama, S. P. P., Livneh, B., Lettenmaier, D. P., and Reichle, R. H.: Skill in streamflow forecasts derived from large-scale estimates of soil moisture and snow, Nature Geosci, 3, 613-616, 2010.

[102] Kodama, M.: A Cosmic-Ray Snow Gauge, International Journal of Applied Radiation and Isotopes, 26, 774-775, 1975.

[103] Kodama, M., Nakai, K., Kawasaki, S., and Wada, M.: An application of cosmic-ray neutron measurements to the determination of the snow-water equivalent, Journal of Hydrology, 41, 85–92, 1979.

[104] Kodama, M.: Continuous monitoring of snow water equivalent using cosmic ray neutrons, Cold Reg. Sci. Technol., 3, 295–303, 1980.

[105] Kodama, M.: An introduction to applied cosmic ray physics, Jpn J. Appl. Phys., 23, 726–728, 1984.

[106] Kodama, M., Kudo, S., and Kosuge, T.: Application of atmospheric neutrons to soil moisture measurement, Soil Sci., 140, 237–242, 1985.

[107] Kool, J.B. and Parker, J.C.: Analysis of the inverse problem for transient unsaturated flow. Water Resources Research, 24, 817-830, 1988.

[108] Kornelsen, K. C., and Coulibaly, P.: Advances in soil moisture retrieval from synthetic aperture radar and hydrological applications, Journal of

Hydrology, 476, 460-489, 2013.

[109] Koyama, C. N., Korres, W., Fiener, P., and Schneider, K.: Variability of Surface Soil Moisture Observed from Multitemporal C-Band Synthetic Aperture Radar and Field Data, Vadose Zone Journal, 9, 1014-1024, 2010.

[110] Köppen, W.: Das geographische System der Klimate, in: Handbuch der Klimatologie, edited by: Köppen, W. and Geiger, G., 1. C. Gebr, Borntraeger, 1–44, 1936.

[111] Krane, K.: Introductory Nuclear Physics, Wiley & Sons, New York, 1988.

[112] Krzeminska, D. M., Steele-Dunne, S. C., Bogaard, T. A., Rutten, M. M., Sailhac, P., and Geraud, Y.: High-resolution temperature observations to monitor soil thermal properties as a proxy for soil moisture condition in clay-shale landslide, Hydrological Processes, 26, 2143-2156, 2012.

[113] Lane, S. N., Reaney, S. M., and Heathwaite, A. L.: Representation of landscape hydrological connectivity using a topographically driven surface flow index, Water Resources Research, 45, W08423, doi: 10.1029/2008wr007336, 2009.

[114] Larson, K. M., A. Bilich, and P. Axelrad (2007), Improving the precision of high-rate GPS, J. Geophys. Res., 112, B05422, doi: 10.1029/2006JB004367.

[115] Larson, K. M., Small, E. E., Gutmann, E. D., Bilich, A. L., Braun, J. J., and Zavorotny, V. U.: Use of GPS receivers as a soil moisture network for water cycle studies, Geophysical Research Letters, 35, L24405, doi: 10.1029/2008gl036013, 2008.

[116] Larson, K. M., Braun, J. J., Small, E. E., Zavorotny, V. U., Gutmann, E. D., and Bilich, A. L.: GPS Multipath and Its Relation to Near-Surface Soil Moisture Content, Selected Topics in Applied Earth Observations and Remote Sensing, IEEE Journal of, 3, 91-99, 2010.

[117] Leblanc, M. J., Tregoning, P., Ramillien, G., Tweed, S. O., and Fakes, A.: Basin-scale, integrated observations of the early 21st century multiyear drought in southeast Australia, Water Resources Research, 45, W04408, doi: 10.1029/2008wr007333, 2009.

[118] Leirião, S., He, X., Christiansen, L., Andersen, O. B., and Bauer-Gottwein, P.: Calculation of the temporal gravity variation from spatially variable water storage change in soils and aquifers, Journal of Hydrology, 365, 302–309, 2009.

[119] Lesch, S. M., Strauss, D. J., and Rhoades, J. D.: Spatial Prediction of Soil Salinity Using Electromagnetic Induction Techniques: 1. Statistical Prediction Models: A Comparison of Multiple Linear Regression and Cokriging, Water Resources Research, 31, 373-386, 1995.

[120] Lettenmaier, D. P., and Famiglietti, J. S.: Hydrology: Water from on high, Nature, 444, 562-563, 2006.

[121] Li, J. and Islam, S.: On the estimation of soil moisture profile and surface fluxes partitioning from sequential assimilation of surface layer soil moisture. Journal of Hydrology, 220, 86-103, 1999.

[122] Li, L., Xu, C.-Y., Xia, J., Engeland, K. and Reggiani, P.: Uncertainty estimates by Bayesian method with likelihood of AR (1) plus Normal model and AR (1) plus Multi-Normal model in different time-scales hydrological models. Journal of Hydrology, 406, 54-65, 2011.

[123] Lunt, I. A., Hubbard, S. S., and Rubin, Y.: Soil moisture content estimation using ground-penetrating radar reflection data, Journal of Hydrology, 307, 254-269, 2005.

[124] Mailhol, J.C., Olufayo, A.A. and Ruelle, P.: Sorghum and sunflower evapotranspiration and yield from simulated leaf area index. Agricultural Water Management, 35, 167-182, 1997.

[125] Mallants, D., Mohanty, B.P., Vervoort, A. and Feyen, J.: Spatial analysis of saturated hydraulic conductivity in a soil with macropores. Soil Technology, 10, 115-131, 1997.

[126] Martínez, G., Vanderlinden, K., Giráldez, J. V., Espejo, A. J., and Muriel, J. L.: Field-Scale Soil Moisture Pattern Mapping using Electromagnetic Induction, gsvadzone, 9, 871-881, doi: 10.2136/vzj2009.0160, 2010.

[127] Martínez-Fernández, J., and Ceballos, A.: Mean soil moisture estimation using temporal stability analysis. Journal of Hydrology, 312, 28-38, 2005.

[128] Matson, M.: NOAA satellite snow cover data, Global and Planetary Change, 4, 213-218, 1991.

[129] Merlin, O., Walker, J. P., Chehbouni, A., and Kerr, Y.: Towards deterministic downscaling of SMOS soil moisture using MODIS derived soil evaporative efficiency, Remote Sensing of Environment, 112, 3935-3946, 2008.

[130] Mertens, J., Madsen, H., Kristensen, M., Jacques, D. and Feyen, J.: Sensitivity of soil parameters in unsaturated zone modelling and the relation between effective, laboratory and in situ estimates. Hydrological

145

Processes, 19, 1611-1633, 2005.

[131] Metsämäki, S., Mattila, O.-P., Pulliainen, J., Niemi, K., Luojus, K., and Böttcher, K.: An optical reflectance model-based method for fractional snow cover mapping applicable to continental scale, Remote Sensing of Environment, 123, 508-521, 2012.

[132] Michot, D., Benderitter, Y., Dorigny, A., Nicoullaud, B., King, D., and Tabbagh, A.: Spatial and temporal monitoring of soil water content with an irrigated corn crop cover using surface electrical resistivity tomography, Water Resources Research, 39, 1138, doi: 10.1029/2002wr001581, 2003.

[133] Miller, E.E. and Miller, R.D.: Physical theory of capillary flow phenomena. Journal of Applied Physics, 27, 324-332, 1956.

[134] Mohanty, B.P. and Zhu, J.: Effective Hydraulic Parameters in Horizontally and Vertically Heterogeneous Soils for Steady-State Land–Atmosphere Interaction. Journal of Hydrometeorology, 8, 715-729, 2007.

[135] Montzka, C., Moradkhani, H., Weihermüller, L., Franssen, H.-J.H., Canty, M. and Vereecken, H.: Hydraulic parameter estimation by remotely-sensed top soil moisture observations with the particle filter. Journal of Hydrology, 399, 410-421, 2011.

[136] Moret, D., Arrúe, J. L., López, M. V., and Gracia, R.: A new TDR waveform analysis approach for soil moisture profiling using a single probe, Journal of Hydrology, 321, 163-172, 2006.

[137] Mualem, Y.: A new model for predicting the hydraulic conductivity of unsaturated porous media. Water Resources Research, 12, 513-522, 1976.

[138] Neutron Monitor Database: available at: http://www.nmdb.eu/, last access: 4 July 2011.

[139] Ollesch, G., Sukhanovski, Y., Kistner, I., Rode, M., and Meissner, R.: Characterization and modelling of the spatial heterogeneity of snowmelt erosion, Earth Surface Processes and Landforms, 30, 197-211, 2005.

[140] Ollesch, G., Kistner, I., Meissner, R., and Lindenschmidt, K.-E.: Modelling of snowmelt erosion and sediment yield in a small low-mountain catchment in Germany, Catena, 68, 161-176, 2006.

[141] Ollesch, G., Demidov, V., Volokitin, M., Voskamp, M., Abbt-Braun, G., and Meissner, R.: Sediment and nutrient dynamics during snowmelt runoff generation in a southern Taiga catchment of Russia,

Agriculture, Ecosystems and Environment, 126, 229-242, 2008a.

[142] Ollesch, G.: Habilitationsschrift "Erfassung und Modellierung der Schneeschmelzerosion am Beispiel der Kleineinzugsgebiete Schäfertal (Deutschland) und Lubazhinkha (Russland)". Habilitation thesis, Fakultät für Geowissenschaften, Geotechnik und Bergbau, TU Bergakademie Freiberg, Freiberg, 2008b.

[143] Olmanson, O. K., and Ochsner, T. E.: Comparing Ambient Temperature Effects on Heat Pulse and Time Domain Reflectometry Soil Water Content Measurements, Vadose Zone Journal, 5, 751-756, 2006.

[144] Onda, Y., Tsujimura, M., Fujihara, J.-i., and Ito, J.: Runoff generation mechanisms in high-relief mountainous watersheds with different underlying geology, Journal of Hydrology, 331, 659-673, 2006.

[145] Omlin, M. and Reichert, P.: A comparison of techniques for the estimation of model prediction uncertainty. Ecological Modelling, 115, 45-59, 1999.

[146] Oswald, S. E., Menon, M., Carminati, A., Vontobel, P., Lehmann, E., and Schulin, R.: Quantitative Imaging of Infiltration, Root Growth, and Root Water Uptake via Neutron Radiography, Vadose Zone Journal, 7, 1035–1047, 2008.

[147] Pan, L. and Wu, L.: A hybrid global optimization method for inverse estimation of hydraulic parameters: Annealing-Simplex Method. Water Resources Research, 34, 2261-2269, 1998.

[148] Pan, Y.-X., and Wang, X.-P.: Factors controlling the spatial variability of surface soil moisture within revegetated-stabilized desert ecosystems of the Tengger Desert, Northern China, Hydrological Processes, 23, 1591-1601, 2009.

[149] Patterson, B. M., and Bekele, E. B.: A novel technique for estimating wetting front migration rates through the vadose zone based on changes in groundwater velocity, Journal of Hydrology, 409, 538-544, 2011.

[150] Paudel, K. P., and Andersen, P.: Monitoring snow cover variability in an agropastoral area in the Trans Himalayan region of Nepal using MODIS data with improved cloud removal methodology, Remote Sensing of Environment, 115, 1234-1246, 2011.

[151] Pauwels, V.R.N., Hoeben, R., Verhoest, N.E.C. and De Troch, F.P.: The importance of the spatial patterns of remotely sensed soil moisture in the improvement of discharge predictions for small-scale basins through data assimilation. Journal of Hydrology, 251, 88-102, 2001.

[152] Parker, E. N.: The passage of energetic charged particles through in-

terplanetary space, Planet. Space Sci., 13, 9–49, 1965.

[153] Pellenq, J., Kalma, J., Boulet, G., Saulnier, G. M., Wooldridge, S., Kerr, Y., and Chehbouni, A.: A disaggregation scheme for soil moisture based on topography and soil depth, Journal of Hydrology, 276, 112-127, 2003.

[154] Piechota, T., Timilsena, J., Tootle, G., and Hidalgo, H.: The western U.S. drought: How bad is it?, Eos, Transactions American Geophysical Union, 85, 301-304, 2004.

[155] Pietroniro, A., and Prowse, T. D.: Applications of remote sensing in hydrology, Hydrological Processes, 16, 1537-1541, 2002.

[156] Piles, M., Camps, A., Vall-llossera, M., Corbella, I., Panciera, R., Rudiger, C., Kerr, Y. H., and Walker, J.: Downscaling SMOS-Derived Soil Moisture Using MODIS Visible/Infrared Data, Geoscience and Remote Sensing, IEEE Transactions on, 49, 3156-3166, 2011.

[157] Ponizovsky, A. A., Chudinova, S. M., and Pachepsky, Y. A.: Performance of TDR calibration models as affected by soil texture, Journal of Hydrology, 218, 35-43, 1999.

[158] Porporato, A., and Rodriguez-Iturbe, I.: Ecohydrology-a challenging multidisciplinary research perspective / Ecohydrologie: une perspective stimulante de recherche multidisciplinaire, Hydrological Sciences Journal, 47, 811-821, doi: 10.1080/02626660209492985, 2002.

[159] Reedy, R., and Scanlon, B.: Soil Water Content Monitoring Using Electromagnetic Induction, Journal of Geotechnical and Geoenvironmental Engineering, 129, 1028-1039, 2003.

[160] Ramillien, G., Frappart, F., Güntner, A., Ngo-Duc, T., Cazenave, A., and Laval, K.: Time variations of the regional evapotranspiration rate from Gravity Recovery and Climate Experiment (GRACE) satellite gravimetry, Water Resources Research, 42, W10403, doi: 10.1029/2005wr004331, 2006.

[161] Rango, A.: Effects of climate change on water supplies in mountainous snowmelt regions, World Resource Review, 7, 315-325, 1995.

[162] Reynolds, W.D., Bowman, B.T., Brunke, R.R., Drury, C.F. and Tan, C.S.: Comparison of Tension Infiltrometer, Pressure Infiltrometer, and Soil Core Estimates of Saturated Hydraulic Conductivity. Soil Science Society of America Journal, 64, 478-484, 2000.

[163] Rinard, P.: Neutron interactions with matter, Los Alamos Technical Report, available at: http://www.fas.org/sgp/othergov/doe/lanl/lib-www/la-pubs/00326407.pdf, 2009.

[164] Rings, J., and Hauck, C.: Reliability of resistivity quantification for shallow subsurface water processes, Journal of Applied Geophysics, 68, 404-416, 2009.

[165] Ritchie, J. T.: Model for predicting evaporation from a row crop with incomplete cover., Water Resources Research, 8, 1204-1213, 1972.

[166] Rivera Villarreyes, C.A., Baroni, G. and Oswald, S.E.: Integral quantification of seasonal soil moisture changes in farmland by cosmic-ray neutrons. Hydrology and Earth System Sciences, 15, 3843-3859, 2011.

[167] Rivera Villarreyes, C.A., Baroni, G. and Oswald, S.E.: Calibration approaches of cosmic-ray neutron sensing for soil moisture measurement in cropped fields. Hydrology and Earth System Sciences Discussions, 10, 4237-4274, 2013a.

[168] Rivera Villarreyes, C. A., Baroni, G., and Oswald, S. E.: Inverse modelling of cosmic-ray soil moisture for field-scale soil hydraulic parameters, European Journal of Soil Science, (Under review), 2013b.

[169] Robinson, D. A., Campbell, C. S., Hopmans, J. W., Hombuckle, B. K., Jones, S. B., Knight, R., Ogden, F., Selker, J., and Wendroth, O.: Soil Moisture Measurement for Ecological and Hydrological Watershed-Scale Observatories: A Review, Vadose Zone Journal, 7, 358–389, 2008.

[170] Rodell, M., Velicogna, I., and Famiglietti, J. S.: Satellite-based estimates of groundwater depletion in India, Nature, 460, 999-1002, 2009.

[171] Rodriguez-Iturbe, I., Vogel, G. K., Rigon, R., Entekhabi, D., Castelli, F., and Rinaldo, A.: On the spatial organization of soil moisture fields, Geophysical Research Letters, 22, 2757-2760, 1995.

[172] Rodriguez-Iturbe, I., and Porporato, A.: Ecohydrology of water-controlled ecosystems: Soil moisture and plant dynamics., Cambridge Univ. Press, Cambridge, UK., 2005.

[173] Rosolem, R., Shuttleworth, W. J., Zreda, M., Franz, T. E., Zeng, X., and Kurc, S. A.: The Effect of Atmospheric Water Vapor on Neutron Count in the Cosmic-Ray Soil Moisture Observing System, Journal of Hydrometeorology, 10.1175/jhm-d-12-0120.1, 2013.

[174] Saatchi, S. S., Houghton, R. A., Dos Santos Alvalá, R. C., Soares, J. V., and Yu, Y.: Distribution of aboveground live biomass in the Amazon basin, Glob. Change Biol., 13, 816–837, 2007.

[175] Samouëlian, A., Cousin, I., Tabbagh, A., Bruand, A., and Richard, G.: Electrical resistivity survey in soil science: a review, Soil and Tillage Research, 83, 173-193, 2005.

[176] Santanello Jr, J.A., Peters-Lidard, C.D., Garcia, M.E., Mocko, D.M.,

Tischler, M.A., Moran, M.S. and Thoma, D.P.: Using remotely-sensed estimates of soil moisture to infer soil texture and hydraulic properties across a semi-arid watershed. Remote Sensing of Environment, 110, 79-97, 2007.

[177] Sayde, C., Gregory, C., Gil-Rodriguez, M., Tufillaro, N., Tyler, S., van de Giesen, N., English, M., Cuenca, R., and Selker, J. S.: Feasibility of soil moisture monitoring with heated fiber optics, Water Resources Research, 46, W06201, doi: 10.1029/2009wr007846, 2010.

[178] Scanlon, B. R., Paine, J. G., and Goldsmith, R. S.: Evaluation of Electromagnetic Induction as a Reconnaissance Technique to Characterize Unsaturated Flow in an Arid Setting, Ground Water, 37, 296-304, 1999.

[179] Schaap, M.G. and Leiji, F.J.: Database related accuracy and uncertainty of pedotransfer functions. Soil Science, 163, 765-779, 1998.

[180] Schelle, H., Iden, S.C., Peters, A. and Durner, W.: Analysis of the Agreement of Soil Hydraulic Properties Obtained from Multistep-Outflow and Evaporation Methods. Vadose Zone Journal, 9, 1080-1091, 2010.

[181] Schuh, W.M. and Cline, R.L.: Effect of Soil Properties on Unsaturated Hydraulic Conductivity Pore-Interaction Factors. Soil Science Society of America Journal, 54, 1509-1519, 1990.

[182] Schwank, M., Wiesmann, A., Werner, C., Mätzler, C., Weber, D., Murk, A., Völksch, I., and Wegmüller, U.: ELBARA II, an L-Band Radiometer System for Soil Moisture Research, Sensors, 10, 584–612, 2009.

[183] Sears, V. F.: Neutron scattering lengths and cross sections, Neutron News, 3, 26–37, 1992.

[184] Selker, J. S., Thévenaz, L., Huwald, H., Mallet, A., Luxemburg, W., van de Giesen, N., Stejskal, M., Zeman, J., Westhoff, M., and Parlange, M. B.: Distributed fiber-optic temperature sensing for hydrologic systems, Water Resources Research, 42, W12202, doi: 10.1029/2006wr005326, 2006.

[185] Seneviratne, S. I., Corti, T., Davin, E. L., Hirschi, M., Jaeger, E. B., Lehner, I., Orlowsky, B., and Teuling, A. J.: Investigating soil moisture–climate interactions in a changing climate: A review, Earth-Science Reviews, 99, 125-161, 2010.

[186] Serbin, G., and Or, D.: Ground-penetrating radar measurement of soil water content dynamics using a suspended horn antenna, Geoscience and Remote Sensing, IEEE Transactions on, 42, 1695-1705, 2004.

[187] Shuttleworth, W. J., Zreda, M., Zeng, X., Zweck, C., and Ferré, T. P. A.: The COsmic-ray Soil Moisture Observing System (COSMOS): a non-invasive, intermediate scale soil moisture measurement network., BHS Third International Symposium, Managing Consequences of a Changing Global Environment., Newcastle, 2010.

[188] Silvapulle, M. J.: On an F-type statistic for testing one-sided hypotheses and computation of chi-bar-squared weights, Statistics & Probability Letters, 28, 137-141, 1996.

[189] Simunek, J., Sejna, M., Saito, H. and Van Genuchten, M.T.: The HYDRUS-1D Software Package for Simulating the One-Dimensional Movement of Water, Heat and Multiple Solutes in Variably-Saturated Media (version 4.0). (ed. Department of Environmental Sciences, U.o.C.R.), Riverside, CA, USA, 2008.

[190] Slater, L., Binley, A. M., Daily, W., and Johnson, R.: Cross-hole electrical imaging of a controlled saline tracer injection, Journal of Applied Geophysics, 44, 85-102, 2000.

[191] Steele-Dunne, S. C., Rutten, M. M., Krzeminska, D. M., Hausner, M., Tyler, S. W., Selker, J., Bogaard, T. A., and van de Giesen, N. C.: Feasibility of soil moisture estimation using passive distributed temperature sensing, Water Resources Research, 46, W03534, doi: 10.1029/2009wr008272, 2010.

[192] Steenbergen, N. V., and Willems, P.: Method for testing the accuracy of rainfall–runoff models in predicting peak flow changes due to rainfall changes, in a climate changing context, Journal of Hydrology, 414–415, 425-434, 2012.

[193] Steer, B.T., Milroy, S.P. and Kamona, R.M.: A model to simulate the development, growth and yield of irrigated sunflower. Field Crops Research, 32, 83-99, 1993.

[194] Sun, H., Nelson, M., Chen, F., and Husch, J.: Soil mineral structural water loss during LOI analyses, Canadian Journal of Soil Science, 89, 603-610, 2009.

[195] Takeshita, Y., Yasui, K., Uekuma, H. and Nishimura, A.: Parameter estimation methods to determine hydraulic properties of aquifers using genetic algorithms. In: Groundwater Updates (eds. Sato, K. and Iwasa, Y.), pp. 469-470. Springer Japan, 2000.

[196] Tapley, B. D., Bettadpur, S., Ries, J. C., Thompson, P. F., and Watkins, M. M.: GRACE Measurements of Mass Variability in the Earth System, Science, 305, 503–505, 2004.

[197] Tiwari, V. M., Wahr, J., and Swenson, S.: Dwindling groundwater resources in northern India, from satellite gravity observations, Geophysical Research Letters, 36, L18401, doi: 10.1029/2009gl039401, 2009.

[198] Topp, G. C., Davis, J. L., and Annan, A. P.: Electromagnetic determination of soil water content: Measurements in coaxial transmission lines, Water Resour. Res., 16, 574-582, 1980.

[199] Team, T. G., Koster, R. D., Dirmeyer, P. A., Guo, Z., Bonan, G., Chan, E., Cox, P., Gordon, C. T., Kanae, S., Kowalczyk, E., Lawrence, D., Liu P., Lu, C. H., Malyshev, S., McAvaney, B., Mitchell, K., Mocko, D., Oki, T., Oleson, K., Pitman, A., Sud, Y. C., Taylor, C. M., Verseghy, D., Vasic, R., Xue, Y., and Yamada, T.: Regions of Strong Coupling Between Soil Moisture and Precipitation, Science, 305, 1138-1140, doi: 10.1126/science.1100217, 2004.

[200] Tetzlaff, D., McDonnell, J. J., Uhlenbrook, S., McGuire, K. J., Bogaart, P. W., Naef, F., Baird, A. J., Dunn, S. M., and Soulsby, C.: Conceptualizing catchment processes: simply too complex?, Hydrological Processes, 22, 1727-1730, 2008.

[201] Travelletti, J., Sailhac, P., Malet, J. P., Grandjean, G., and Ponton, J.: Hydrological response of weathered clay-shale slopes: water infiltration monitoring with time-lapse electrical resistivity tomography, Hydrological Processes, 26, 2106-2119, 2012.

[202] Tumlinson, L. G., Liu, H., Silk, W. K., and Hopmans, J. W.: Thermal Neutron Computed Tomography of Soil Water and Plant Roots, Soil Sci. Soc. Am. J., 72, 1234–1242, 2008.

[203] Vachaud, G., Passerat De Silans, A., Balabanis, P., and Vauclin, M.: Temporal Stability of Spatially Measured Soil Water Probability Density Function, Soil Science Society of America Journal, 49, 822-828, 1985

[204] Van Camp, M., Williams, S. D. P., and Francis, O.: Uncertainty of absolute gravity measurements, Journal of Geophysical Research: Solid Earth, 110, B05406, doi: 10.1029/2004jb003497, 2005.

[205] Van Camp, M., Métivier, L., de Viron, O., Meurers, B., and Williams, S. D. P.: Characterizing long-time scale hydrological effects on gravity for improved distinction of tectonic signals, Journal of Geophysical Research: Solid Earth, 115, B07407, doi: 10.1029/2009jb006615, 2010.

[206] van Dam, J.C. and Feddes, R.A.: Modeling of water flow and solute transport for irrigation and drainage. In: Pereira, L.S., Feddes, R.A., Gilley, J.R., and Lesaffre, B., Sustainability of Irrigated Agriculture (ed. Academic, K.), pp. 211-231, The Netherlands, 1996.

[207] van Genuchten, M.T.: A numerical model for water and solute movement in and below the root zone, Res. Rep. 121. U.S. Salinity Lab., Agric. Res. Ser., U.S. Dep. of Agric., Riverside, California, 1987.

[208] Venkatesh, B., Lakshman, N., Purandara, B. K., and Reddy, V. B.: Analysis of observed soil moisture patterns under different land covers in Western Ghats, India, Journal of Hydrology, 397, 281-294, 2011.

[209] Vereecken, H., Huisman, J. A., Bogena, H. R., Vanderborght, J., Vrugt, J. A., and Hopmans, J. W.: On the value of soil moisture measurements in vadose zone hydrology: a review., Water Resour. Res., 44, W00D06, doi: 10.1029/2008WR006829, 2008.

[210] Vico, G., and Porporato, A.: From rainfed agriculture to stress-avoidance irrigation: I. A generalized irrigation scheme with stochastic soil moisture, Advances in Water Resources, 34, 263-271, 2011.

[211] Vivoni, E. R., Rodríguez, J. C., and Watts, C. J.: On the spatiotemporal variability of soil moisture and evapotranspiration in a mountainous basin within the North American monsoon region, Water Resources Research, 46, W02509, doi: 10.1029/2009wr008240, 2010.

[212] Vrugt, J.A., Hopmans, J.W. and Simunek, J.: Calibration of a Two-Dimensional Root Water Uptake Model. Soil Science Society of America Journal, 65, 1027-1037, 2001.

[213] Vrugt, J.A. and Dane, J.H.: Inverse Modeling of Soil Hydraulic Properties. In: Encyclopedia of Hydrological Sciences. John Wiley and Sons, Ltd, 2006.

[214] Watson, F. G. R., Anderson, T. N., Newman, W. B., Alexander, S. E., and Garrott, R. A.: Optimal sampling schemes for estimating mean snow water equivalents in stratified heterogeneous landscapes, Journal of Hydrology, 328, 432-452, 2006.

[215] Werth, S., Güntner, A., Petrovic, S., and Schmidt, R.: Integration of GRACE mass variations into a global hydrological model, Earth and Planetary Science Letters, 277, 166-173, 2009.

[216] Western, A. W., Blöschl, G., and Grayson, R. B.: Geostatistical characterisation of soil moisture patterns in the Tarrawarra catchment, Journal of Hydrology, 205, 20-37, 1998.

[217] Western, A. W., and Blöschl, G.: On the spatial scaling of soil moisture, Journal of Hydrology, 217, 203-224, 1999.

[218] Western, A. W., Grayson, R. B., and Blöschl, G.: Scaling of soil moisture: A hydrologic perspective, Annual Review of Earth and Planetary Sciences, 30, 149–180, 2002.

[219] Western, A. W., Zhou, S.-L., Grayson, R. B., McMahon, T. A., Blöschl, G., and Wilson, D. J.: Spatial correlation of soil moisture in small catchments and its relationship to dominant spatial hydrological processes, Journal of Hydrology, 286, 113-134, 2004.

[220] Whitaker, A. C., Sugiyama, H., and Hayakawa, K.: Effect of Snow Cover Conditions on the Hydrologic Regime: Case Study in a Pluvial-Nival Watershed, Japan1, JAWRA Journal of the American Water Resources Association, 44, 814-828, 2008.

[221] Wiebe, H., Heygster, G., Zege, E., Aoki, T., and Hori, M.: Snow grain size retrieval SGSP from optical satellite data: Validation with ground measurements and detection of snow fall events, Remote Sensing of Environment, 128, 11-20, 2013.

[222] Wildenschild, D. and Jensen, K.H.: Numerical modeling of observed effective flow behavior in unsaturated heterogeneous sands. Water Resources Research, 35, 29-42, 1999.

[223] Woli, K. P., Hayakawa, A., Kuramochi, K., and Hatano, R.: Assessment of river water quality during snowmelt and base flow periods in two catchment areas with different land use, Environmental monitoring and assessment, 137, 251-260, 2008.

[224] Wu, W. and Dickinson, R. E.: Time Scales of Layered Soil Moisture Memory in the Context of Land-Atmosphere Interaction, J. Climate, 17, 2752–2764, 2004.

[225] Wziontek, H., Wilmes, H., Wolf, P., Werth, S., and Güntner, A.: Time series of superconducting gravimeters and water storage variations from the global hydrology model WGHM, Journal of Geodynamics, 48, 166-171, 2009.

[226] Yakirevich, A., Gish, T.J., Simunek, J., van Genuchten, M.T., Pachepsky, Y.A., Nicholson, T.J. and Cady, R.E.: Potential Impact of a Seepage Face on Solute Transport to a Pumping Well. Vadose Zone Journal, 9, 686-696, 2010.

[227] You, Y., Yu, Q., Pan, X., Wang, X., and Guo, L.: Application of electrical resistivity tomography in investigating depth of permafrost base and permafrost structure in Tibetan Plateau, Cold Regions Science and Technology, 87, 19-26, 2013.

[228] Yu, Z., Liu, D., Lü, H., Fu, X., Xiang, L. and Zhu, Y.: A multi-layer soil moisture data assimilation using support vector machines and ensemble particle filter. Journal of Hydrology, 475, 53-64, 2012.

[229] Zhou, H., Aizen, E., and Aizen, V.: Deriving long term snow cover ex-

tent dataset from AVHRR and MODIS data: Central Asia case study, Remote Sensing of Environment, 136, 146-162, 2013.

[230] Zhu, J. and Mohanty, B.P.: Effective hydraulic parameters for steady state vertical flow in heterogeneous soils. Water Resources Research, 39, 2003.

[231] Zreda, M., Desilets, D., Ferré, T. P. A., and Scott, R. L.: Measuring soil moisture content non-invasively at intermediate spatial scale using cosmic-ray neutrons, Geophysical Research Letters, 23, 949–952, 2008.

[232] Zreda, M., Shuttleworth, W.J., Zeng, X., Zweck, C., Desilets, D., Franz, T., Rosolem, R. and Ferre, T.P.A.: COSMOS: The COsmic-ray Soil Moisture Observing System. Hydrology and Earth System Sciences, 16, 4079-4099, 2012.

[233] Zribi, M., Saux-Picart, S., Andr, C., Descroix, L., Ottl, C., and Kallel, A.: Soil moisture mapping based on ASAR/ENVISAT radar data over a Sahelian region, International Journal of Remote Sensing, 28, 3547-3565, 2007.

[234] Zribi, M., Pardé, M., De Rosnay, P., Baup, F., Boulain, N., Descroix, L., Pellarin, T., Mougin, E., Ottlé, C., and Decharme, B.: ERS scatterometer surface soil moisture analysis of two sites in the south and north of the Sahel region of West Africa, Journal of Hydrology, 375, 253-261, 2009.

Acknowledgements

Furthermore, I would like to thank to my colleagues at the institute Thomas Graeff, Alexandre Cunha Costa, Peter Biro, Christian Mohr, Abbas Dara, Nicole Rudolph-Mohr, Matthias Munz, Jan Busch, Christoph Kormann, Sabine Schrader, Daniel Bazant, Till Francke and Isabel Martinez for providing me a friendly working atmosphere along these three years.

Last, but not least, I thank to all my family in Peru and Germany, who guided my way. Special thanks are going to Hanna for her patience with my never ending work, love, encourage and unconditional support always.

Appendix A

Transformation of calibration function

This appendix provides a transformation approach to adapt the calibration function with already fitted parameters to other reference conditions, e.g. drier ones, than those used so far for normalizing neutron count rates. This can be done a posteriori at any time, and without changes to the evaluated soil moisture values, provided that the calibration function is transformed as described in the following.

Count rates for normalization are preferably taken from a period with relatively dry conditions, and corresponding count rates and atmospheric pressure are named $N_{\mathrm{dry\_raw}}$ and P_{dry}, respectively. When a count rate for a different period shall be used for normalization ($N'_{\mathrm{dry\_raw}}$) it goes along with a different local atmospheric pressure (P'_{dry}) during that period. The calibration function, Eq. (2.1), can be transformed and updated to the use of counting rates with new normalization. For the transformation procedure, two factors α and γ for neutron count rates (Eq. A-1) and atmospheric pressure (Eq. A-2), respectively, are defined as follows:

$$N'_{\mathrm{dry\_raw}} = \alpha \cdot N_{\mathrm{dry\_raw}} \qquad (\text{A-1})$$

$$P'_{\mathrm{dry}} = \gamma \cdot P_{\mathrm{dry}} \qquad (\text{A-2})$$

Local corrections of neutron count rates by atmospheric pressure is applied as described in Eq. (2.2)

$$N'_{\mathrm{dry}} = N'_{\mathrm{dry\_raw}} \cdot e^{\beta\left(P_{\mathrm{dry}} - P_{\mathrm{mean}}\right)} \qquad (\text{A-3})$$

Inserting Eq. (A-1) in Eq. (A-3) gives

$$N'_{\text{dry}} = \alpha \cdot N_{\text{dry\_raw}} \cdot e^{\beta\left(P'_{\text{dry}} - P_{\text{mean}}\right)}$$

Re-arranging the exponential term yields

$$N'_{\text{dry}} = \alpha \cdot N_{\text{dry\_raw}} \cdot e^{\beta\left(P_{\text{dry}} - P_{\text{mean}}\right)} \cdot e^{\beta\left(P'_{\text{dry}} - P_{\text{dry}}\right)} \qquad \text{(A-4)}$$

Since $N_{\text{dry}} = N_{\text{dry\_raw}} \cdot e^{\beta\left(P_{\text{dry}} - P_{\text{mean}}\right)}$, Eq. (A-4) can be written as

$$N'_{\text{dry}} = \alpha \cdot N_{\text{dry}} \cdot e^{\beta\left(P'_{\text{dry}} - P_{\text{dry}}\right)} \qquad \text{(A-5)}$$

Equation (A-5) specifies how old and new normalized counting rates are related, where α and $e^{\beta\left(P'_{\text{dry}} - P_{\text{dry}}\right)}$ are constants. Then, if Eq. (A-2) is inserted in Eq. (A-5) and constants are re-grouped, we get

$$N'_{\text{dry}} = \left(\alpha \cdot e^{\beta\left(\gamma \cdot P_{\text{dry}} - P_{\text{dry}}\right)}\right) \cdot N_{\text{dry}} = \alpha \cdot e^{\beta \cdot P_{\text{dry}}(\gamma - 1)} \cdot N_{\text{dry}} \qquad \text{(A-6)}$$

Because of parameters inside the parenthesis are all constants, the expression in the parenthesis can be named by another constant λ yielding the following relation

$$N'_{\text{dry}} = \lambda \cdot N_{\text{dry}} \qquad \text{(A-7)}$$

In the calibration function, Eq. (2.1), relative neutron count rates are used, and the ones used so far can now be related to neutron count rates normalized via the new reference conditions as follows:

$$N_R = \frac{N}{N_{\text{dry}}} = \lambda \frac{N}{N'_{\text{dry}}} \qquad \text{(A-8)}$$

Replacing this term in the calibrated function Eq. (2.1) by Eq. (A-8) gives

$$\rho_{\text{wat}}/\rho_{\text{b}} \quad \theta(N) = \frac{a_0}{\frac{N}{N_{\text{dry}}} - a_1} - a_2 = \frac{a_0}{\lambda \frac{N}{N'_{\text{dry}}} - a_1} - a_2 \qquad \text{(A-9)}$$

Finally, simplifying Eq. (A-9) to

$$\rho_{\text{wat}}/\rho_{\text{b}} \quad \theta = \frac{a_0/\lambda}{\frac{N}{N'_{\text{dry}}} - \frac{a_1}{\lambda}} - a_2 = \frac{a_0/\lambda}{N'_R - \frac{a_1}{\lambda}} - a_2 \qquad \text{(A-10)}$$

This demonstrates that this calibration function of a GANS probe may be adjusted during on-going measurements or even retrospectively, if besides using the differently normalized neutron counting rates the parameters a_0 and a_1 in the calibration function are divided by the constant λ.

Appendix B

Calibration results

This is a revised version of the one published by Rivera Villarreyes, C. A., Baroni, G., and Oswald, S. E.: Calibration approaches of cosmic-ray neutron sensing for soil moisture measurement in cropped fields, Hydrology and Earth System Sciences Discussions, 10, 4237-4274, 2013; a proceedings-type publication.

Table B-1: Fully-empirical calibration approach and its four calibration cases: (C1) constant z* and no neutron weighting scheme, (C2) variable z* and no neutron weighting scheme, (C3) constant z* and neutron weighting scheme, and (C4) variable z* and neutron weighting scheme. The RMSE was calculated for the validation period.

Cases	Datasets	Crop	a_0 [-]	a_1 [-]	a_2 [-]	k [-]	RMSE [$\mathrm{m^3\,m^{-3}}$]
C1	D1	Sunflower	0.071	0.380	0.070		0.031
C1	D2	Sunflower	0.102	0.001	0.055		0.056
C1	D3	Sunflower	0.024	0.480	0.002		0.030
C1	D4	Sunflower	0.054	0.317	0.001		0.033
C2	D1	Sunflower	0.066	0.434	0.091		0.041
C2	D2	Sunflower	0.168	0.001	0.143		0.047
C2	D3	Sunflower	0.070	0.355	0.091		0.028
C2	D4	Sunflower	0.043	0.366	0.001		0.030
C3	D1	Sunflower	0.071	0.380	0.071	-0.010	0.031
C3	D2	Sunflower	0.215	0.001	0.202	-2.934	0.039
C3	D3	Sunflower	0.278	0.062	0.322	-3.409	0.031
C3	D4	Sunflower	0.049	0.339	0.001	-0.808	0.031
C4	D1	Sunflower	0.071	0.381	0.071	-0.010	0.031
C4	D2	Sunflower	0.190	0.001	0.169	-1.659	0.043
C4	D3	Sunflower	0.275	0.065	0.318	-2.162	0.031
C4	D4	Sunflower	0.049	0.337	0.001	-0.558	0.031
C1	D5	Winter rye	0.049	0.440	0.028		0.046
C1	D6	Winter rye	0.245	0.001	0.199		0.031
C1	D7	Winter rye	0.136	0.001	0.090		0.046
C1	D8	Winter rye	0.021	0.540	0.001		0.039
C2	D5	Winter rye	0.075	0.385	0.095		0.030
C2	D6	Winter rye	0.304	0.001	0.297		0.023
C2	D7	Winter rye	0.052	0.377	0.046		0.030
C2	D8	Winter rye	0.038	0.470	0.031		0.024
C3	D5	Winter rye	0.198	0.215	0.266	-3.346	0.030
C3	D6	Winter rye	0.282	0.001	0.259	-1.155	0.026
C3	D7	Winter rye	0.113	0.167	0.100	-1.427	0.036
C3	D8	Winter rye	0.047	0.443	0.045	-1.890	0.024
C4	D5	Winter rye	0.153	0.261	0.204	-1.440	0.030
C4	D6	Winter rye	0.286	0.001	0.267	-0.906	0.025
C4	D7	Winter rye	0.078	0.275	0.071	-1.085	0.034
C4	D8	Winter rye	0.035	0.482	0.028	-1.172	0.026

Table B-2: Semi-empirical calibration approach and its four calibration cases: (C1) constant z* and no neutron weighting scheme, (C2) variable z* and no neutron weighting scheme, (C3) constant z* and neutron weighting scheme, and (C4) variable z* and neutron weighting scheme. The RMSE was calculated for the validation period.

Cases	Datasets	Crop	f_{cal} [-]	k [-]	RMSE [$\mathrm{m^3\,m^{-3}}$]
C1	D1	Sunflower	1.310		0.051
C1	D2	Sunflower	0.923		0.024
C1	D3	Sunflower	0.825		0.031
C1	D4	Sunflower	0.981		0.022
C2	D1	Sunflower	1.206		0.039
C2	D2	Sunflower	0.873		0.027
C2	D3	Sunflower	0.845		0.029
C2	D4	Sunflower	0.899		0.026
C3	D1	Sunflower	1.256	-0.958	0.045
C3	D2	Sunflower	0.898	-5.231	0.025
C3	D3	Sunflower	0.855	-2.884	0.028
C3	D4	Sunflower	0.875	-10.00	0.027
C4	D1	Sunflower	1.241	-0.846	0.043
C4	D2	Sunflower	0.898	-3.839	0.025
C4	D3	Sunflower	0.853	-1.786	0.028
C4	D4	Sunflower	0.873	-10.00	0.028
C1	D5	Winter rye	1.205		0.042
C1	D6	Winter rye	1.192		0.037
C1	D7	Winter rye	1.051		0.024
C1	D8	Winter rye	1.060		0.025
C2	D5	Winter rye	1.088		0.030
C2	D6	Winter rye	1.068		0.026
C2	D7	Winter rye	1.023		0.023
C2	D8	Winter rye	1.119		0.030
C3	D5	Winter rye	1.081	-3.198	0.029
C3	D6	Winter rye	1.023	-4.102	0.023
C3	D7	Winter rye	1.052	-3.076	0.024
C3	D8	Winter rye	1.132	-1.920	0.031
C4	D5	Winter rye	1.077	-1.682	0.029
C4	D6	Winter rye	1.020	-2.472	0.023
C4	D7	Winter rye	1.056	-2.390	0.025
C4	D8	Winter rye	1.134	-1.446	0.031

Table B-3: N_0-calibration approach and its four calibration cases: (C1) constant z* and no neutron weighting scheme, (C2) variable z* and no neutron weighting scheme, (C3) constant z* and neutron weighting scheme, and (C4) variable z* and neutron weighting scheme. The RMSE was calculated for the validation period.

Cases	Datasets	Crop	N_0 [cph]	k [-]	RMSE [$\mathrm{m^3\,m^{-3}}$]
C1	D1	Sunflower	1376.4		0.032
C1	D2	Sunflower	1278.6		0.029
C1	D3	Sunflower	1233.0		0.043
C1	D4	Sunflower	1288.0		0.028
C2	D1	Sunflower	1349.4		0.025
C2	D2	Sunflower	1261.5		0.034
C2	D3	Sunflower	1240.4		0.040
C2	D4	Sunflower	1259.7		0.035
C3	D1	Sunflower	1373.4	-0.184	0.031
C3	D2	Sunflower	1266.8	-6.221	0.033
C3	D3	Sunflower	1244.1	-2.907	0.039
C3	D4	Sunflower	1251.0	-10.00	0.037
C4	D1	Sunflower	1372.0	-0.189	0.030
C4	D2	Sunflower	1266.9	-4.603	0.033
C4	D3	Sunflower	1243.3	-1.808	0.040
C4	D4	Sunflower	1250.5	-10.00	0.037
C1	D5	Winter rye	1357.0		0.030
C1	D6	Winter rye	1352.1		0.026
C1	D7	Winter rye	1319.2		0.023
C1	D8	Winter rye	1315.3		0.023
C2	D5	Winter rye	1322.0		0.022
C2	D6	Winter rye	1315.1		0.023
C2	D7	Winter rye	1308.3		0.024
C2	D8	Winter rye	1330.6		0.023
C3	D5	Winter rye	1320.3	-3.102	0.022
C3	D6	Winter rye	1301.6	-4.011	0.024
C3	D7	Winter rye	1312.8	-3.046	0.023
C3	D8	Winter rye	1337.4	-2.242	0.023
C4	D5	Winter rye	1319.1	-1.623	0.021
C4	D6	Winter rye	1300.5	-2.418	0.024
C4	D7	Winter rye	1313.8	-2.360	0.023
C4	D8	Winter rye	1337.4	-1.667	0.023

Author's declaration

I prepared this dissertation without illegal assistance. The work is original except where indicated by special reference in the text and no part of the dissertation has been submitted for any other degree.

This dissertation has not been presented to any other University for examination, neither in Germany nor in another country.

Carlos Andres Rivera Villarreyes

Potsdam, October 2013